N O T I C E

THIS DOCUMENT HAS BEEN REPRODUCED FROM MICROFICHE. ALTHOUGH IT IS RECOGNIZED THAT CERTAIN PORTIONS ARE ILLEGIBLE, IT IS BEING RELEASED IN THE INTEREST OF MAKING AVAILABLE AS MUCH INFORMATION AS POSSIBLE

DOE/NASA/0046-81/1
NASA CR-165171

ADVANCED DC MOTOR CONTROLLER FOR BATTERY-POWERED ELECTRIC VEHICLES

(NASA-CR-165171) ADVANCED dc MOTOR CONTROLLER FOR BATTERY-POWERED ELECTRIC VEHICLES (Franklin Inst. Research Labs.) 98 p HC A05/MF A01 CSCL 13F
N81-29036
Unclas
G3/85 26980

Charles A. Belsterling
George R. Simmons
John Stone
Franklin Research Center

July, 1981

Prepared for
NATIONAL AERONAUTICS AND SPACE ADMINISTRATION
Lewis Research Center
Under Contract DEN3-46

AUG 1981
RECEIVED
NASA STI FACILITY
ACCESS DEPT.

for
U.S. DEPARTMENT OF ENERGY
Conservation and Renewable Energy
Office of Vehicle and Engine R&D

DOE/NASA/0046-81/1
NASA CR-165171

ADVANCED DC MOTOR CONTROLLER FOR BATTERY-POWERED ELECTRIC VEHICLES

C.A. Belsterling, G.R. Simmons, and J. Stone
Franklin Research Center
20th & Benjamin Franklin Parkway
Philadelphia, PA 19103

July, 1981

Prepared for
NATIONAL AERONAUTICS AND SPACE ADMINISTRATION
Lewis Research Center
Cleveland, Ohio 44135
Under Contract DEN3-46

for
U.S. DEPARTMENT OF ENERGY
Conservation and Renewable Energy
Office of Vehicle and Engine R&D
Washington, D.C. 20545
Under Interagency Agreement DEAI01-77CS51044

CONTENTS

	Page
SUMMARY	1
INTRODUCTION	1
CONCEPT DEFINITION	2
Statement of the Problem	2
REQUIREMENTS FOR AN ADVANCED CONTROLLER	3
ANALYSIS OF THE CONTROLLER CONCEPT	5
Description of Operation	5
Basic Analysis	6
Computer Simulation	8
PROOF-OF-PRINCIPLE DEMONSTRATION	11
Proof-of-Principle Tests & Discussion	12
VALIDATION OF THE COMPUTER PROGRAM	14
CRITICAL TECHNOLOGY AND SUPPORTING DEVELOPMENT	15
FUNCTIONAL MODEL DESIGN	15
Selection of Machines	15
Transient Response to Field Changes	16
Efficiency Characteristics	17
Rating of Machines for the Functional Model	18
ENGINEERING MODEL DESIGN	19
Introduction	19
Minimizing MG Set Rating	20
Controller Design	22
Controller Description	24
Controller Layout	25
Controller Performance with Traction Motor	26
Controller Efficiency	27
Summary	27

CONTENTS (Cont'd)

	Page
LIFE-CYCLE COST ANALYSIS	27
Introduction	27
Purchase Price	28
Maintenance	29
Repair	29
Salvage Value	29
Energy Burden	30
Warranty	30
Cost Analysis	30
SUMMARY	30
RECOMMENDATIONS	31
REFERENCES	32

APPENDIX A. List of Symbols

APPENDIX B. Validation of the Computer Program

APPENDIX C. Additional Engineering Model Controller Drawings

LIST OF FIGURES

1. A Typical Electric Vehicle Propulsion System
2. SAE J227a/D Power Profile
3. Advanced DC Motor Controller Block Diagram
4. Ward Leonard System Power Transfer
5. Franklin MG System Power Transfer
6. DC Controller Simulation Block Diagram
7. Sketch of Proof-of-Principle System
8. Advanced DC Motor Controller Circuit Schematic Diagram
9. Proof-of-Principle Electrical System Schematic Diagram
10. Photograph of Proof-of-Principle Demonstration System
11. Closeup of Control Panel
12. Closeup of Proof-of-Principle Machines
13. Typical Proof-of-Principle Test Results - Acceleration and Deceleration on a Level Grade
14. Simulation of Transient Response of Controller with 50% Generator Field
15. Simulated Performance with Constant Traction Motor Current During Deceleration
16. Simulated Performance with Constant Traction Motor Armature Current During Acceleration
17. Simulated Performance with Constant Battery Power Control
18. Computed Efficiency of the Functional Model Controller with Various Field Currents
19. Predicted Efficiency of Vehicle Using Functional Model Controller
20. Predicted Efficiency of Vehicle in Regenerative Braking Mode
21. Arrangement for the MG Set for the Functional Model DC Motor Controller
22. Electrical Schematic of the Functional Model in Test Facility
23. DC Controller Block Diagram
24. Conceptual Sketch of Rotary Amplifier
25. Schematic of Rotary Amplifier Field Control
26. Assembly Drawing of Engineering Model Advanced Motor-Generator Set
27. Sketch Showing Controller Layout in an Electric Vehicle

LIST OF FIGURES (Cont'd)

28. Simulated Engineering Model Performance During SAE Profile

29. Traction Motor Shaft Output During SAE Profile

30. Traction Motor Horsepower Versus Vehicle Speed

31. Controller Output Power During SAE Profile

32. Battery Output Power During SAE Profile

33. Controller Efficiency During SAE Profile

34. Controller Efficiency Versus Vehicle Speed

35. Summary of Life Cycle Costs

B-1 Simulated Proof-of-Principle System--Acceleration and Deceleration on Level Grade

B-2 Proof-of-Principle Demonstration System Test Results--Acceleration and Deceleration of a Vehicle on Level Grade

B-3 Superposition of Figures B-1 and B-2 to Validate Computed Dynamic Performance

ADVANCED DC MOTOR CONTROLLER

FOR

BATTERY POWERED ELECTRIC VEHICLES

Charles A. Belsterling, George R. Simmons, John Stone
Franklin Research Center

SUMMARY

This Final Report covers the development of a new concept for an advanced DC motor controller using rotating machines. A motor-generator set is connected to run from the DC source and generate a voltage in the traction motor armature circuit that normally opposes the source voltage. When the generator voltage equals the source voltage, no voltage is applied to the traction motor. When the generator voltage is reduced, the traction motor accelerates. When the generator voltage is increased, the traction motor reverses torque or, if torque is reversed, regeneration braking is effective to zero speed. The functional feasibility of the concept is demonstrated with tests on a Proof-of-Principle System. An analog computer simulation is developed and validated with the results of the tests. It is then applied to predict the performance of a full-scale Functional Model DC Controller. The results indicate high efficiencies over wide operating ranges and exceptional recovery of regenerated energy. The Functional Model was designed with off-the-shelf machines, and resulted in excessive weight; it was not built. The Engineering Model design covers the development of a new machine and control strategies that minimize the weight and maximize performance. The new machine integrates both motor and generator on a single two-bearing shaft. The control strategy produces a controlled bi-directional $\pm$ 48 volts dc output from the generator permitting full control of a 96 volt dc traction motor from a 48 volt battery. The Advanced DC Motor Controller was designed to control a 20 hp traction motor. The controller weighs 63.5 kg (140 lb.) and has a peak efficiency of 90% in random driving modes and 96% during the SAE J227a/D driving cycle.

INTRODUCTION

For nearly 30 years the staff of the Franklin Research Center (FRC) has been active in advancing the state of the technology of rotating machines and controllers. In response to a 1978 solicitation from NASA, Lewis Research Center, this background was applied to meeting the requirement for an advanced motor controller for electric vehicles. The concept proposed is intended to avoid the detrimental characteristics of high-power electronic choppers yet maintain competitive levels of efficiency,

size and weight. The concept employs a rotating machine connected into the traction motor armature circuit to oppose or boost the battery voltage. The effect is achieved through low-current field control directly from the accelerator potentiometer without the need for electronic amplification.

Contract DEN3-46 was awarded to the Franklin Research Center in August 1978 to develop this concept for an advanced DC motor controller. The scope of the project to date has covered concept analysis, proof-of-principle demonstration, functional model design, prediction of full-scale performance, engineering model design and life cycle cost analysis. The work was done using a computer simulation of the controller in a typical electric vehicle to conduct parameter studies and predict performance on the SAE J227a/D driving cycle. For the engineering model design, we retained an industrial design consultant, Mr. Jeffrey Major, Prestolite Motor Division, Eltra Corp., to insure that the new controller is suitable for low-cost mass production.

Prior to submitting our proposal, a patent disclosure on this controller concept was filed at FRC. NASA acquired the rights to it at the signing of the contract, but FRC later petitioned successfully for the return of those rights. An application was filed in the U.S. Patent Office in May 1980.

The results of the work are significant to the field of electric vehicles as well as industrial machine control. It establishes that this concept provides a new and competitive means to control a DC motor conveniently and efficiently for a relatively low cost.

CONCEPT DEFINITION

Statement of the Problem

The problem of controlling the speed of an electric vehicle can be reduced to its simplest terms as illustrated in Figure 1. The battery is the source of stored energy carried on-board the vehicle. The vehicle requires a wide range of forces and velocities to perform its intended mission. Therefore, if a transmission is not included that can reflect either a constant load or a constant speed to the traction motor, the motor must deliver variable torques at variable speeds on command of the driver.

Except for internal losses the battery is essentially a fixed-terminal-voltage device. The traction motor, on the other hand, requires variable voltages and currents to deliver variable torques and speeds. This then defines the basic functional problem that the controller must solve: how to control the output from a fixed-voltage source to deliver variable voltage to a variable load. A secondary problem is how to return energy from the load to the source whenever it becomes available.

The controller must perform the functions necessary to solve these problems. Some of the existing ways to control electric vehicles are as follows.

The most obvious method of controlling a load connected to a fixed-voltage source is by means of a variable series resistance. However, this is extremely inefficient because large amounts of energy (equal to the load at the half-voltage point) are dissipated as heat.

The method most widely-used in early electric vehicles was battery switching, where cells were connected into several equal groups and the total voltage was varied in steps by means of mechanical contactors. This method has historically suffered from the arcing effects of switching extremely high dc currents in an inductive circuit.

For many years the accepted way to control high-power variable speed dc motors was by means of the Ward-Leonard System which employs a motor-generator set with low-power generator field controls (ref 1). This highly efficient and versatile system is still used on large off-the-road vehicles, where a lingering weight penalty can be tolerated.

In recent years the solid-state electronic "chopper" has become most common in controls for electric vehicles. It is operated as a fast-acting line switch to modulate the average voltage to the motor according to the ratio of on-time to off-time. Claims are made for very high chopper efficiencies but when motor losses, battery stresses and radiated noise are considered, it is not, in the opinion of many, the "best" choice (ref 2 and 3).

REQUIREMENTS FOR AN ADVANCED CONTROLLER

The following requirements for the advanced controller were originally expressed.

1. Application of the advanced controller shall result in significant improvements to vehicle range and performance.

2. Typical DC motors will be operable from a variable voltage as provided by the controller.

3. The controller shall be capable of controlling the DC motor to provide the typical motor horsepower versus time profile shown in Figure 2.

4. The controller and motor shall operate and interface with existing and advanced (1983) batteries.

5. Battery system voltage will comply with constraints imposed by motor, controller and battery within a battery pack voltage range of 100 to 240 volts.

6. Peak battery current level shall be limited to and comply with constraints imposed by battery characteristics (typically 600 amps for a 100 volt battery).

7. Low ratios of peak and rms to average controller currents are highly desirable to minimize battery internal losses.

8. For regenerative braking, the controller must limit battery currents to the maximum values specified in 6 above.

9. Controller must provide stable operation at low speeds (0 to 10 mph) for good maneuverability and parking.

10. Acceleration control must be smooth at an operator-selected rate to the desired speed.

11. Deceleration control must be smooth at an operator-selected rate to the desired speed.

12. Electromagnetic radiation from the controller and its electromagnetic susceptability shall conform to the latest revision of SAE J551.

13. Target ambient temperature range, -34.44°C (-30°F) to +48.89°C (+120°F).

14. Air cooling is required unless an alternate method is justified by overall vehicle considerations.

15. The controller input command signal corresponding to the accelerator pedal shall be a torque demand signal.

16. Reversing control may be accomplished external to the controller but a simple internal method is preferred.

17. Suitable safety features (circuit breakers, fuses, etc.) shall be incorporated into the controller to protect personnel and equipment.

Additional requirements defined for the Engineering Model of the FRC Controller are the following:

18. The controller shall be an integrated rotating machine based on the concept demonstrated in Proof-of-Principle tests.

19. The controller shall be designed to control the General Electric Type 2366 motor rated for 20 hp at 2500 rpm, 96 volts and 175 amps.

20. Power ratings of the integrated controller shall be the minimum allowable and shall conform with the results of the Engineering Model design.

21. The controller shall be designed so that production models will exhibit low life cycle costs not to exceed existing, comparably-rated controllers.

ANALYSIS OF THE CONTROLLER CONCEPT

Description of Operation

The Advanced DC Motor Controller concept developed by the Franklin Research Center is designed to meet all of the requirements expressed for the controller. It does so by employing a rotating machine to modulate and recirculate the power that must be handled by the controller thereby providing smooth and efficient operation in both the accelerating and regenerative modes.

The Franklin DC Motor Controller concept is implemented with a dc motor-generator (MG) set as shown in Figure 3. The output of the field-controlled generator is connected in series with the traction motor with its polarity normally opposing the battery. The MG set drive motor is also connected to the battery. When the traction motor is at rest the generator terminal voltage is controlled through its field to be exactly equal to the battery voltage and no current flows in the traction motor armature circuit. To accelerate and run the vehicle, the generator field is decreased, reducing the generator voltage and allowing the difference between battery and generator volts to be applied to the traction motor. Current flowing "backwards" through the generator makes it a motor and its drive motor a generator, recirculating the absorbed power back to the battery.

When the generator field is reversed, the generator voltage adds to the available battery voltage to provide an extended speed range above the base speed of the motor without the need for a gear-shift.

For regenerative braking the generator field is increased, raising the sum of the traction motor back-EMF and the generator voltage above the battery voltage, feeding current back to the battery and reversing the torque on the traction motor. The power required to boost the traction motor voltage is circulated from the battery through the MG set. This mode can also be used to reverse the rotation of the traction motor without the need for heavy electrical contactors.

Basic Analysis

One's first reaction to the MG set as a dc motor controller is to compare it with the classic Ward Leonard System illustrated in Figure 4. Input power is transmitted directly through the drive motor M and the generator G to the load R_L. Therefore the power transmission equations are:

Case 1 - Normal operation

$$P_o = P_{in} \times \text{motor efficiency} \times \text{generator efficiency}$$

$$\text{or } P_o = P_{in} eff_m eff_g \qquad 1)$$

Case 2 - Regeneration

Similarly when regenerating power from the load

$$P_{in} = P_o eff_m eff_g \qquad 2)$$

The power rating of the MG set can be derived from the generator requirements. Assuming that we want to deliver the maximum equivalent battery voltage E_b to the load, the generator maximum power is

$$P_g = E_g I_L = E_b I_L$$

and the load current I_L is

$$I_L = \frac{E_b}{R_g + R_L}$$

then

$$P_g = \frac{E_b^2}{R_g + R_L} \qquad 3)$$

Thus the MG set <u>must be rated to handle the maximum power delivered to the load</u>.

Now consider the Franklin MG System illustrated in Figure 5.

Case 1 - Normal operation - G motoring ($E_g < E_b$)

$$P_2 = P_{in} + P_m \qquad 4)$$

$$P_o = P_2 - P_g \qquad 5)$$

$$P_m = P_g eff_m eff_g \qquad 6)$$

combining to get the power transfer equation we have

$$P_o = P_{in} - P_g(1 - eff_m eff_g) \qquad 7)$$

Case 2 - Regeneration - G generating ($E_g > E_b$)

$$P_2 = P_{in} - P_m \qquad 8)$$

$$P_o = P_2 + F_g \qquad 9)$$

$$P_g = P_m eff_m eff_g \qquad 10)$$

combining to get the power transfer equation gives

$$P_{in} = P_o + P_d\left(\frac{1}{eff_m eff_g} - 1\right) \qquad 11)$$

Note that in this case the losses are a function of generator power. To derive this quantity we have

$$P_g = E_g I_L$$

and the load current is

$$I_L = \frac{E_b - E_g}{R_g + R_L} \quad \text{(assuming negligible battery resistance)}$$

then

$$P_g = \frac{E_g E_b - E_g^2}{E_g + R_L} \qquad 12)$$

When $E_g = E_b$ there is no generated power P_g and no power is delivered to the load, so for low power levels this System is at least competitive with the Ward Leonard System in its efficiency.

On the other hand, when the System delivers maximum power to the load $E_g = 0$ and again the generated power is zero. With reference to equations 7) and 1), it is clear that the Franklin MG System is far superior to the Ward Leonard System in this case.

Even more important is the difference in the ratings of the machines required. The peak power point occurs when $E_g = E_b/2$. Substituting this point into equation 2), we have

$$P_g = \frac{E_g E_b - E_g^2}{R_g + R_L} = \frac{E_b^2/2 - E_b^2/4}{R_g + R_L}$$

and

$$P_g = \frac{E_b^2}{4(R_g + R_L)} \qquad 13)$$

Comparing this result with the calculation in equation 3) shows that the rating of the MG set in the Franklin System can be only 1/4 of the rating for the MG set in the Ward Leonard System. Thus the Franklin MG System has the potential for delivering all the benefits of the Ward Leonard System (and more) without the weight penalty normally associated with an MG set controller.

The above analysis shows that the FRC concept inherently provides the following potential advantages and benefits as an advanced dc motor controller for electric vehicles.

Advantages	Potential Benefits
Familiar components	Low-cost service
Regenerative braking and motor reversal	Low-current control circuits
Continuous smooth current flow	Long-life rugged design
Extended speed range	Eliminates transmission
No high-energy transients	Low E/M interference

Disadvantages

MG set must be disconnected at standstill

Computer Simulation

The dynamic performance of a motor controller for battery-powered vehicles cannot be established with a few steady-state calculations alone. It can only be evaluated under cyclic conditions such as those imposed by the SAE driving cycles or, at the minimum, accelerate-run-decelerate conditions. Computer simulation was judged to be the most efficient and economical way to predict the performance of the new controller operating in the specified driving cycle (Figure 2). It provides the means to include the effects of vehicle dynamics and test control strategies for optimizing performance and minimizing weight.

FRC chose to simulate the motor controller in a complete vehicle and propulsion system on an analog computer. The simulation included the battery, the new motor controller and the traction motor with vehicle characteristics reflected to the motor shaft. The vehicle characteristics (mass, drag) were determined from the specified load profile (Figure 2) so wheel diameter and gear ratios need not be defined separately. They are inherent in our assumption that the rated speed of the motor, 2500 rpm, corresponds to cruising speed of the vehicle 72 km/h (45 mph). The results obtained from the computer simulation are compared to the actual performance of the Proof-of-Principle Controller later in this report to firmly establish the validity of the program.

Figure 6 is the block diagram of the computer program for simulating the propulsion system behavior. It simultaneously solves the motor/generator equations as energized by the battery and loaded by the vehicle. Beginning at the upper left corner of Figure 4, the battery voltage E_b is applied to the drive motor and the back-EMF, $K_e\phi_D S\theta_D$, subtracted from it. The difference is applied to the armature with resistance R_D to drive current I_D into the circuit. This part of the computer program solves the motor equation

$$E_b = K_e\phi_D S\theta_D + I_D R_D \qquad 14)$$

or

$$I_D = \frac{E_b - K_e\phi_D S\phi_D}{R_D} \qquad 15)$$

The resulting current I_D is then multiplied in the computer program by the torque constant times field flux $K_T\phi_D$ to calculate the torque T_D developed by the armature or

$$T_D = K_T\phi_D I_D \qquad 16)$$

The resulting torque of the drive motor is applied to three components of loading.

1. The friction and windage, $K_D S\theta_D$, of the drive motor
2. The accelerating torque, $J_D S^2\theta_D$, of the drive motor, and
3. The friction, windage, accelerating and load torques of the generator (ΣT).

The first and third components are subtracted from the developed torque to provide the torque to accelerate the motor. This solves the equation

$$T_D - \Sigma T - K_D S\theta_D = J_D S^2\theta_D \qquad 17)$$

The result is divided by the inertia, J_D, and integrated by the operator S to compute the motor speed $S\theta_D$.

The generator is simulated in the center of the block diagram of Figure 6. The field flux ϕ_g is the input variable controlled from the accelerator pedal. The flux is multiplied by the torque constant K_T to become one input to a two-input multiplier. The other input is the generator armature current I_g which is the same as the traction motor current I_m because they are in series. The product $K_T\theta_g I_m$ is the electrical torque on the generator shaft which is one of the load torques on the drive motor.

In the other branch, ϕ_g is multiplied by the generated voltage constant K_e to become one input to a two-input multiplier. The other input is the generator shaft speed $S\theta_g$ which is the same as the drive motor shaft speed $S\theta_D$. The product is the generated voltage which is then added to the I_gR_g drop to become the generator's terminal voltage E_g.

Now E_g is subtracted from the battery voltage E_b and the difference E_m is applied to the terminals of the traction motor, simulated in the lowest network in Figure 6. The motor back-EMF is computed from the product of the generated voltage constant K_e, the field flux ϕ_m and the traction motor shaft speed $S\phi_m$. The product is subtracted from the applied terminal voltage E_m and divided by the motor armature resistance R_m to develop armature current I_m. This current is then multiplied by the torque constant K_t and the field flux ϕ_m to compute the total developed torque, T_m. The friction and windage torque $K_D S\theta_m$ and the external load torque due to grades T_L are both subtracted from the developed torque to compute the net available for acceleration. This torque is divided by the sum of the motor inertia J_m and the reflected vehicle inertia J_L, then integrated by the operator S to compute the traction motor speed $S\theta_m$. This solves the equation:

$$T = (J_m + J_L)S^2\theta_m \qquad 18)$$

or

$$S\theta_m = \frac{T}{(J_m + J_L)S} \qquad 19)$$

With the computer program of Figure 6, one can "drive" the vehicle by manually controlling generator field flux. To simulate the performance of the vehicle and propulsion system in the SAE J227 driving cycle, the computed traction motor speed was continuously subtracted from the equivalent profile speed to generate an error signal controlling generator field flux.

PROOF-OF-PRINCIPLE DEMONSTRATION

A Proof-of-Principle Model was required to demonstrate, in a convenient and economical way, that the proposed concept would function as predicted. Our Proof-of-Principle Demonstration Controller was built with the most economical rotating machines available. They are 4 DC generators built for mid-1960's Chevrolet automobiles identical except that one has ball bearings instead of sleeve bearings.

When these machines were first received at FRC, they were tested to determine the design parameters necessary to compute static and dynamic performance. The measure parameters, within $\pm$ 5%, are as follows:

- armature resistance R_a = 0.165 ohms
- field resistance R_f = 7.27 ohms
- torque constant K_t = .052 $N_m/I_m/I_f$ 90.46 lb.in/I_m/I_f
- generated voltage constant K_e = 0.0067 volts/rpm/I_f
- rotating inertia J_m = .00122 N_m/rpm/sec (0.0108 lb.in/rpm/sec)
- friction K_f = 2.26 x 10^{-4} N_m/rpm (0.002 lb.in/rpm)

Armature circuit resistance (including brush resistance), friction and windage are very nonlinear characteristics so fixed values were chosen at nominal operating points. This means that computed results will be accurate over a limited dynamic range.

The Proof-of-Principle Demonstration System is shown schematically in Figure 7. Two machines are used to make up the Controller MG set. A third is the traction motor and the fourth is used as the motor loading device to simulate operations on grades. A flywheel is also mounted on the traction motor shaft to simulate vehicle inertia.

The circuit schematic of Figure 8 shows the armature and field connections of the basic FRC Controller. Arrows indicate the directions of current flow during the accelerating, running and regenerating modes of operation.

Figure 9 is a schematic of the complete Proof-of-Principle Demonstration System showing the instrumentation and control circuits necessary for the planned tests. It also shows the loading dynamometer, capable of simulating up-grade and down-grade conditions. Ammeter shunts are connected in every branch of the circuit to measure the current to each individual element and the total current from the battery. The generator field is controlled through a power transistor connected to a manually-operated potentiometer simulating the accelerator pedal in an electric vehicle. The loading motor is supplied from a separate adjustable constant-current source.

Photographs of the System are shown in Figures 8-10 with closeup views of the control panel, motor controller and traction motor with load.

There is a speed transducer on the controller shaft and a torque-speed transducer on the traction motor shaft.

Proof-of-Principle Tests & Discussion

The initial test program was to demonstrate the functions of the Franklin Controller and establish technical feasibility. The tests performed but not recorded were as follows:

Run No.	To Demonstrate	Procedure
1	Speed Control	• Generator field at maximum, traction motor at zero speed. • Generator field reduced to half maximum, traction motor accelerated and ran at half maximum speed. • Generator field reduced to zero, traction motor accelerated to maximum speed. • Traction motor speed varied smoothly with generator field current.
2	Up-hill Run	• Generator field at zero, traction motor accelerated to maximum speed. • Loading motor field increased to oppose traction motor and simulate up-hill run. • Traction motor speed decreased slightly-armature current increased for extra load.
3	Down-hill Run	• Generator field at half maximum, traction motor accelerated to half maximum speed. • Loading motor field increased to aid traction motor and simulate down-hill run. • Traction motor speed increased slightly--armature current decreased and reversed, demonstrating regeneration.

Run No.	To Demonstrate	Procedure
4	Regenerative Braking	• Generator field at zero, traction motor accelerated to maximum speed. • Generator field suddenly decreased to zero. • Traction motor armature current momentarily reversed to brake the motor.
5	Overspeed	• Generator field at zero, traction motor accelerated to maximum speed. • Generator field reversed to add generated voltage to battery voltage. • Traction motor speed increased above nominal maximum.
6	Reversing	• Generator field at nominal maximum, traction motor at zero speed. • Generator field increased above nominal maximum, generated voltage greater than battery voltage. • Traction motor accelerated in reverse direction.

Further testing was carried out to record the performance of the System under a normal start, run and stop cycle as shown in Figure 13. In this case (prior to Reference #201) the vehicle is initially at rest on level ground and the generated voltage exactly cancels the battery voltage. There is zero voltage to the traction motor and zero current in the armature circuit. The Controller is idling on the battery bus.

At Reference #201 the control field flux is reduced to zero, allowing most of the battery voltage to be applied to the traction motor. A large current flows in the armature circuit, accelerating the vehicle and momentarily forcing the generator to become a motor, recirculating the absorbed power back through the MG set. The vehicle accelerates at a rate determined by the available traction motor torque and the mass of the vehicle, drawing increased power from the battery.

At Reference #202, the vehicle has reached top speed so the armature current is reduced to a value just high enough to overcome vehicle friction and drag losses. Under these conditions the increased power from the battery is low and some power is still recirculating through the controller (MG drive current reduced; speed increased) because of residual magnetism in the control field.

At Reference #203, the control field flux is reapplied and the vehicle decelerates. The decay in traction motor speed is different from the rise because of the nonlinearity of the friction and windage in the machines and the slow decay of current in the armature circuit. Note the momentary reversal in traction motor armature current indicating regenerative braking.

In summary, the Proof-of-Principle tests described above clearly demonstrate the feasibility of the new DC Motor Controller. They show that the Controller has the potential for meeting or exceeding all of the functional requirements of an electric vehicle as established for the NASA program. It delivers a smoothly-varying voltage to the traction motor from an existing EV battery. It does not draw excessive peaks or pulses of current from the battery or deliver pulsed voltage to the traction motor. It provides regenerative braking without high pulses of current into the battery. Accleration, deceleration and low speed control are smooth and stable at an operator-selected rate. Reversing and overspeed ranges are provided by means of low-power field control. All of these functions are provided with simple, rugged and widely-understood rotating machines. Therefore it has outstanding potential for use in improved electric vehicles.

The major problems to be overcome to realize this potential are 1) reducing the size and weight and 2) maximizing performance efficiency on the SAE J227a/D driving cycle. These problems may be solved with the application of advanced technology in the design of DC machines; specifically two-bearing, high-speed configurations.

VALIDATION OF THE COMPUTER PROGRAM

In order to use the analog computer to predict the performance of both Functional and Engineering Model Controllers, the computer program was verified as being an accurate simulation of the Advanced DC Controller. This was accomplished by manual calculations of the balance of power at several steady state operating points and by graphical comparison of the dynamic characteristics of the simulated and experimental tests. The results are given in Appendix B.

In summary, the validity of the computer simulation program has been firmly established in manual calculations and in a direct comparison with the results of tests on the Proof-of-Principle System. The computing accuracy is better than $\pm$ 5%. Differences are shown to be mainly a result of non-linearities which are not included in the simulation but are only predominant in small machines. For example, the brush friction in the Proof-of-Principle machines is [illegible] of the no-load losses while in a 20 hp machine, it is in the order of 40%. Therefore the computer simulation, with the proper parameter adjustments, is a reliable tool for predicting the performance of full-scale systems with good reliability.

CRITICAL TECHNOLOGY AND SUPPORTING DEVELOPMENT

It has been predicted and demonstrated that the new DC Motor Controller has the potential for satisfying all of the functional requirements. The functional requirements can, in fact, be satisfied today with readily-available machines and controls but two areas of critical technology must be addressed to realize the full potential of the concept. One area is the software (logic) to optimize control strategies. The other area is the hardware making up the MG set.

Considering the optimization of control strategies, several characteristics of the new controller have been recognized. The most obvious handicap in the system's performance is the fact that the MG set runs continuously and its losses are consuming battery energy at standstill. To overcome this handicap, it will be necessary to disconnect the MG set whenever the vehicle is stopped. It can be restarted in a fraction of a second so the time delay is not critical. However, energy is required to accelerate it and that energy is not easily recovered when it is disconnected. A simple timer is adequate to command the shutdown for minimum energy consumption. The shutdown delay time is calculated as the idling time at which the running energy equals the startup energy.

In the design of the MG set, the need for minimum weight and maximum efficiency are the most important factors. Minimum size follows. The MG set need not be power rated as high as the traction motor, so it is not equivalent to two traction motors. Beyond that, the most advanced materials and concepts should be applied to the development of a new MG set to maximize efficiency and reduce size and cost.

FUNCTIONAL MODEL DESIGN

The Functional Model of the Advanced DC Motor Controller is to extend the controller concept to a full-scale, rated power, functioning unit to operate with a typical traction motor and provide the means to obtain a realistic evaluation of its performance. It also is intended to demonstrate practicality and define critical problems.

Selection of Machines

As shown by the Proof-of-Principle demonstration the performance of the Franklin Controller is highly-dependent on the characteristics of the MG set, the power-handling component. For example, low armature resistance is a key factor in achieving high efficiency. Losses of all types should be minimized. Therefore to implement an acceptable Functional Model, DC machines with high efficiency over a wide range of loading are required. For a realistic evaluation, the characteristics of available high-efficiency machines in the 10-20 hp range were investigated. Machine parameters were scaled down to the same rating as those used in the Proof-of-Principle System so a direct comparison can be made to establish the

sensitivity of certain parameters in Controller performance. The scaled rating is 175 watts maximum shaft power with 91% efficiency. The calculated parameters for a typical machine with this efficiency are:

armature resistance	R_a = 0.0181 ohms
field resistance	R_f = 54.5 ohms
torque constant	K_t = 0.49 Nm/I_m/I_f (4.34 lb. in/I_m/I_f)
generated voltage constant	K_e = 0.055 volts/rpm/I_f
rotating inertia	J_m = 1.22 x 10^{-4} Nm/rpm/sec (0.011 lb.in/rpm/sec)
friction and windage	K_f = 6.22 x 10^{-5} Nm/rpm (0.00055 lb.in/rpm)

These above parameters were inserted into the validated computer program and simulated tests run to record the predicted performance characteristics of the Functional Model. Sample recordings are discussed in the following paragraphs.

Transient Response to Field Changes

The transient response to step changes in generator field excitation is shown in Figure 14. The field is initially at 50% (Reference #1) and the traction motor is running at 500 rpm. Battery power is low because the vehicle is at half speed on level ground. The field is suddenly reduced to zero (Reference #2) allowing more current to reach the traction motor and the vehicle accelerates. Although the increased armature current also flows through the generator, its field is zero so it cannot act as a motor and recirculate power to the battery. Therefore all the necessary power is drawn from the battery.

After the vehicle has reached its new cruising speed, the field is suddenly increased to 50% (Reference #3). The generator voltage adds to the motor back-EMF to reverse the current in the armature circuit and feed it back to the battery. The additional torque required by the generator is provided through an increase in current in the MG set drive motor, drawing power from the battery. The net result is that braking energy returned to the battery is approximately 30% of the amount used to accelerate.

In view of the foregoing test results, it becomes clear that a larger portion of the kinetic energy in the vehicle can be returned to the battery if the generator field is controlled in an optimal manner. One approach is to control the field profile to maintain <u>constant traction motor current</u> (braking force) during deceleration. This case is shown in Figure 15. (Note the scale change for traction motor current and battery power.)

This figure shows the battery power returned during deceleration with constant armature current. Figure 16 shows the battery power drain during acceleration with constant armature current. The regenerated energy (area under the power curve) is nearly half the energy consumed during acceleration.

Carrying this approach one step further, Figure 17 shows the response in the case when the field is controlled to maintain constant power during acceleration and deceleration. In this case, approximately 1/3 of the stored energy is regenerated. Armature current rises much higher than in the previous case to stop the vehicle in a shorter time. Armature circuit losses subtract more from the available regenerated energy.

Efficiency Characteristics

The efficiency characteristics of the Controller were computed by fixing the field current of the generator and varying the load in the traction motor. Results were measured for field currents of 0%, 25%, 50% and 75% of rated field current. Efficiency is calculated for the ratio of output power to battery power.

Figure 18 shows the efficiency characteristics of the Advanced DC Motor Controller predicted for the full-scale Functional Model. The efficiency is plotted versus power output for various constant values of field current. Note that the Controller is between 80 and 90% efficient over most of the load range when the field is less than 50% of its maximum value. This represents running at approximately half to full rated speed, equivalent to an electric car operating loaded at 48-88 km/hr (30-55 mph).

The 0% generator field current curve represents the case where the generator is completely inactive and the MG set is simply idling on the battery bus. Then at low output power, the MG set losses are significant but at high power output the additional losses are only the I^2R losses in the generator armature. The latter condition is typical of acceleration and cruising at high speed.

At 75% field current, less than 25% of the battery voltage is available to the traction motor. In this mode the generator is a motor simply recirculating up to 75% of the power from the battery, creating greater losses and dramatically reducing the efficiency.

The efficiency characteristics of the overall vehicle propulsion system were computed by maintaining constant speed while varying the load on the traction motor. Results were measured for speeds from 8.8 km/hr (5.5 mph) to 88 km/hr (55 mph).

Figure 19 shows the overall propulsion system efficiency (less battery) for a vehicle using the Advanced DC Motor Controller. These

characteristics reflect the high Controller efficiencies over a broad operating envelope shown in Figure 18 holding a maximum of nearly 80% for a wide range of load conditions.

These characteristics represent the case of running the vehicle at constant speed on varying grades. Again the highest efficiency is obtained when the vehicle is at top speed, the generator terminal voltage is lowest and the MG set is nearly idling on the battery bus. At the lower speeds the MG set is recirculating greater amounts of power so the efficiency is lower.

Finally, Figure 20 shows the overall system efficiency in the regenerative braking mode. Again it indicates outstanding recovery (around 80%) in the most critical region; near maximum speed.

In summary, the computer simulation of the full-scale Franklin Controller mounted in a typical vehicle has been used to predict performance of the Functional Model. The vehicle characteristics were calculated from the required SAE J227a/D power profile (Figure 2) as follows:

Gross weight = 1730 kg (3814 lbs.)

$$\text{Drag} = \frac{4.34n}{\text{km/hr}}\left(\frac{1.57\ \text{lb.}}{\text{mph}}\right)$$

Results of transient responses to manually-controlled field changes and efficiency characteristics with fixed-field or closed-loop speed control (Figures 14 through 20) show that:

1. substantial amounts of power can be regenerated through the controller
2. with constant current controls, the energy regenerated is nearly half the energy consumed in acceleration
3. controller efficiency is between 80 and 90% from half to full rated speed (generator field 50% to 0%)
4. overall propulsion system efficiency (less battery) is between 70 and 80% for a wide range of load conditions at high speed, and
5. overall system efficiency during regenerative braking is in the vicinity of 80% at maximum speed.

Rating of Machines for the Functional Model

The power rating for the traction motor has been determined by taking the rms value of horsepower as determined from the SAE J227a driving cycle, Schedule D (Figure 2). This calculation indicates that a 20 hp motor is more than adequate for this application.

The generator design is based on maximum voltage and maximum current levels. In the case of the Functional Model these are 108V and 175A, respectively for a 20 hp traction motor. The size of the generator can be minimized in a design operating at high shaft speeds. A search of the available designs showed that a Prestolite DC machine (Model No. MTC-4001) was available to operate at the desired voltage and current ratings and run at 5000 rpm. It is available as a series-wound motor. This machine was selected as the generator and the series field was to be removed and replaced by a shunt field winding. The same machine was also to be used as the loading motor for the Functional Model tests.

The sizing of the MG-set drive motor was based on the power required by the generator. Computer studies and tests performed on the Proof-of-Principle machine showed that control of field excitation on the drive motor, generator and traction motor can be exercised to minimize the power requirement of the drive motor. Therefore computer studies were conducted to determine the optimum field control strategy for minimum sizing of the drive motor. It was found that the drive motor could be rated at only 60% of the generator power rating.

The one problem which remained an obstacle to the fabrication of the Functional Model Controller was the procurement of a drive motor that would not be oversize for the power required of it. The temporary solution was to use the oversized Prestolite MLR-4001 motor with a modified field until a suitable drive motor was procured.

The design layout of the MG set for the Functional Model DC Controller is shown in Figure 21. The Prestolite MTC-4001 generator and MLR-4001 motor are flange-mounted on an L-shaped bracket with mounting holes. The shafts are coupled with gears or belts inside a protective shroud. The overall size is approximately 0.06 m^3 (2 $ft.^3$) and the estimated weight, 63.5 kg (140 lbs.).

Figure 22 shows the connection of the Functional Model Controller in a proposed test facility.

At the conclusion of the Functional Model design, it was recognized that, using off-the-shelf machines, it would be too large and heavy. Therefore it was decided to design a special machine as a part of the Engineering Model design.

ENGINEERING MODEL DESIGN

Introduction

The purpose of the Engineering Model is to provide the equipment for conducting comprehensive performance tests in a vehicle under controlled conditions. It is intended to be an integrally-assembled representatively-packaged unit which physically resembles a proposed Production Model in

form and function. In this case, the Engineering Model will be an integrated rotating machine controller based on the concept demonstrated by the Proof-of-Principle Model. It is to be designed to be compatible with the General Electric Near-Term traction motor rated at 96 volts, 175 amps and 2500 rpm. It is to meet all specified requirements as defined at the beginning of this report.

The Engineering Model of the Franklin DC Motor controller has been designed as a compact, two-bearing, DC MG set with associated contactors and control logic.

Minimizing MG Set Rating

In the early stages of design there was a final analysis of the control strategies to minimize the loading of the MG set and thereby its required size. It was found that the generator size was primarily determined by the fact that it is directly in series with the traction motor and therefore must be capable of generating full battery voltage and conducting maximum traction motor armature current. The generator drive motor, however, runs from the fixed battery voltage and its maximum current is a function of the amount of power circulated through the MG set during the regenerative mode. Therefore its rating can be varied using different control strategies. The strategies studied in the final analysis were:

- traction motor field forcing
- limited mechanical braking
- bi-directional versus uni-directional generator field control.

Forcing of the traction motor field during regeneration reduces the drive motor armature current because the traction motor develops more generated voltage, thereby reducing the amount to be developed by the generator. Thus the drive motor power (current) to drive the generator is less.

Providing mechanical braking during the instant when the drive motor current peaks is effective in reducing the drive motor rating; however, it reduces the amount of energy returned to the battery during regenerative braking.

Finally, the concept of bi-directional versus uni-directional control of the generator field results in a major reduction in drive motor rating. This concept is described as follows.

The original (uni-directional) control scheme was to design the generator with a rated voltage just equal to the battery and the traction motor voltages. At standstill, generator and battery voltage are equal, and at rated speed the generator voltage is zero.

A better control system was found to be bi-directional control of the generator field. In this case, the generator and battery are rated at just half the voltage of the traction motor. Again at standstill, the generator and battery voltage are equal. However, to reach rated speed, the generator voltage is completely reversed to add to the battery so the total voltage equals the rated voltage of the traction motor. The net result is that the rating of the generator is practically half its rating in the uni-directional scheme.

As specified by the power profile of Figure 2, the rms power requirement for the traction motor is approximately 15 horsepower. The power required to move the vehicle up a 10% grade at 48 km/h (30 mph) is 35 horsepower for a limited time period. The peak power required from the traction motor is 57 horsepower during the regenerative portion of the profile. In our design the rated speed of the traction motor is matched to a vehicle speed of 72 km/hr (45 mph). The traction motor field is weakened to 82% to run at 89 km/h (55 mph) without an increase in generator output voltage. Computer investigations of optimum control strategies for the Controller are evaluated in terms of these traction motor ratings.

Table 1. Effects of Control Strategies

Type of Generator Field Control	Mechanical Braking	RMS MG SET HORSEPOWER	
		% Traction Motor Field During Deceleration	
	% of Rated Traction Motor Torque	100	125
Uni-directional	0	13.2	10.6
	15	11.6	10.0
	40	9.6	9.0
Bi-directional	0	8.0	7.6

With reference to Table 1, the bi-directional control of the generator field shows a very significant advantage, reducing the MG set rating from 13.2 to 8.0 horsepower. Mechanical braking indicates a potential advantage but we judge it not to be worth the sacrifice of regenerated energy. Forcing the traction motor field during deceleration reduces the rating an additional, but limited, amount. Based on these results, the optimum control strategies are:

1. Bi-directional generator field control,

2. Traction motor field forcing to 125% during deceleration.

3. Traction motor field weakening to 82% at 89 km/h.

Then using this control strategy the MG set rating for the power profile in Figure 2 is 7.6 horsepower.

Further simulations show that the MG set must develop 13.5 horsepower when the vehicle climbs a 10% grade at 48 km/h (30 mph). This is only a 178% overload, but since the time on grade was not defined, we chose to design the MG set for a 9.0 horsepower RMS rating.

Controller Design

To evaluate the Franklin Advanced Controller for an existing vehicle the Engineering Model was designed for use with the General Electric-Chrysler Near-Term Vehicle Motor, rated at 96 volts and 175 amperes. The bi-directional output from the generator requires only a 48 volt battery to drive the 96 volt traction motor and only the rated current flows in the armature circuit. This demonstrates another outstanding advantage of the Franklin System. It provides the means to realize the benefits of a high voltage motor and a low voltage battery bus.

Considering the Franklin DC Motor Controler as a "black box" with battery input and motor voltage output, it has been designed as a compact package rated as follows:

Controller RMS output power	13.44 kw
Drive Motor RMS horsepower	9 hp
Input (battery) voltage	48 volts
Output voltage	96 volts
RMS current	140 amperes
Maximum current	175 amperes

The unit is built on a single shaft within a two-bearing housing designed for forced-air cooling.

Design studies were made to determine the optimum design for minimum losses, weight and volume. Calculations were made using an armature diameter of 11.43 cm (4.5 in.) and a total motor diameter of 18.42 cm (7.25 in.). The armature stack and field length were varied from 10.16 cm (4.0 in.) to 17.78 cm (7.0 in.). The speed range was varied from 2000 to 5000 rpm. The optimum design was found to be at 4000 rpm.

The tabulation of losses in this design at rated output are given in Table 2. Brush drag and electrical loss are expected to be reduced by experimenting with materials after the Engineering Model is built.

Table 2. Tabulation of Controller MG Set Losses at Rated Output

Drive Motor Core	76.5 watts
Generator Core	75.6
Drive Motor Windage	84.9
Generator Windage	84.9
Drive Motor Brush Drag	360.0
Generator Brush Drag	360.0
Drive Motor Field	56.0
Generator Field	56.0
Drive Motor Armature	102.2
Generator Armature	98.0
Drive Motor Brush Electrical Loss	214.5
Generator Brush Electrical Loss	210.0
	1777.7 watts

The rated output of the Controller is the battery voltage (E_b) plus the generator voltage (E_g) multiplied by the rated generator current (I_g).

$$P_o = (E_b + E_g)\ I_g$$

$$P_o = (48 + 48)(140) = 13.44\ \text{KW}$$

The input to the Controller is the Controller output plus the total losses in the Controller.

Then the Controller efficiency is calculated as:

$$\%\ \text{Efficiency} = \frac{\text{Output}}{\text{Output+Losses}} = \frac{(E_b+E_g)(I_g)}{(E_b+E_g)(I_g) + \text{Losses}}$$

$$\%\ \text{Efficiency} = \frac{(48+48)(140)}{(48+48)(140) + 1777.7} = 88.3\%\ \text{at rated power}$$

The DC Controller block diagram is shown in Figure 23. A key switch closes a contactor which energizes the drive motor and all field controls. As the drive motor accelerates the MG set to rated speed, a differential sensor compares the generator output voltage to the battery voltage and closes the generator/battery contactor when the voltages are equal. At this time, there is zero voltage across the traction motor and the controller is awaiting a signal from the accelerator pedal.

As the accelerator pedal is depressed approximately halfway, the generator output voltages varies from 48 volts to 0 volts and the traction motor increases to half speed. Pressing the accelerator further causes the generator output polarity to reverse and the output voltage now adds to the 48 volt battery until a sum of 96 volts is applied to the traction motor. The vehicle is now traveling at about 45 mph and the accelerator is almost completely depressed. Pressing the accelerator even further energizes a traction motor field weakening circuit which allows the vehicle to accelerate up to 55 mph.

When the brake pedal is depressed, the field of the traction motor is forced to 125% of nominal value to provide maximum regenerative braking. Reverse is accomplished by reversing the traction motor field.

A thermal sensor located in the drive motor brush assembly activates the cooling fan at a temperature of 194°F (90°C). Another thermal sensor located in the drive motor field assembly lights a dashboard indicator if the MG set overheats at a temperature of 248°F (120°C).

The field control of the generator is accomplished with a rotary amplifier shown in Figure 24. It is a low-power field-controlled DC generator operated from the accelerator potentiometer and driving the generator field. The rotary amplifier eliminates the need for electronics in the field control, creating a more rugged and dependable controller. An electrical input signal of 1.5 watts controls up to 120 watts of power to the generator field. The eight pole rotary amplifier is mounted on the end bell of the MG set and its armature spins at 4000 rpm along with the MG set armature. The diameter of the amplifier is 7.25 inches, the same as the MG set diameter and it weighs 3.6 kg (8 lbs.). The controller schematic including the rotary amplifier is shown in Figure 25.

The choice of a rotary amplifier instead of a semiconductor circuit is the result of a tradeoff between improved reliability and serviceability versus a minimal reduction in losses.

Controller Description

The assembly drawing in Figure 26 has been prepared to show the physical arrangement of the major components of the motor generator (MG) set of the DC Controller.

The four field windings are assembled in each stator frame on pole pieces that are bolted to the frame by two bolts. Field terminals are preconnected to the windings. The drive motor field is designed to operate directly from the battery voltage. The generator field is designed to operate from a rotary amplifier and may not be the same as the drive motor field. The rotary amplifier is not shown in this drawing.

The estimated characteristics for the complete DC Controller are given as follows:

Weight	63.5 kg	140 lb.
Volume	$14.7 \times 10^3 cm^3$	$0.58 ft.^3$
Rating	13.44 kw	13.44 kw
Speed	4000 rpm	4000 rpm
Allowable Temperature Rise	115^oC	207^oF

Materials of construction are identified in Appendix C.

Controller Layout

Figure 27 illustrates the layout of elements in the DC Controller as mounted in a vehicle.

The MG set must have forced-air cooling and needs the most cooling when operating at higher vehicle speeds. A scoop is provided to bring in ram air and is effective alone at high speeds. The air flow enters the MG set through a centrifugal blower that is thermostatically-controlled by the temperature of the drive motor to supplement the ram air when necessary. A drain is provided at the bottom of the blower cage to remove any water that may be pulled in with the air. The MG set will be mounted above the level of the blower in order to further minimize the possibility of water entering either the drive motor or generator.

A junction box is provided to house the electronics for logic control in starting the MG set and weakening the traction motor field. The accelerator pedal and brake pedal will provide input signals to control the generator field current and the field of the traction motor.

A second junction box is used to house a contactor to connect the battery to the system and a contactor to connect the traction motor armature to the Controller output.

Controller Performance with Traction Motor

The traction motor power requirements for a typical electric vehicle are shown in Figure 2. The specified power profile is derived from the SAE J227a driving cycle, Schedule D. Dashed lines are added to indicate the specified power level for a vehicle cruising at 89 km/hr (55 mph) on a level grade and for a vehicle traveling at 48 km/hr (30 mph) up a 10% grade.

Figure 28 is a strip chart recording showing the performance of the Engineering Model Controller. These results were obtained from the analog computer simulation. By controlling the generator field (Channel 1), the traction motor shaft horsepower (Channel 7) was made to closely follow the specified power requirement of Figure 2.

During deceleration the traction motor field is increased to 125% of nominal value since it enables the controller to regenerate a greater amount of energy and it reduces the armature currents in both traction motor and controller. Throughout the entire profile, excellent control is maintained over the traction motor.

A comparison of the traction motor shaft power to the specified SAE Power requirement is shown in Figure 29. The correlation between the two curves is excellent, with only small differences due to controller time constants. This comparison demonstrates the controller's ability to meet the SAE power profile requirements.

The rms power requirement for the traction motor to meet the requirements of the SAE J227a, D profile is approximately 15 hp. The power required to move the vehicle up a 10% grade at 30 miles per hour is 35 hp for a limited time period. The maximum peak power required from the traction motor is 57 hp during the regenerative portion of the profile. The traction motor provided for this design is rated for 20 hp continuous operation. From this we find that during the 30 mph mode of operation on a 10% grade, the motor will operate at 175% load. During the deceleration portion of the SAE profile, 285% peak power must be supplied by the traction motor.

The plot of Figure 30 shows horsepower versus speed delivered to the traction motor with the vehicle on a level grade and on a 10% grade. At a constant 35 mph (88.5 km/hr) on a level grade, the controller will supply 16 horsepower to the traction motor. At a constant speed of 30 mph (48.3 km/hr) on a 10% grade, the controller is capable of delivering at least 35 horsepower to the traction motor. The Engineering Model Controller clearly meets the horsepower requirements for constant speed specified.

Controller Efficiency

Figure 31 is a plot of Controller output power versus time during the SAE J227a/D driving cycle. Figure 32 is a plot of battery output power versus time for the same driving cycle. These plots were obtained from the analog computer program results of Figure 30 which were used to determine the energy efficiency of the Engineering Model Controller.

The results show that 1112.7 kw-sec of energy are drawn from the battery each cycle of the SAE J227a/D driving profile. During the 25 second idle time when the vehicle is at rest, 17.6 kw-sec (1.6% of the total) is drawn. During deceleration, 201.5 kw-sec (18.1% of the total) of energy is regenerated into the battery. The net energy used in one cycle is therefore 911.2 kw-sec using regeneration. A vehicle could theoretically travel 18.1% further than if no regeneration were used for the SAE J227a/D driving cycle.

The energy efficiency of the Engineering Model Controller over the entire SAE J227a/D driving cycle is 86.8%.

The Controller efficiency versus time for the SAE driving profile is plotted in Figure 33. The efficiency was calculated from the battery power and Controller output power of Figure 28. During the regeneration portion of the curve, the efficiency represents the power flow from traction motor to battery.

The Controller efficiency versus constant speed at 0% and 10% upgrades is shown in Figure 34. The efficiency peaks at better than 91%.

Summary

In summary, the Engineering Model has been designed to meet all requirements. Considering its flexibility of control, the inherent regenerative braking and the smooth flow of current, its weight and efficiency are competitive with other existing DC Motor Controllers.

LIFE-CYCLE COST ANALYSIS

Introduction

The objective of a life-cycle analysis is to establish the cost per kilometer (mile) of a Franklin DC Motor Controller over a designated operating lifetime. Factors entering into this cost are as follows:

- Purchase price
- Maintenance
- Repair
- Salvage value
- Energy expended moving its weight
- Warranty

Two guidelines imposed on the Life Cycle Cost Analysis are:

- Purchase price is to be based on production rates of 10,000 and 100,000 units per year.

- Operating lifetime is defined as 100,000 cycles of the SAE J227a, Schedule D driving cycle (approximately 3,500 hours and 164,000 km).

To establish other guidelines necessary to evaluate costs, we assume the following:

- Vehicle lifetime is 10 years and 164,000 km (102,000 mi.)
- Costs are expressed in 1980 dollars.
- Purchase price is the sum of the original equipment manufacturer (O.E.M.) cost plus the O.E.M. and dealer's markup, estimated at 30%. Taxes are not included.
- Cost of electricity is 5 cents per kwh.
- Maintenance and repair costs are based on a labor rate of $16 per hour.
- A complete set of replacement brushes costs $20.
- Commutators can be resurfaced by turning on a machine lathe in one hour.

Purchase Price

The manufacuring costs for the D.C. Controller have been established for production rates of 10,000 and 100,000 units per year. To these figures our consultant has applied other factors (overhead, profit, etc) used by manufacturing companies to arrive at a selling price to an original equipment manufacturer (O.E.M.). We add 30% to cover the O.E.M. and vehicle dealer's markups to arrive at the following costs for the motor-generator (MG) set.

Quantity/Year	Consumer's Cost (MG Set Only)
10,000	$745.
100,000	$595.

The amplifiers (including rotary amplifier) and logic devices necessary for field control, the thermostatically-controlled blower system, and the contactors for connecting the MG set to the battery are estimated at $25, $25 and $5 respectively, in a quantity of 10,000 per year. In the larger quantity of 100,000, we anticipate a 20% discount or a total cost of $40. Then the total purchase price for the FRC DC Motor Controller is:

Quantity/Year	Consumer's Cost
10,000	$795.
100,000	$635.

Maintenance

The motor-generator set has been designed with double-sealed, permanmanently-lubricated bearings so no routine maintenance is required. The only maintenance anticipated for the MG set is an occasional cleaning, with compressed air, of the area around the commutators and the cooling air passages. This can be accomplished in about 1/2 hour at a cost of $8 one time each year.

The electronic circuits are sealed and will require no periodic maintenance.

Repair

Calculations have been made to determine the operating lifetime of the bearings of the MG set. Since the shaft is not connected to a mechanical load and there is no thrust, the bearings are very lightly loaded and the calculated lifetime is more than 1 million hours.

Based on statistics of the Prestolite Company, the minimum lifetime for brushes in DC motors and generators is 2,000 hours, but they usually last for 4,000 hours. Therefore we will anticipate a brush replacement in the 7th year of operation at a parts cost of $20.

It is good practice to turn the commutator on a lathe whenever the brushes are replaced. We estimate that this can be done, including the labor for replacing and seating the brushes, in one hour at a cost of $20.

Electrical insulation and wiring are rated for more than 20,000 hours, and the electronic components for far more than the required 3,500 hours, so no replacements are expected.

Salvage Value

A realistic salvage value can be established by first determining the useful lifetime of the DC Controller itself than pro-rating the

purchase price from the 3,500 hours required.

An analysis of the FRC DC Motor Controller has shown that the first major component to wear out will be the commutators. The commutators must be turned down approximately every 3,000 hours and this process can be repeated 5 to 10 times before removing too much metal. It is usually not economical to rebuild the armature to replace the commutator so the machine can be considered scrap at that time. Using a figure of 7 commutator turnings, the useful life of the FRC DC Motor Controller is 21,000 hours. This is 6 times the life of the vehicle so it could be used in other vehicles or in other applications for many more years. Therefore its salvage value should be at least 50% of the purchase price.

Energy Burden

The cost associated with moving the weight of the Controller is calculated from typical figures for existing electric vehicles. Assuming a vehicle gross weight of 1588 kg (3500 lbs.) with an energy consumption of 0.31 kwh/km (0.50 kwh/mile), 0.000195 kwh/km (0.000143 kwh/mile) is required to move each kilogram (pound). The Franklin DC Motor Controller weighs approximately 63.50 kg (140 lbs.) so the rate of consumption is 0.0124 kwh/km (0.0200 kwh/mi.). At 16,400 km (10,200 mi.) per year, the energy consumed is 203 kwh. With an energy cost of 5¢ per kwh, the annual cost is $10.17.

Warranty

The costs associated with a warranty on equipment of this type are 3 to 5% of the total sale price. Since they are costs incurred by the manufacturer, they are included in the purchase price to the vehicle owner.

Cost Analysis

A summary of life cycle costs is shown in Figure 35 for an assumed production rate of 100,000 units per year. For a rate of 10,000 units per year, the Total Lifetime Cost is $615.70 which amounts to 0.00375 per kilometer and $0.0060 per mile.

SUMMARY

The design of the Engineering Model dc motor controller has been completed. The results of the analog computer simulation demonstrate the potential of the controller to meet all requirements imposed. This unique approach to controlling a dc voltage with rotating machines yields distinct advantages over "chopper" type controllers. The arrangement of the drive motor and generator combined with an effective control

strategy make the controller extremely competitive. Advantages of the FRC advanced dc motor controller are addressed below.

- Optimum Voltage Levels - Bi-directional generator permits the use of a high-voltage motor with a low voltage battery.

- Dependable - The controller is constructed using rotating electric machines which are proven to be rugged and reliable.

- Low Life Cycle Cost - Due to long life expectancy and minimal maintenance requirements, the life cycle cost is estimated to be $0.0033/km ($0.0052/mile).

- Available Service - Widespread auto repair stations and electric motor repair shops possess the necessary technical skills for service.

- Overload Tolerance - FRC controller can withstand high overload currents for short periods of time.

- Regeneration - Energy regeneration is inherent in this controller down to zero speed.

- Smooth Control - Speed control of the traction motor is infinitely variable over full range.

- Negligible EMI - Electromagnetic interference is negligible because smooth dc currents are drawn from the battery.

- Good System Efficiency - According to References 2 and 3, traction motor efficiency is 5 to 10 percent higher when controlled by smooth dc voltage as compared to electronic chopper controlled voltage. Smooth dc currents are also expected to result in longer battery life.

RECOMMENDATIONS

The Engineering Model Controller is designed to be a rugged, compact and practical unit compatible with the operating environment of electric vehicles. Although the services of a manufacturing design consultant were employed producibility problems and brush drag losses can only be firmly established by building the controller.

REFERENCES

1. Fink, Donald G., ed. Standard Handbook for Electrical Engineers, Eleventh Edition, McGraw Hill Book Company 1978, pg 20-90.

2. Schwab, John R., NASA-Lewis Research Center, "Performance of a 22.4 kW Nonlaminated-Frame dc Series Motor with Chopper Controller", DOE/NASA/1044-79/4, NASA TM-79252, Sept. 1979.

3. Schwab, John R., NASA-Lewis Research Center, "Performance of a 14.9 kW Laminated-Frame dc Series Motor with Chopper Controller", DOE/NASA/1044-79-2, NASA TM-79177, June 1979.

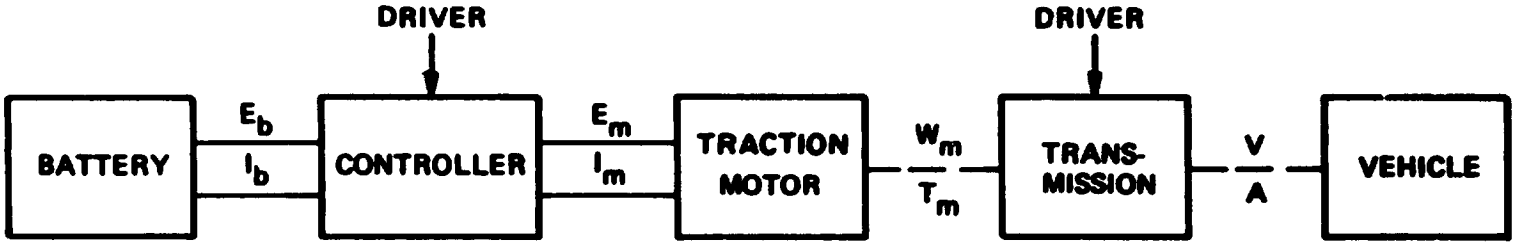

Figure 1. A Typical Electric Vehicle Propulsion System

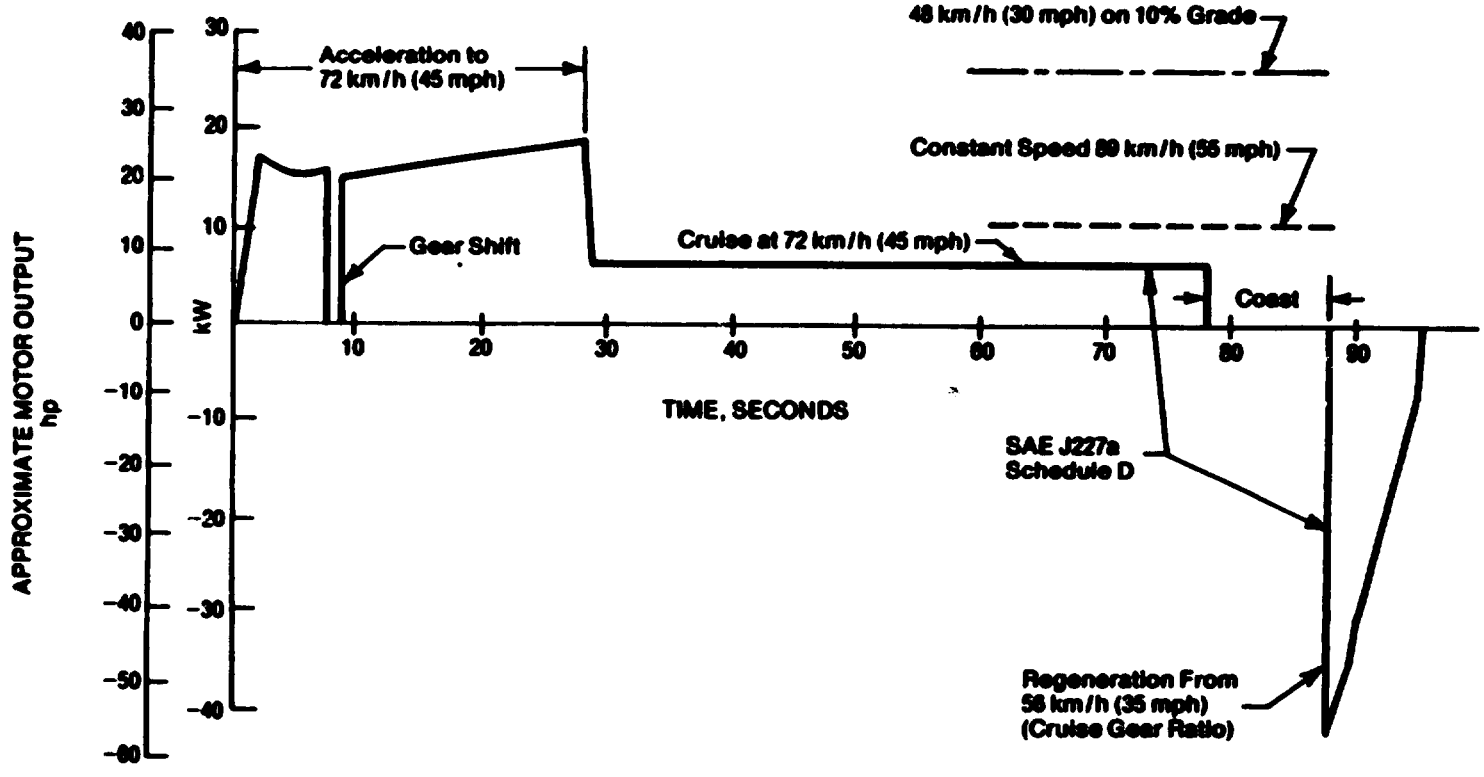

Figure 2. SAE J227a/D Power Profile

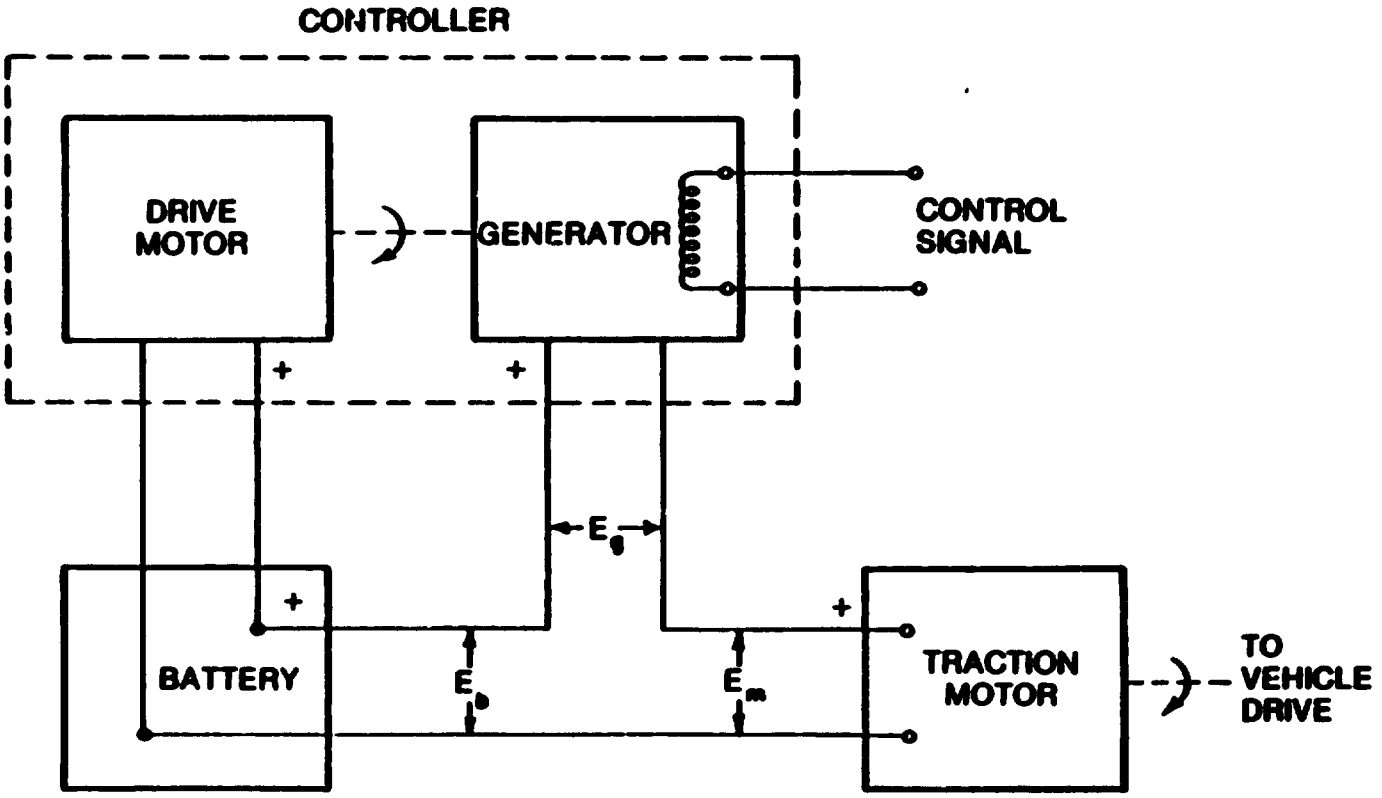

Figure 3. Advanced DC Motor Controller Block Diagram

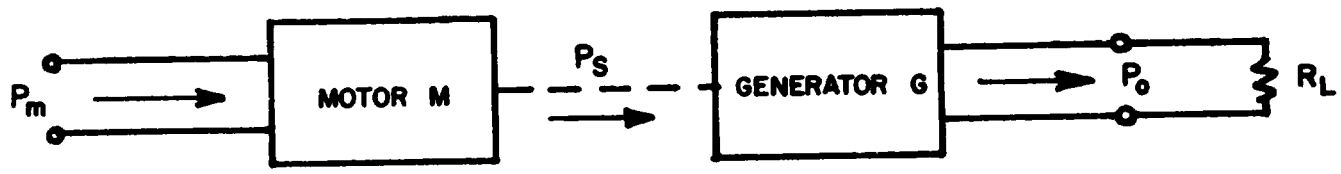

Figure 4. Ward Leonard System Power Transfer

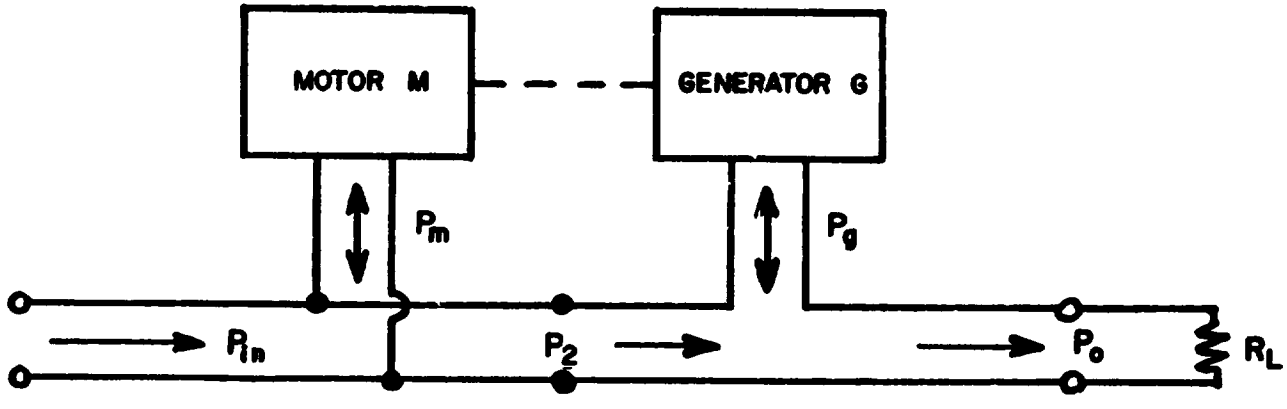

Figure 5. Franklin MG System Power Transfer

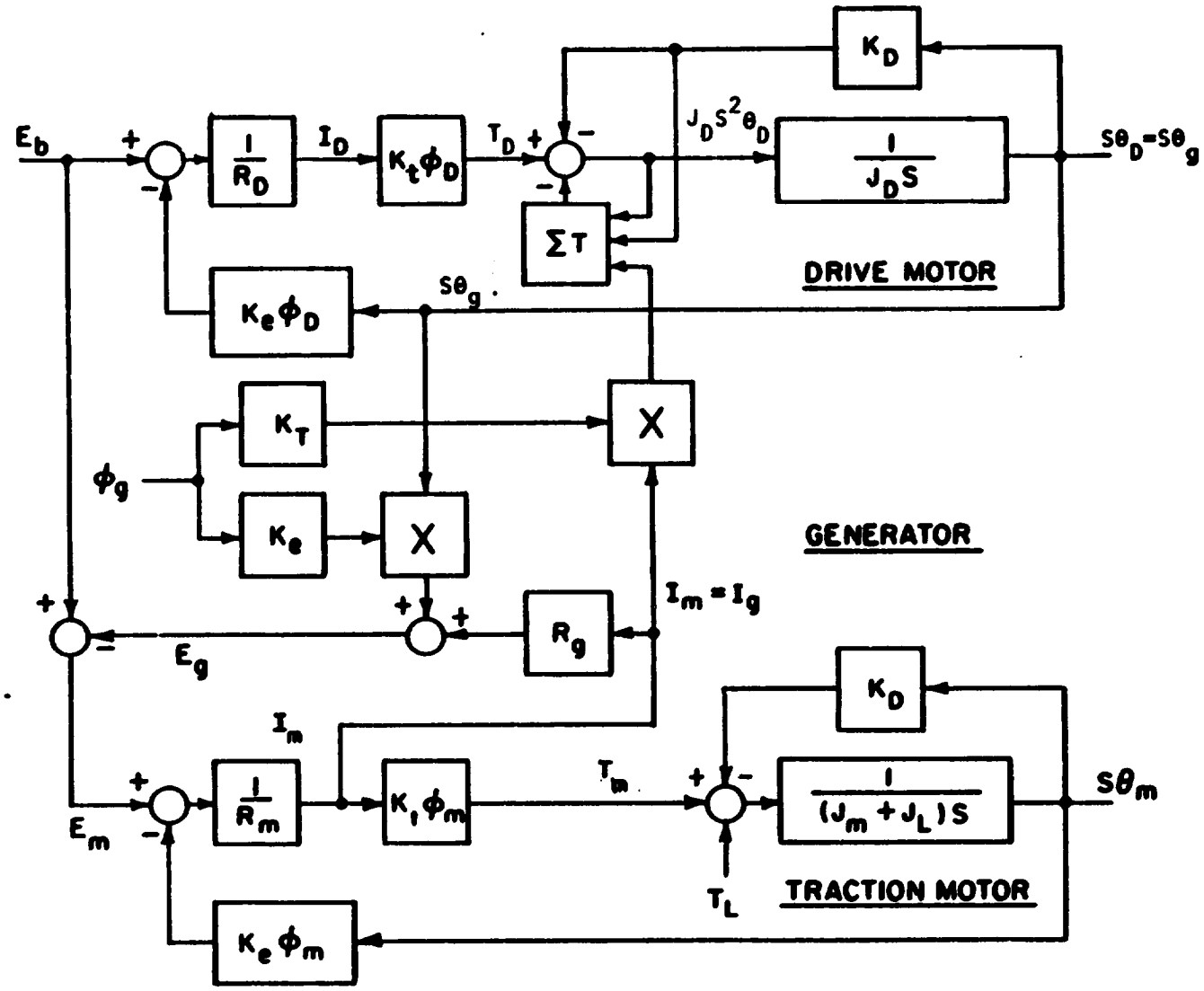

Figure 6. DC Controller Simulation Block Diagram

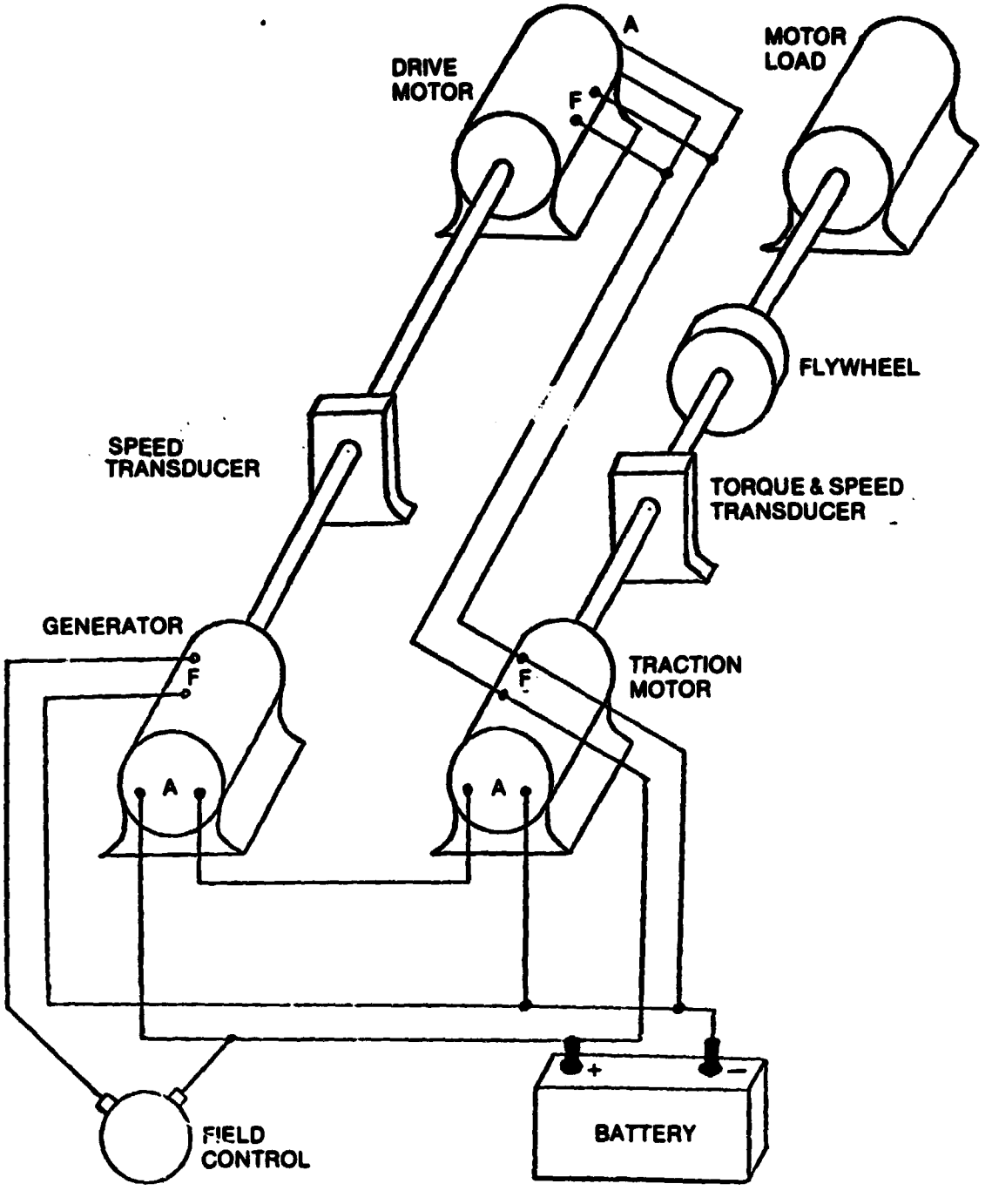

Figure 7. Sketch of Proof-of-Principle System

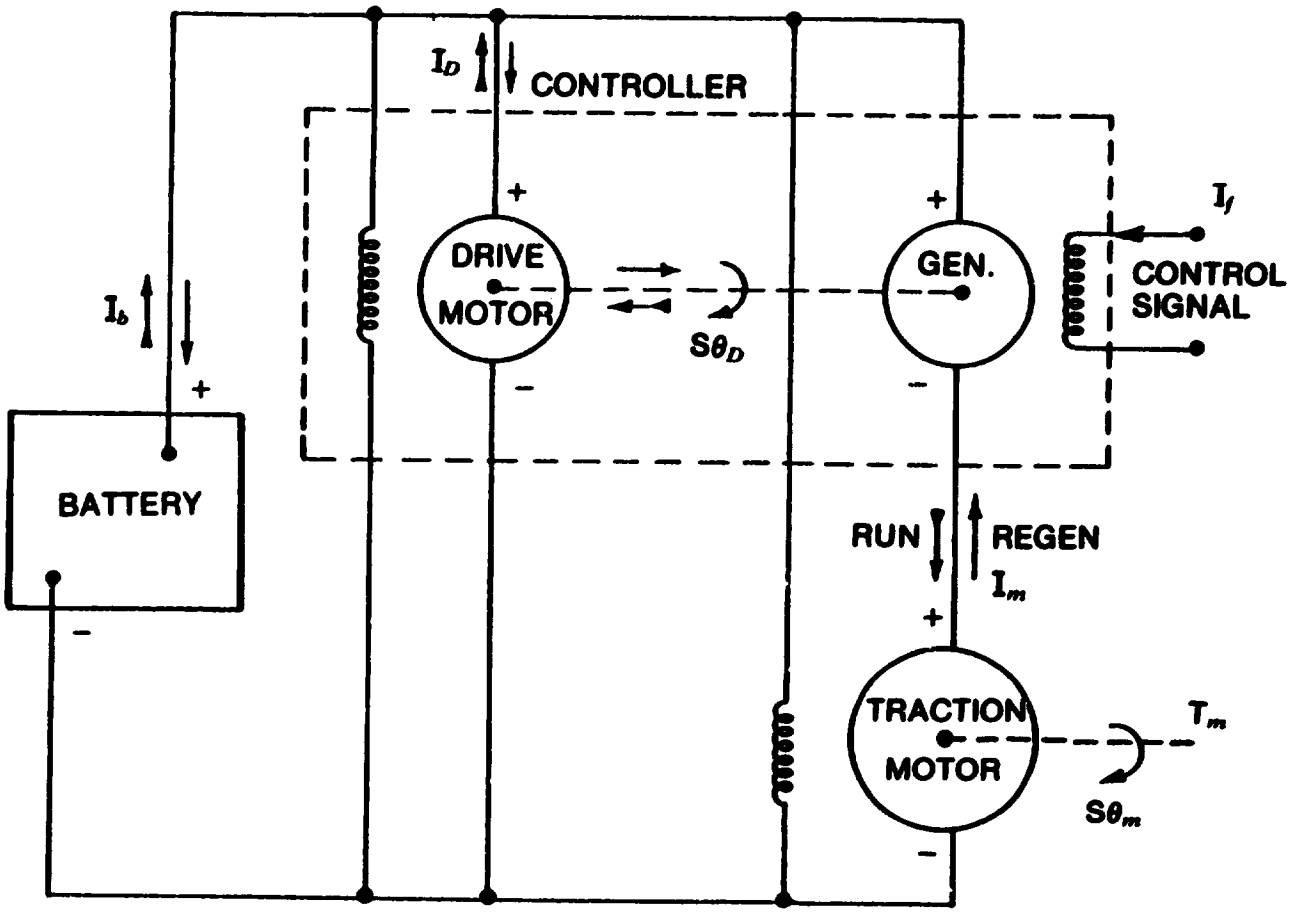

Figure 8. Advanced DC Motor Controller Circuit Schematic Diagram

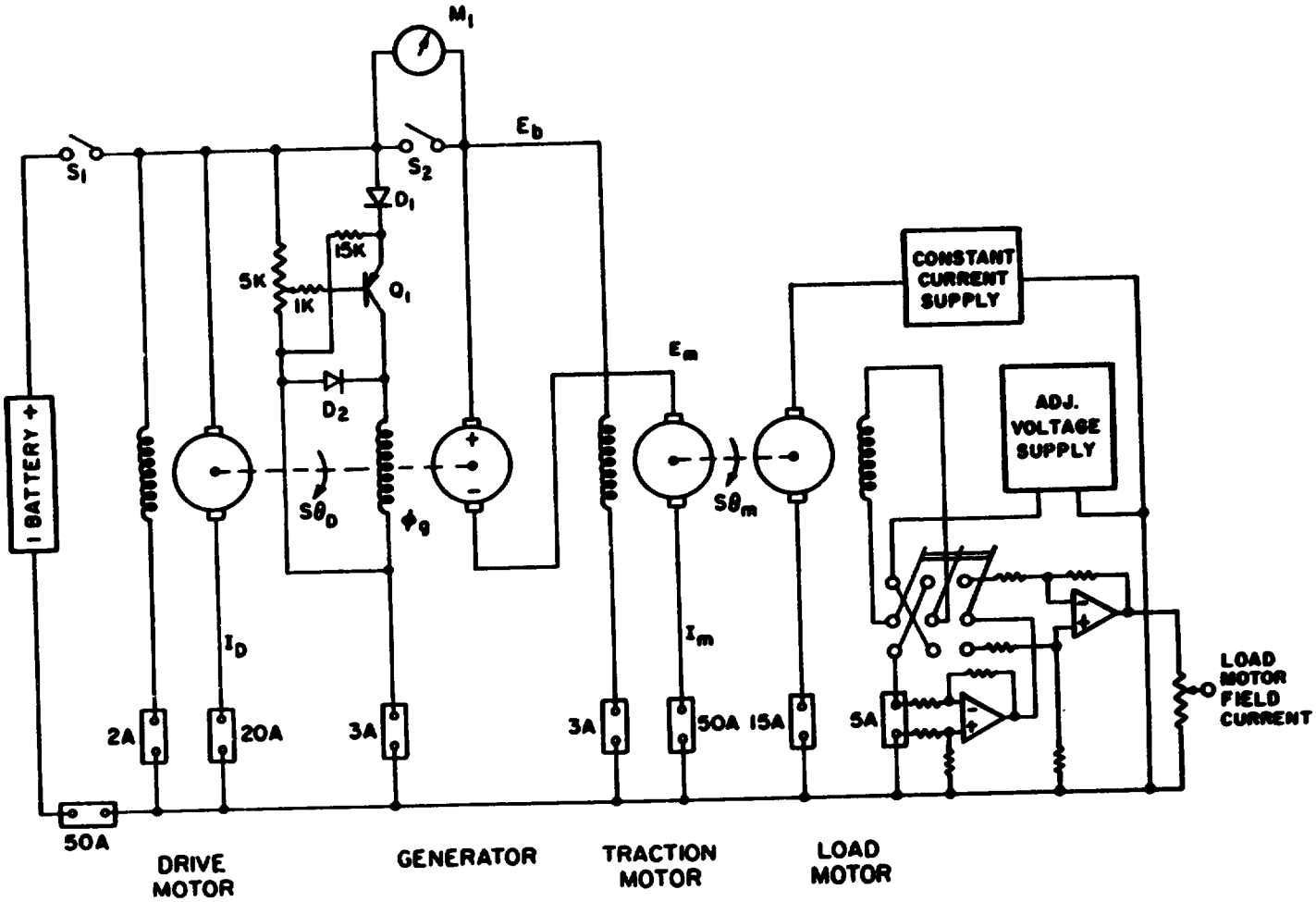

Figure 9. Proof-of-Principle Electrical System Schematic Diagram

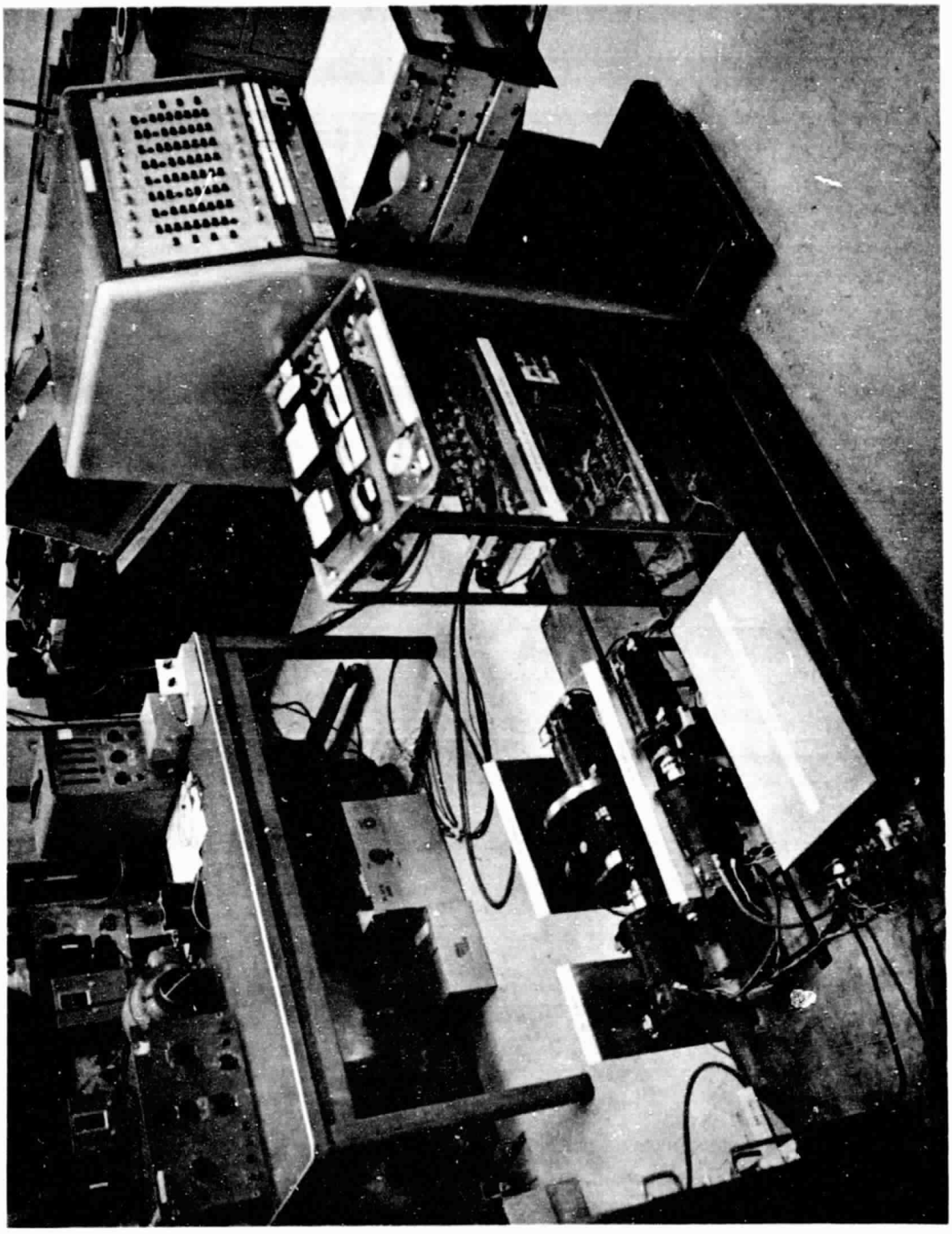

Figure 10. Photograph of Proof-of-Principle Demonstration System

ORIGINAL PAGE IS
OF POOR QUALITY

Figure 11. Closeup of Control Panel

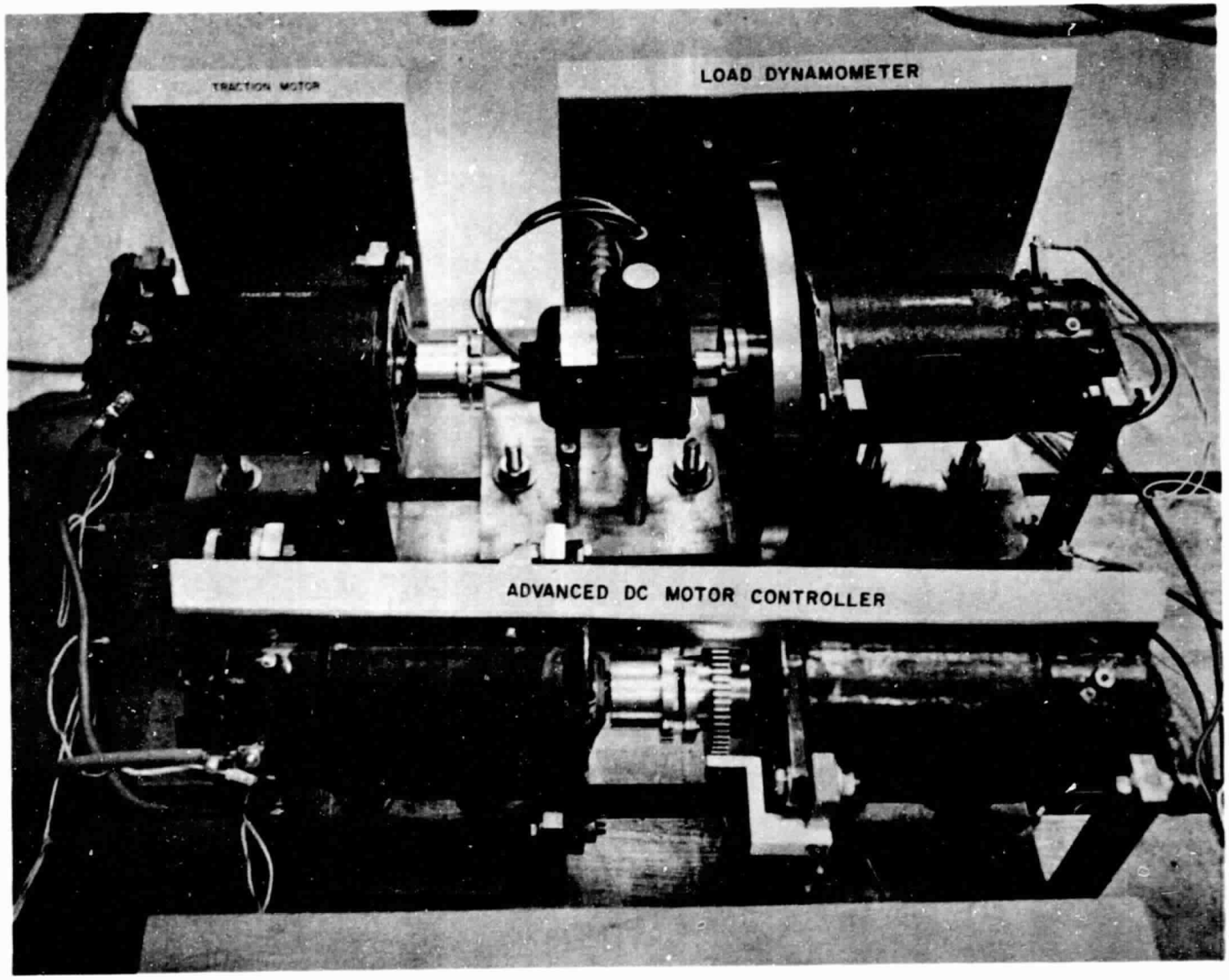

Figure 12. Closeup of Proof-of-Principle Machines

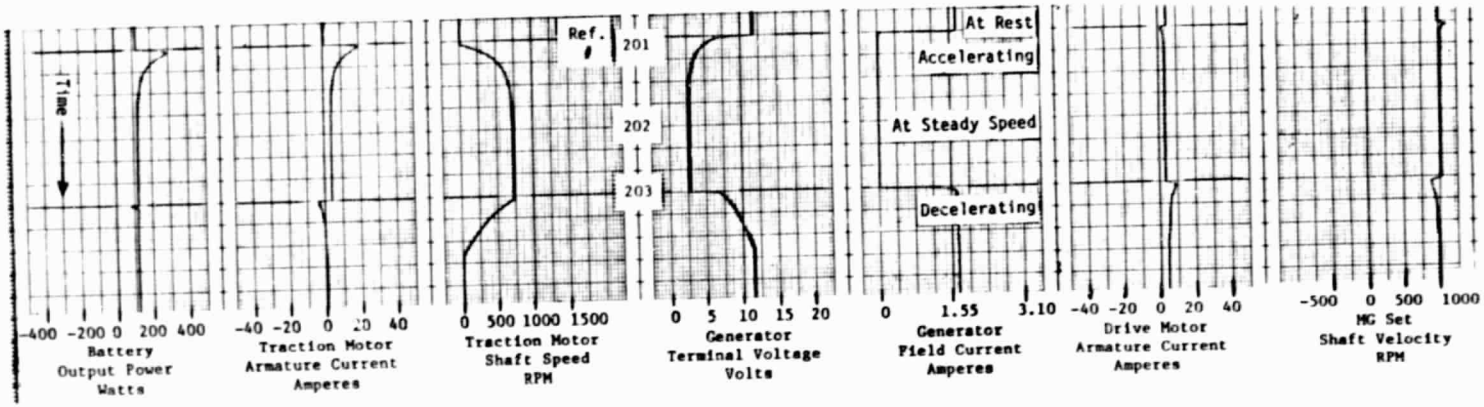

Figure 13. Typical Proof-of-Principle Test Results - Acceleration and Deceleration on a Level Grade

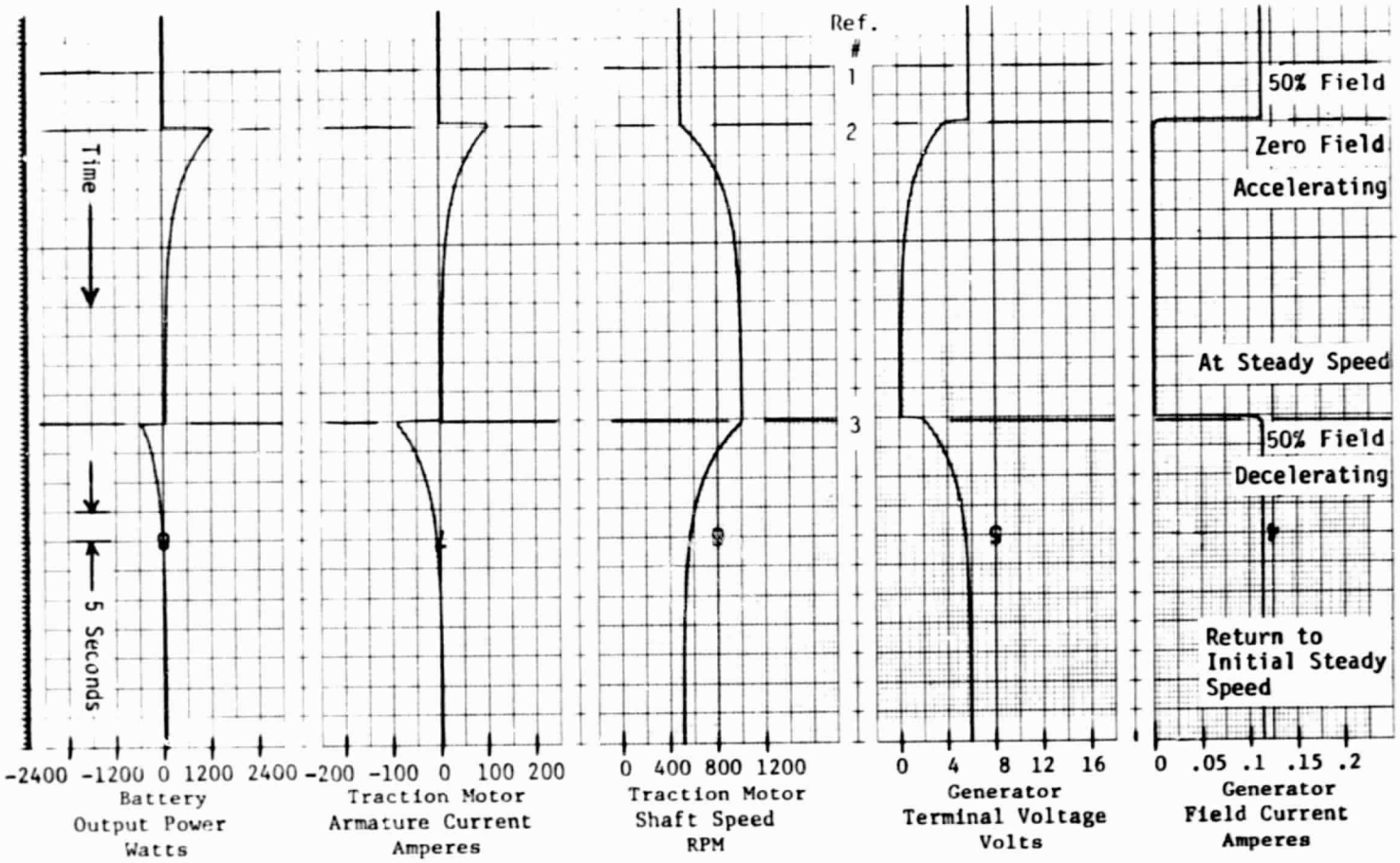

Figure 14. Simulation of Transient Response of Controller with 50% Generator Field

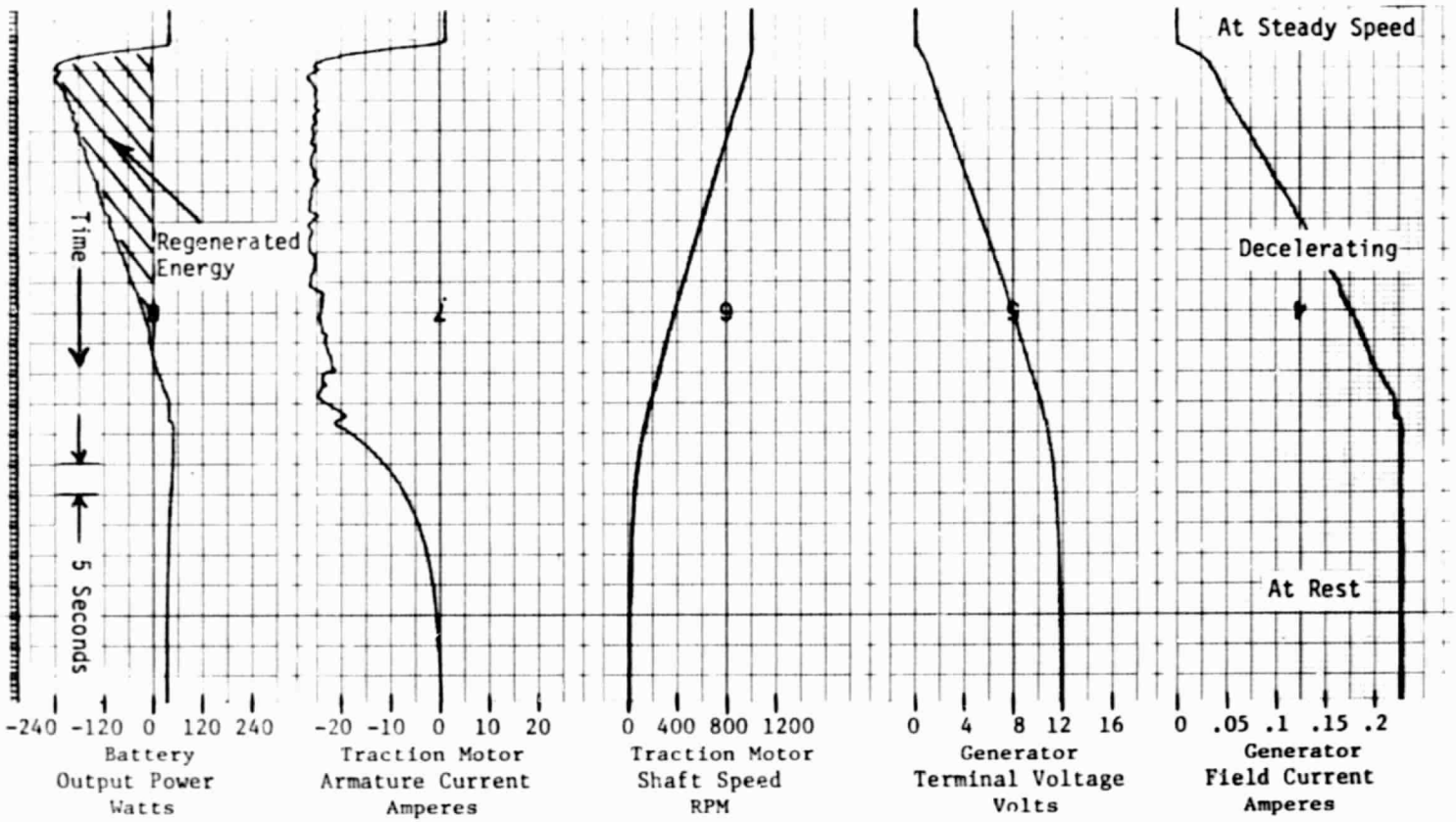

Figure 15. Simulated Performance with Constant Traction Motor Current During Deceleration

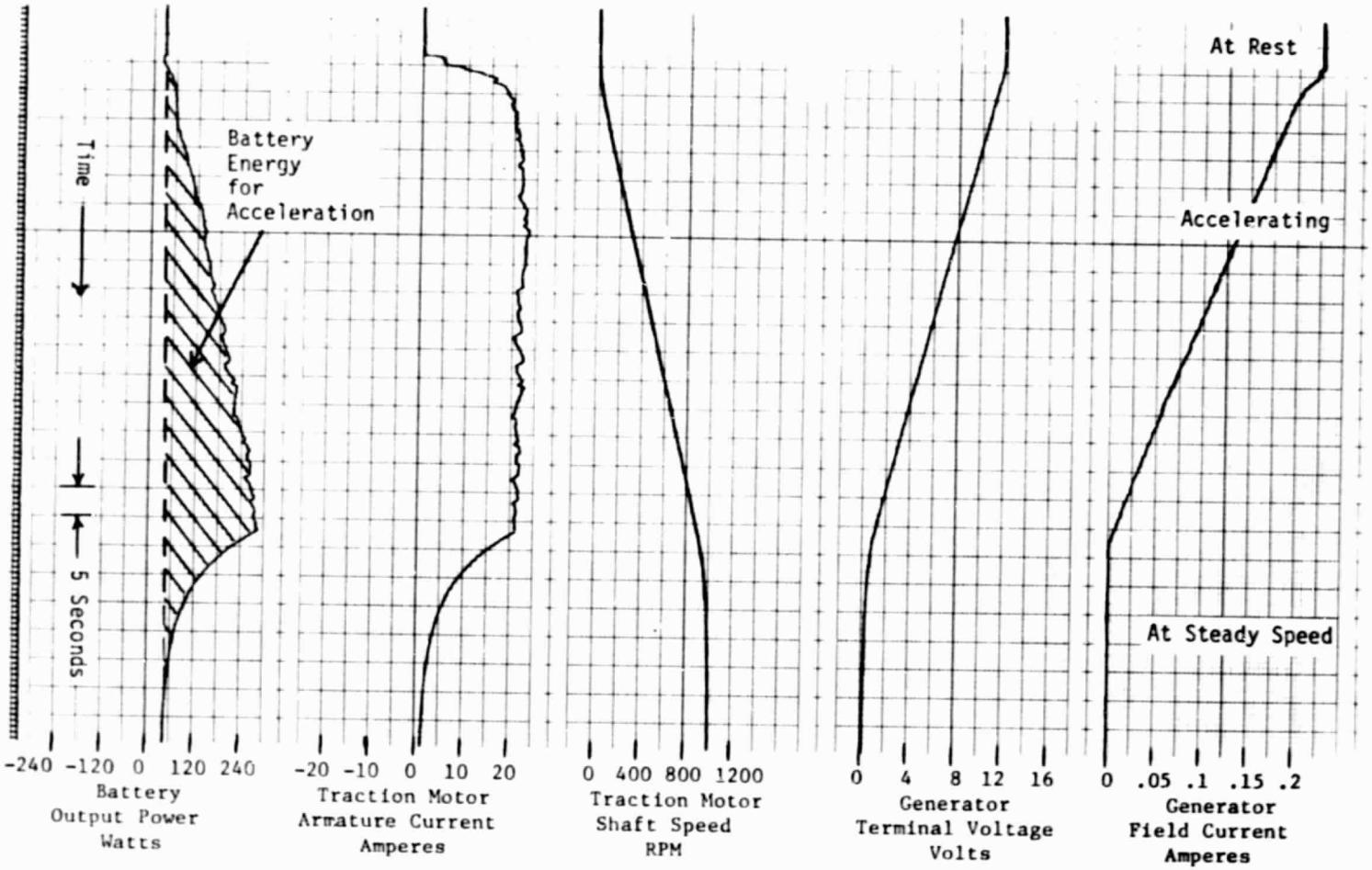

Figure 16. Simulated Performance with Constant Traction Motor Armature Current During Acceleration.

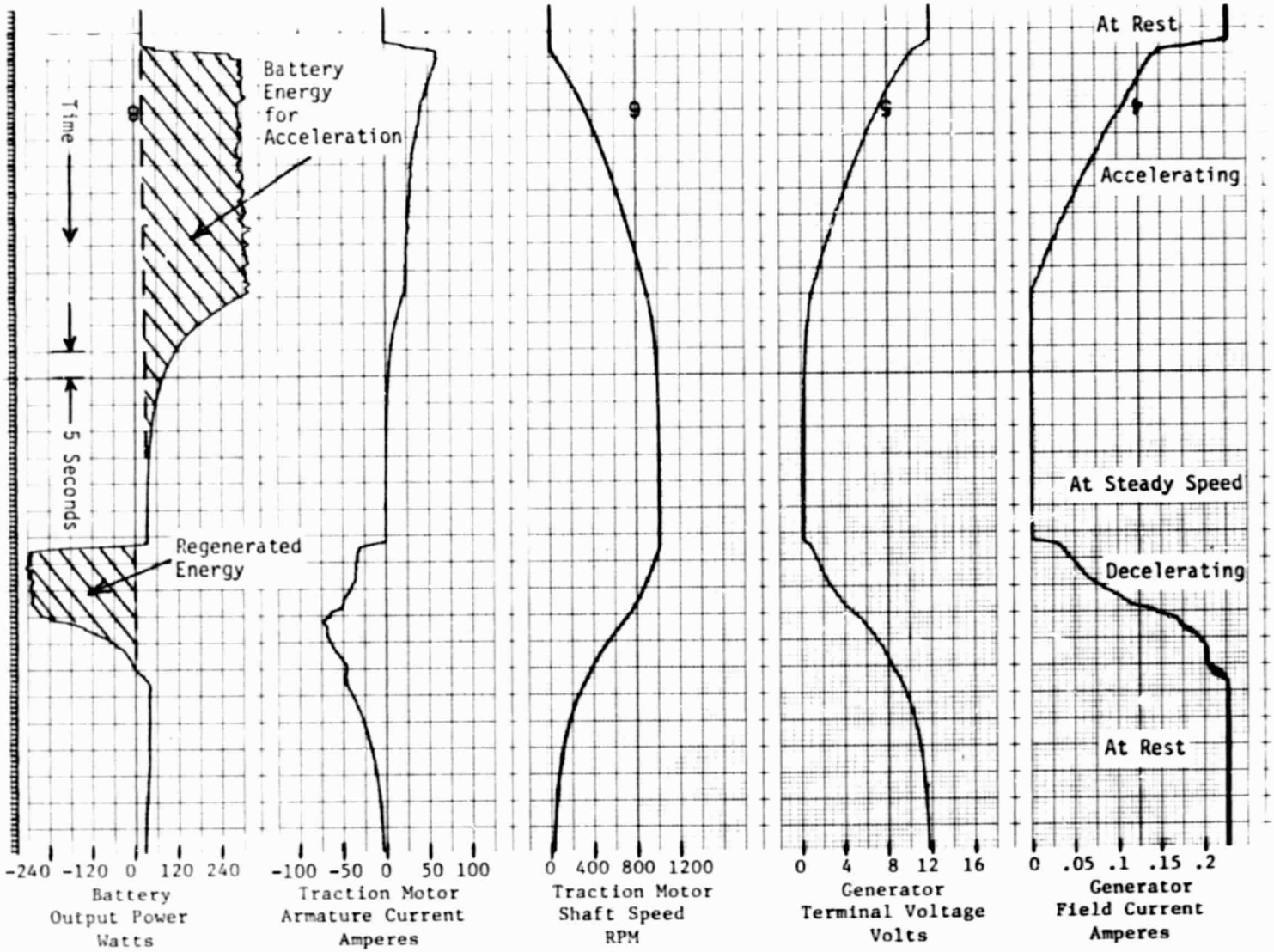

Figure 17. Simulated Performance with Constant Battery Power Control

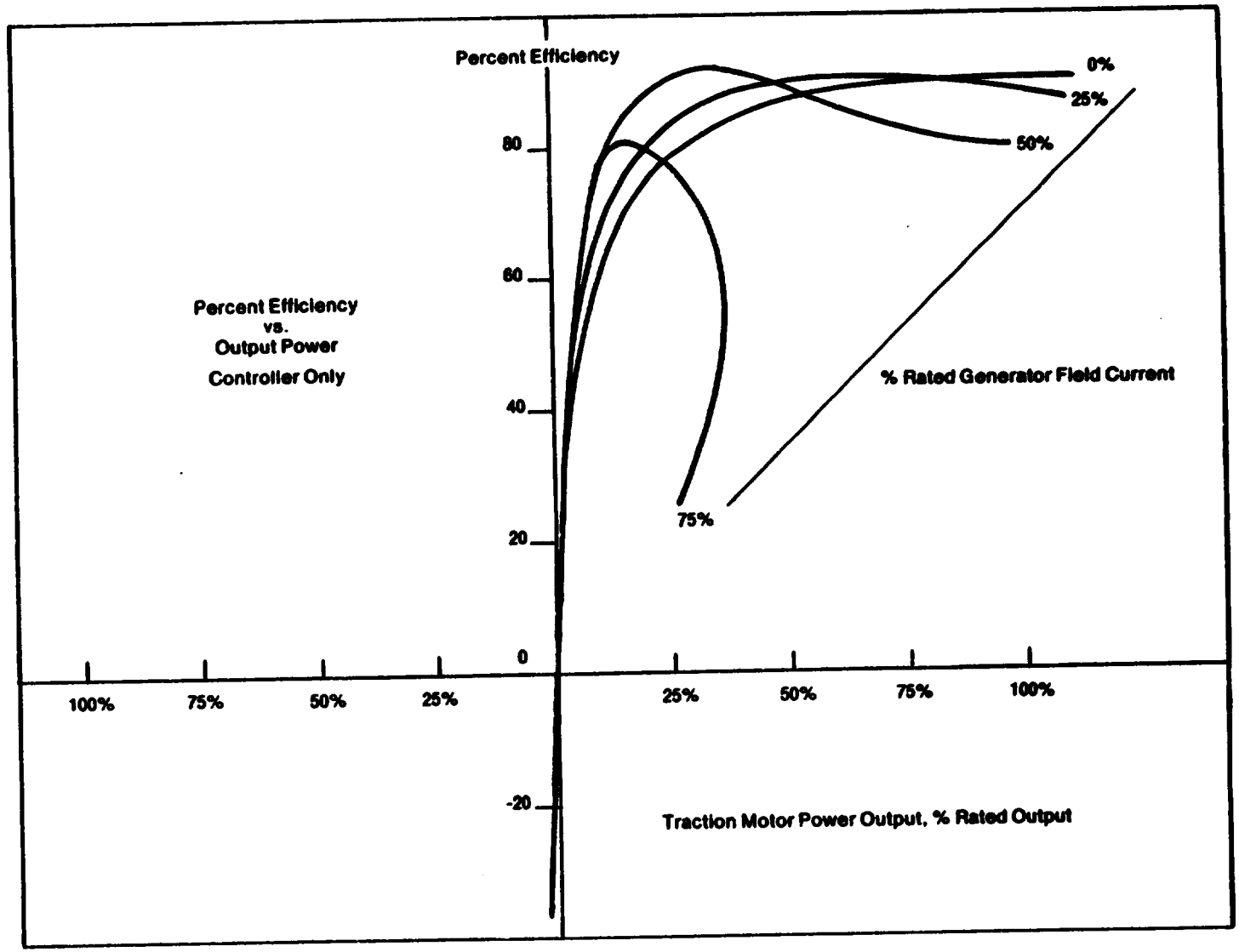

Figure 18. Computed Efficiency of the Functional Model Controller with Various Field Currents

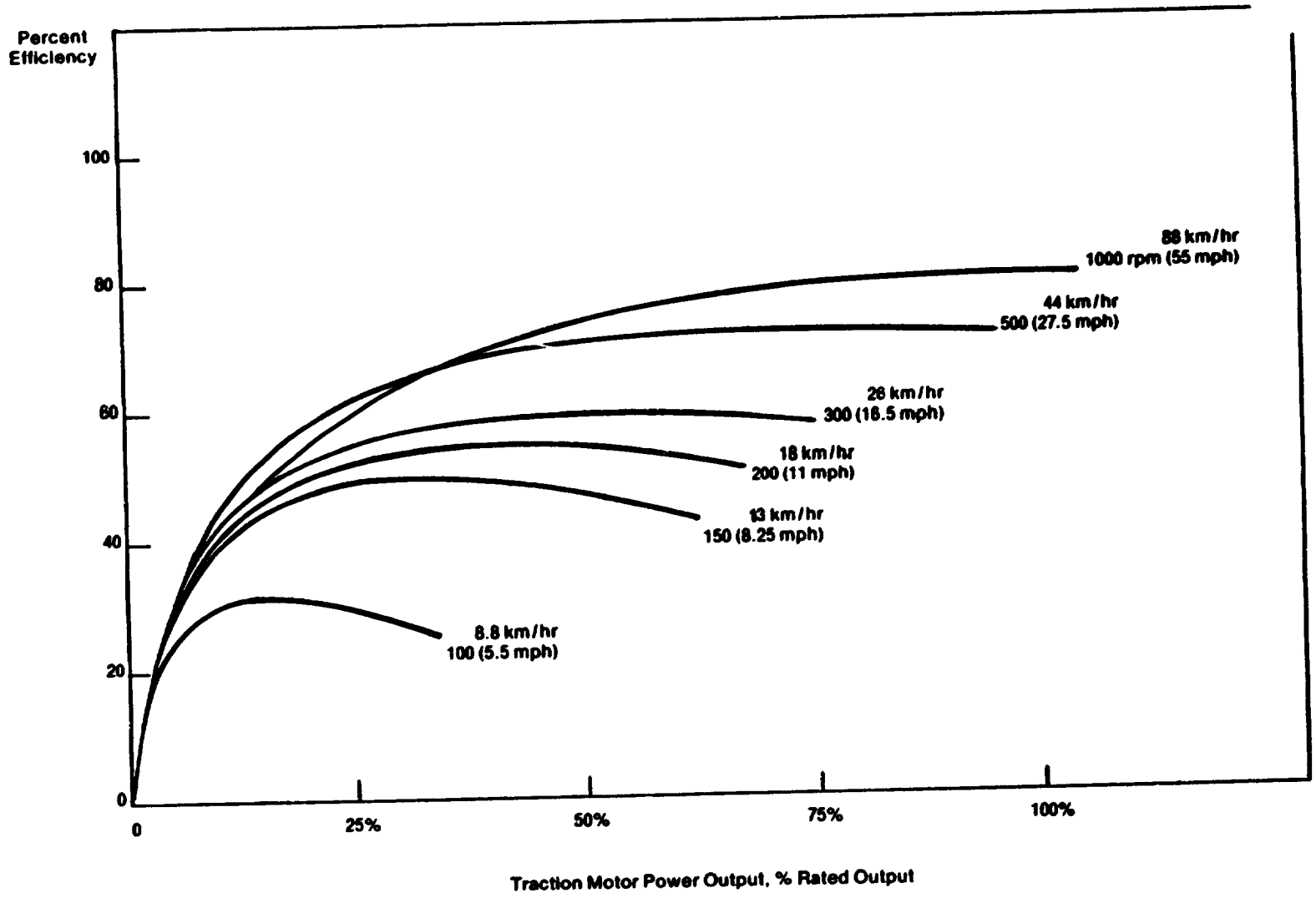

Figure 19. Predicted Efficiency of Vehicle Using Functional Model Controller

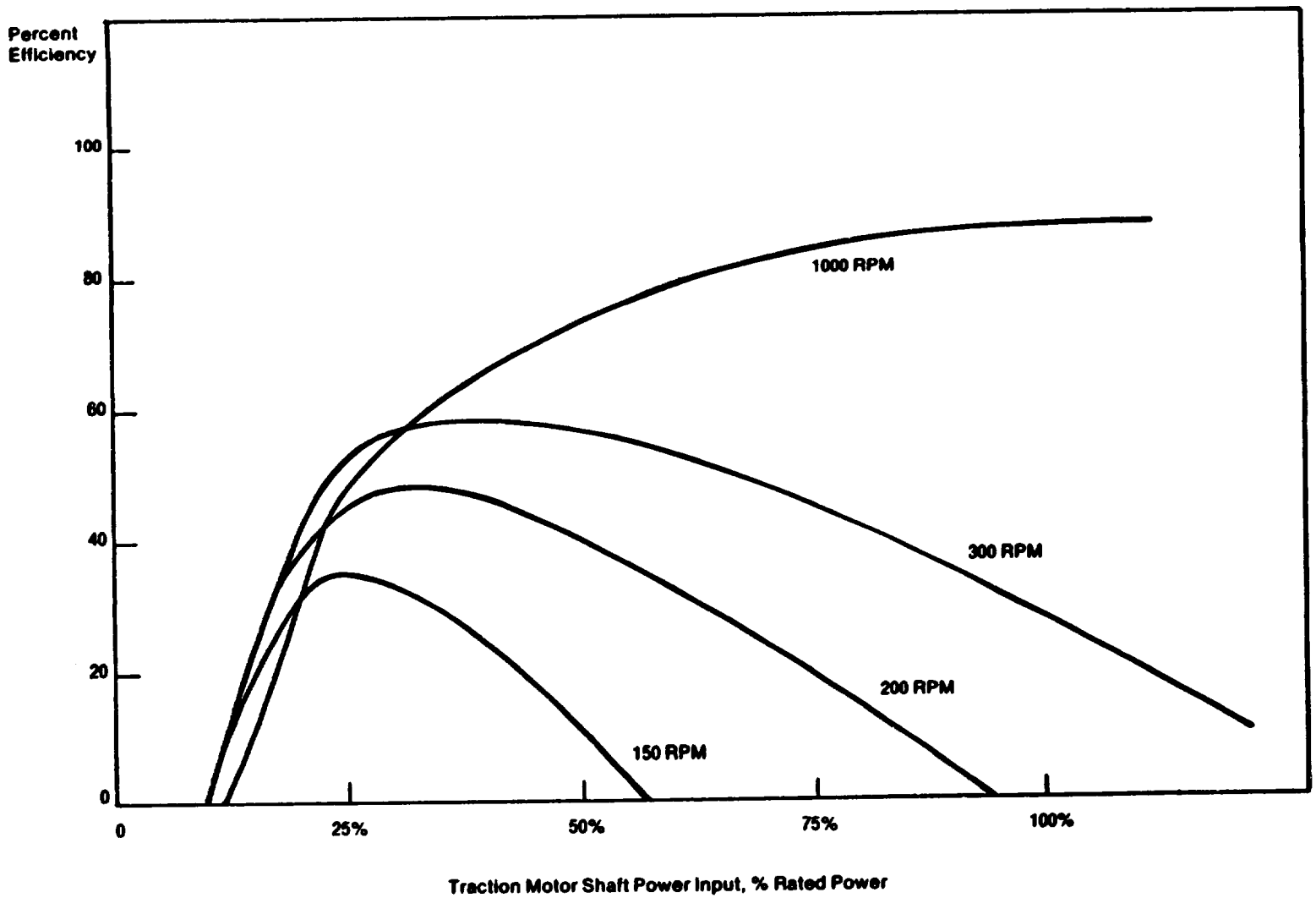

Figure 20. Predicted Efficiency of Vehicle in Regenerative Braking Mode

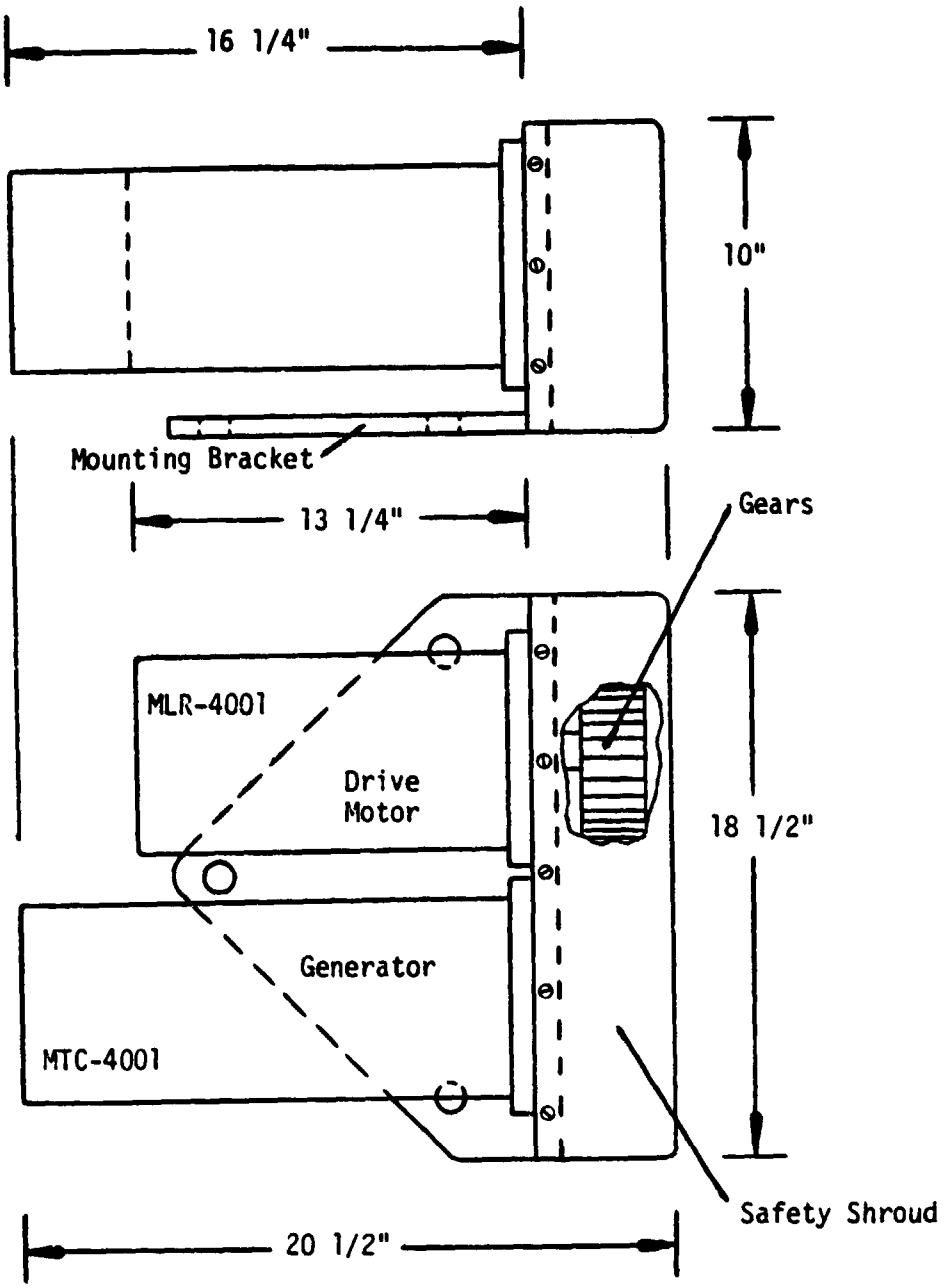

Figure 21. Arrangement for the MG Set for the Functional Model DC Motor Controller

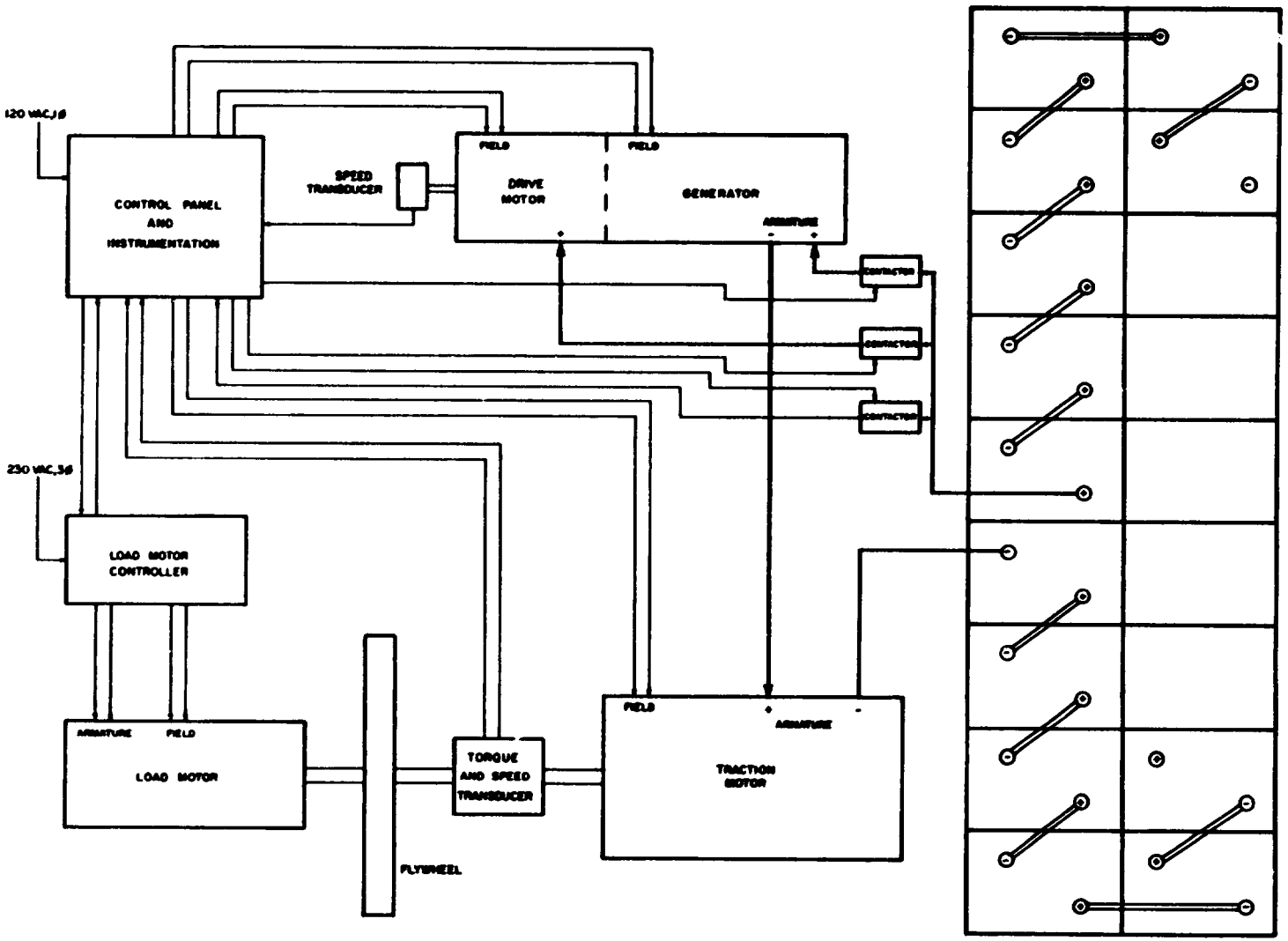

Figure 22. Electrical Schematic of the Functional Model in Test Facility.

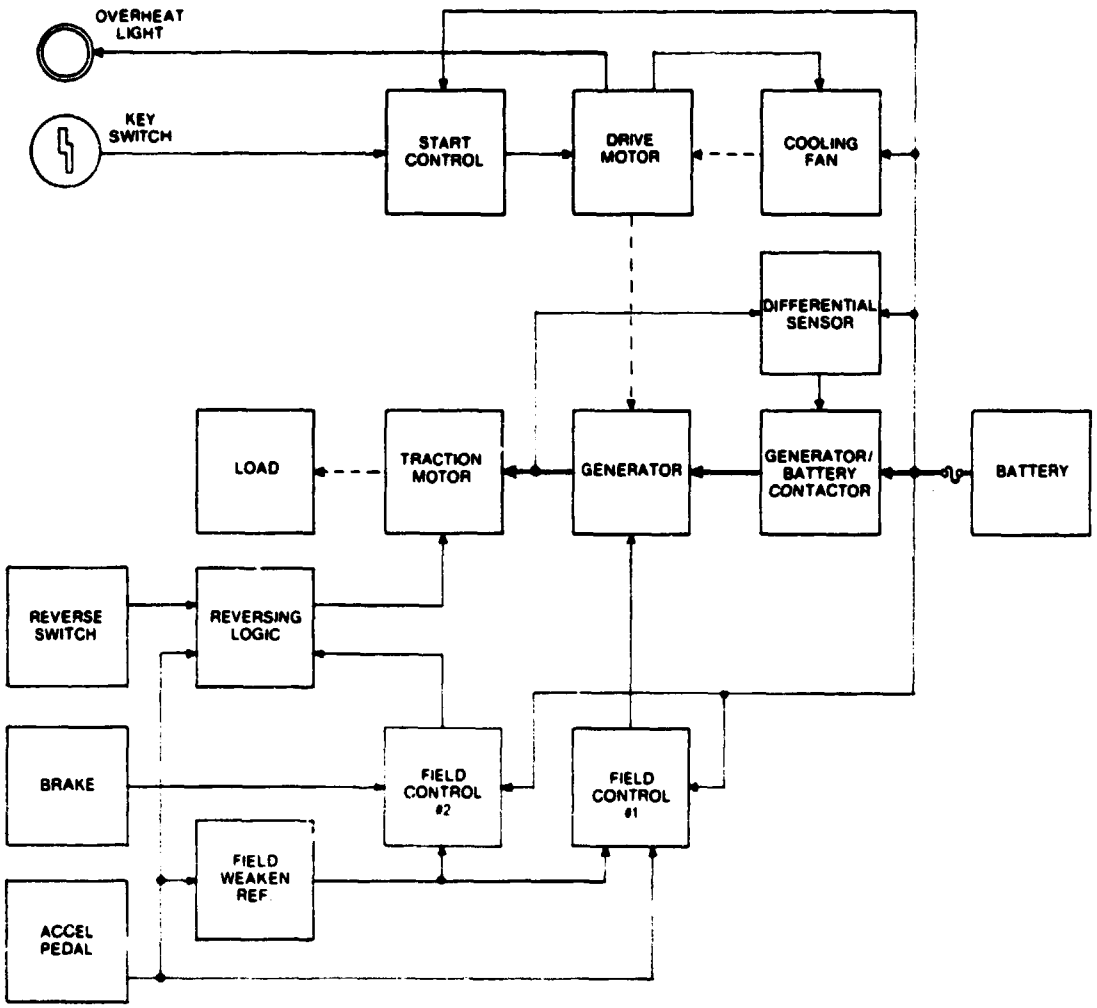

Figure 23. DC Controller Block Diagram

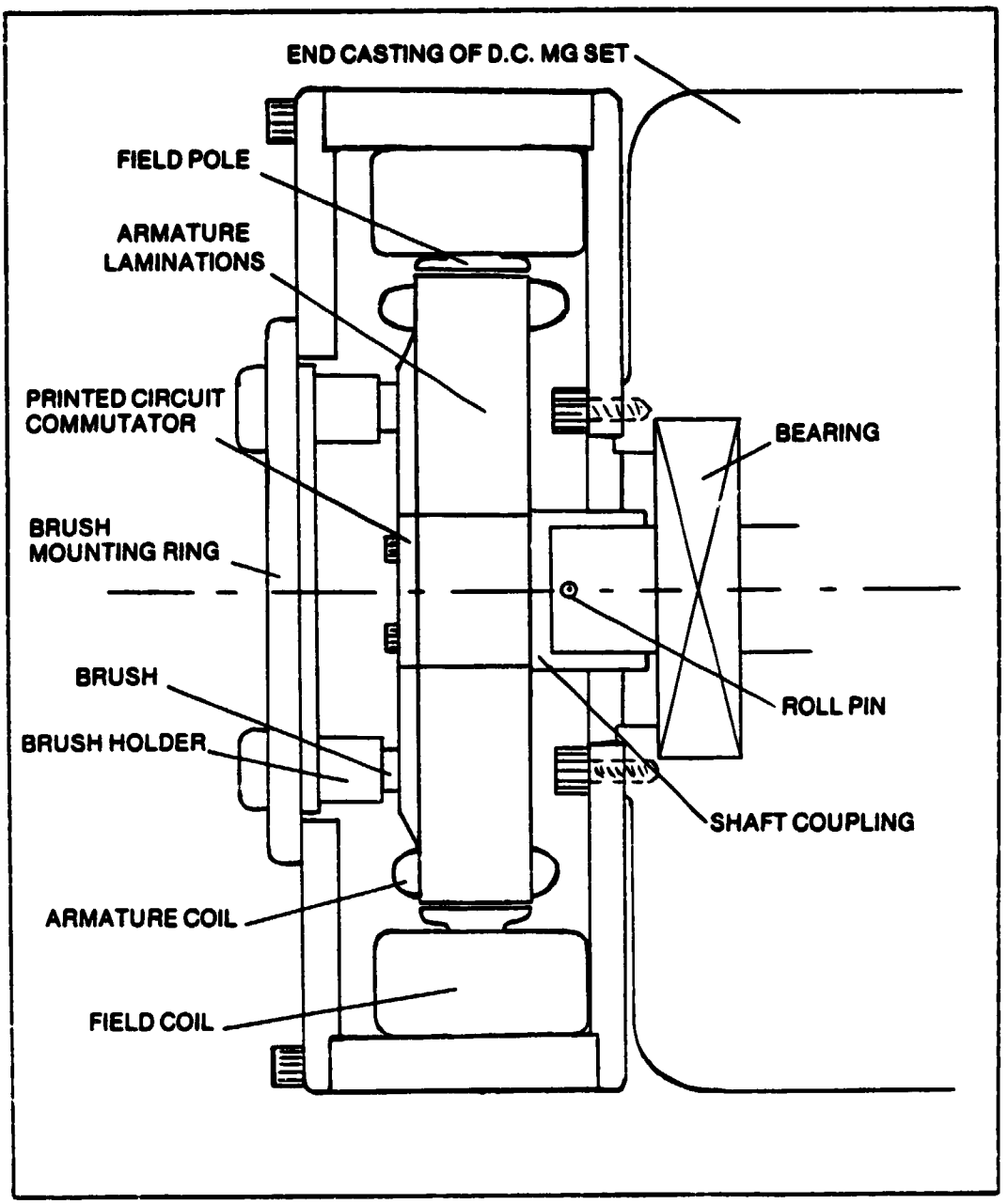

Figure 24. Conceptual Sketch of Rotary Amplifier

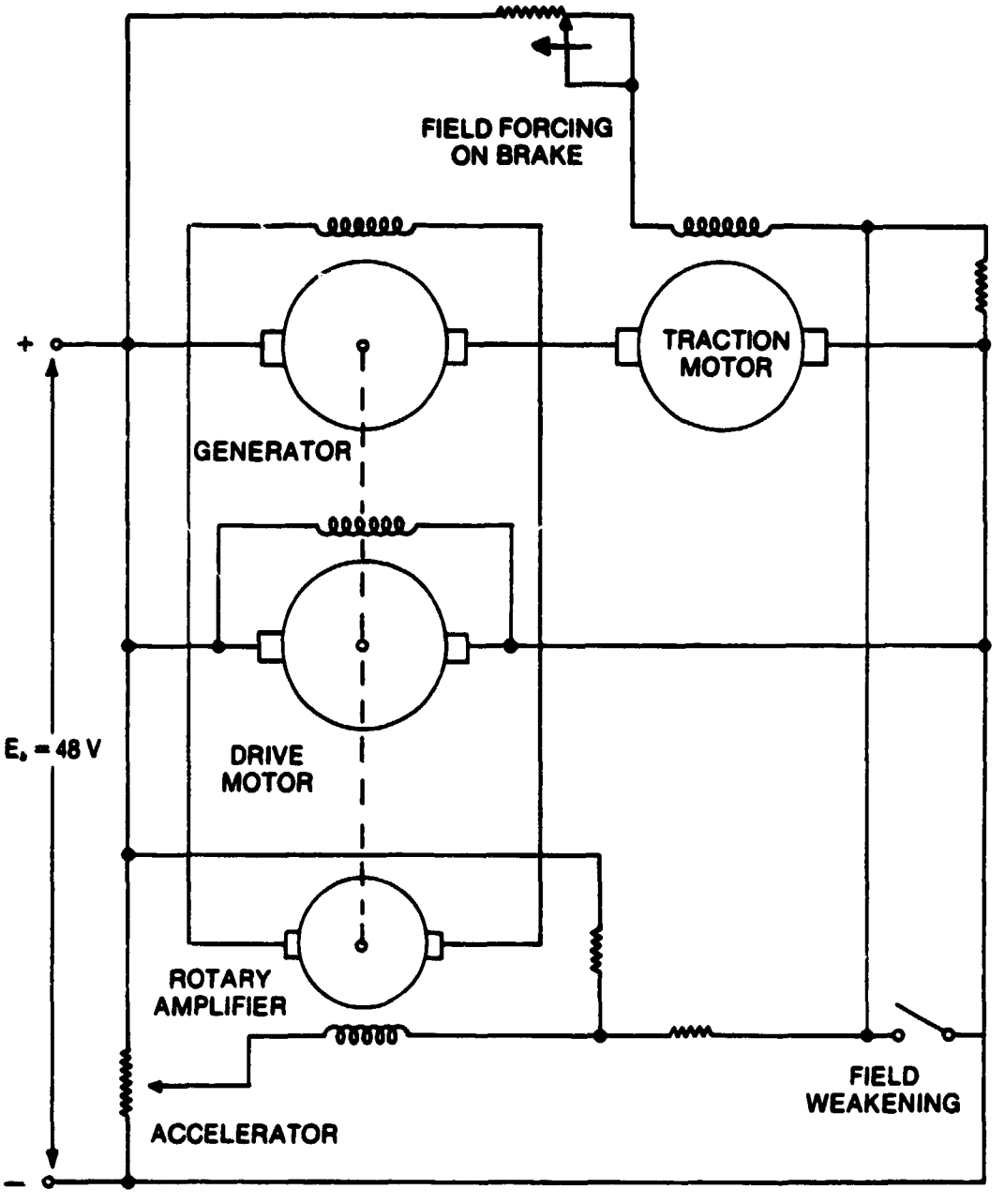

Figure 25. Schematic of Rotary Amplifier Field Control

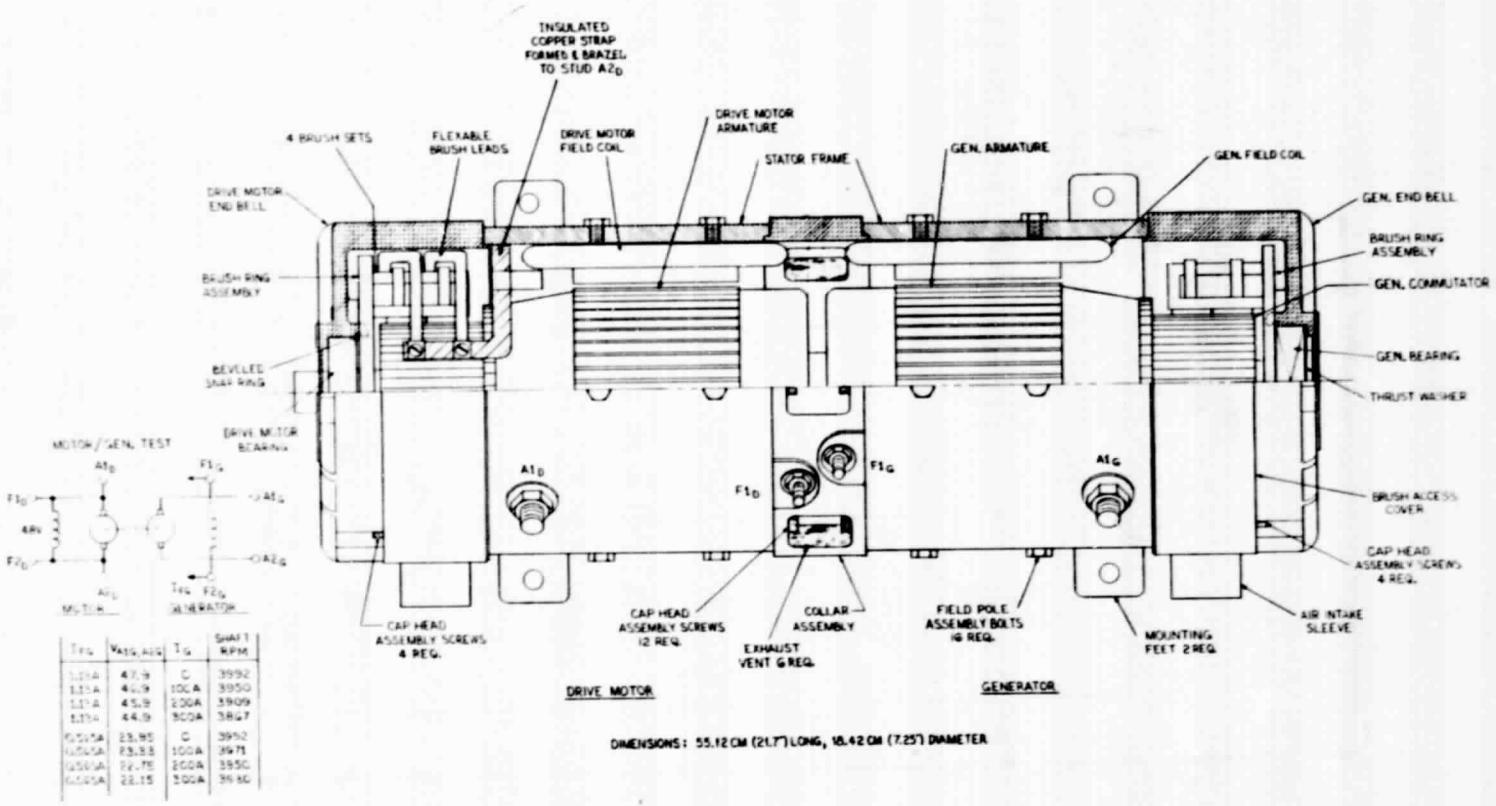

I_{FG}	$V_{AG,AVG}$	I_G	SHAFT RPM
1.13A	47.9	C	3992
1.13A	46.9	100A	3950
1.13A	45.9	200A	3909
1.13A	44.9	300A	3867
0.565A	23.95	C	3952
0.565A	23.33	100A	3971
0.565A	22.75	200A	3950
0.565A	22.15	300A	3930

Figure 26. Assembly Drawing of Engineering Model Advanced Motor-Generator Set

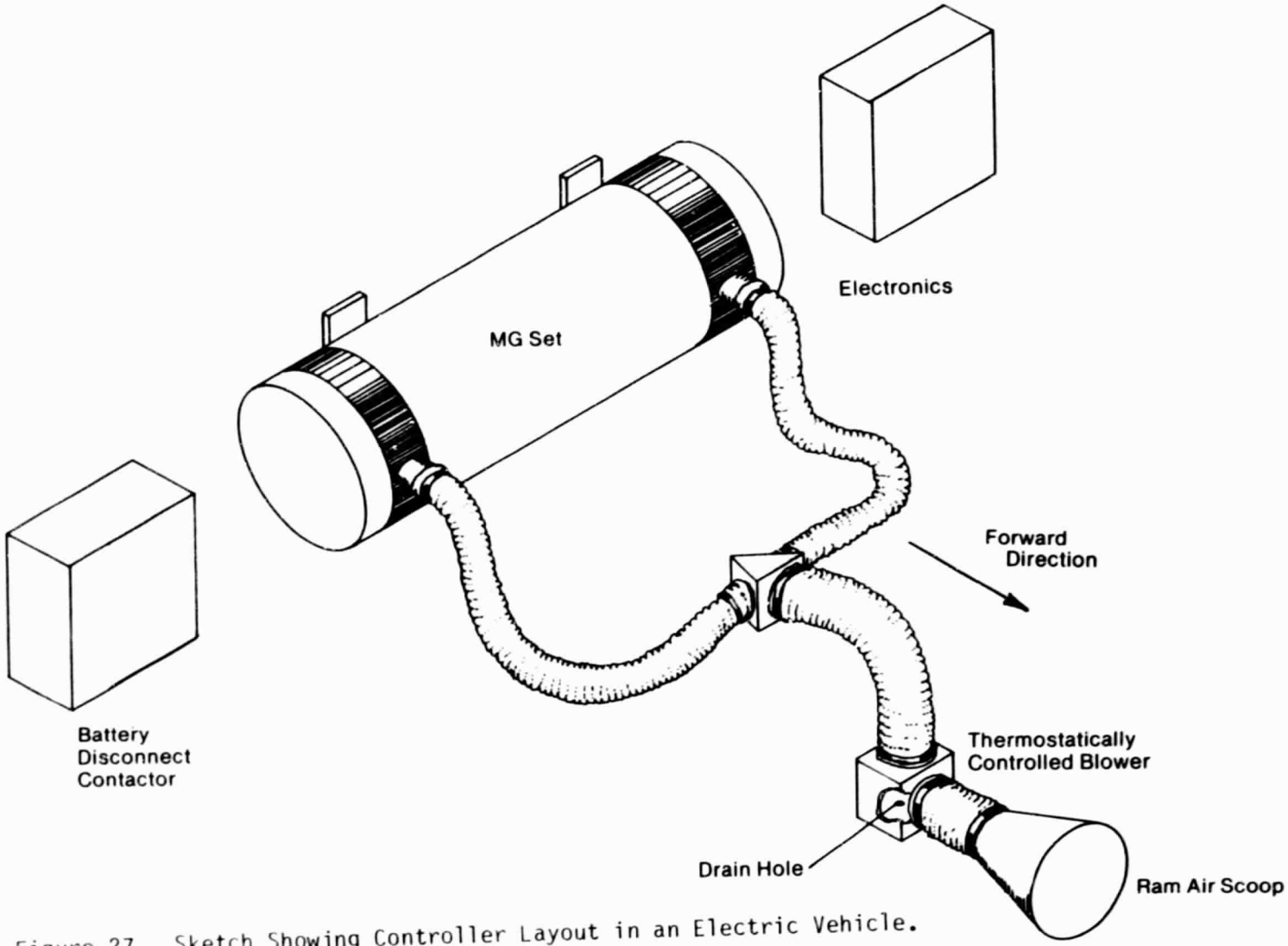

Figure 27. Sketch Showing Controller Layout in an Electric Vehicle.

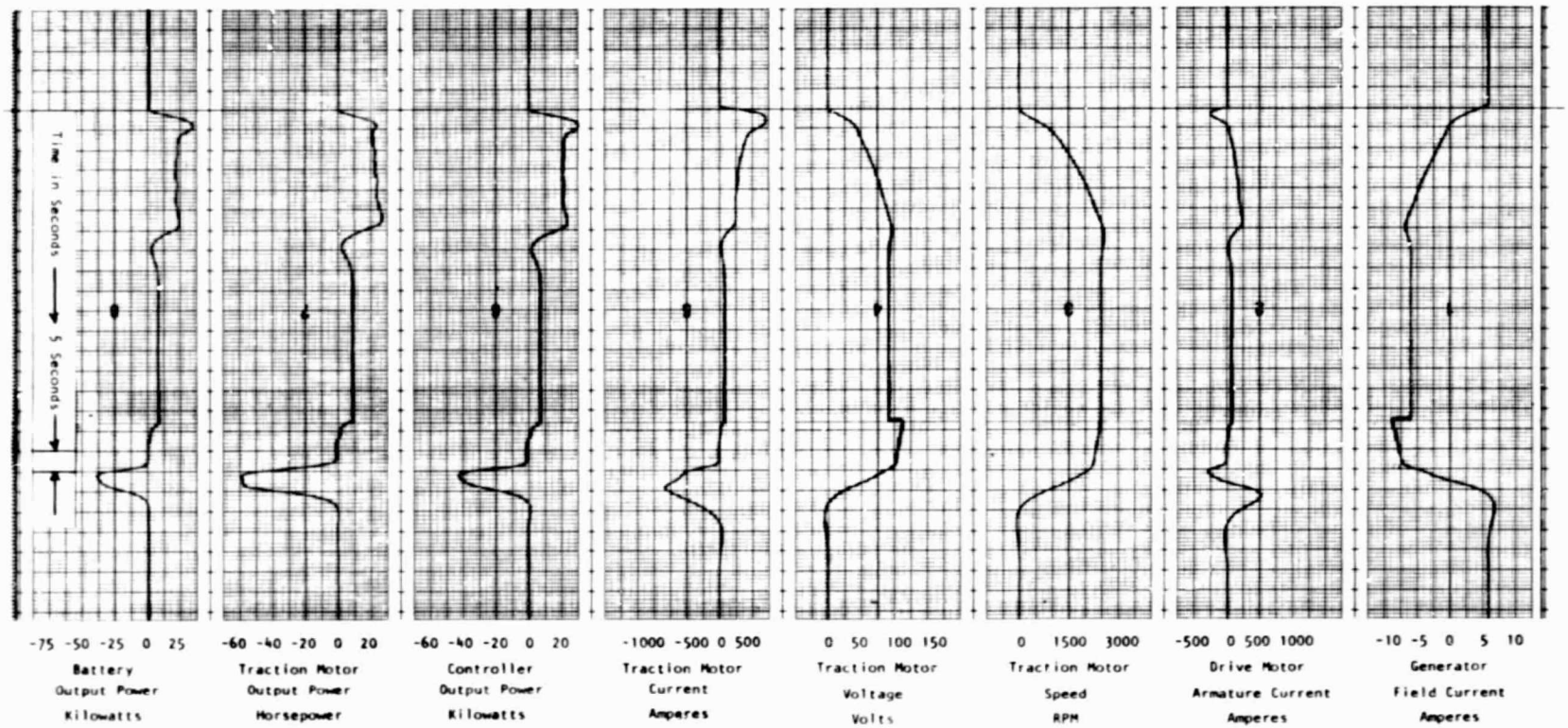

Figure 28. Simulated Engineering Model Performance During SAE Profile

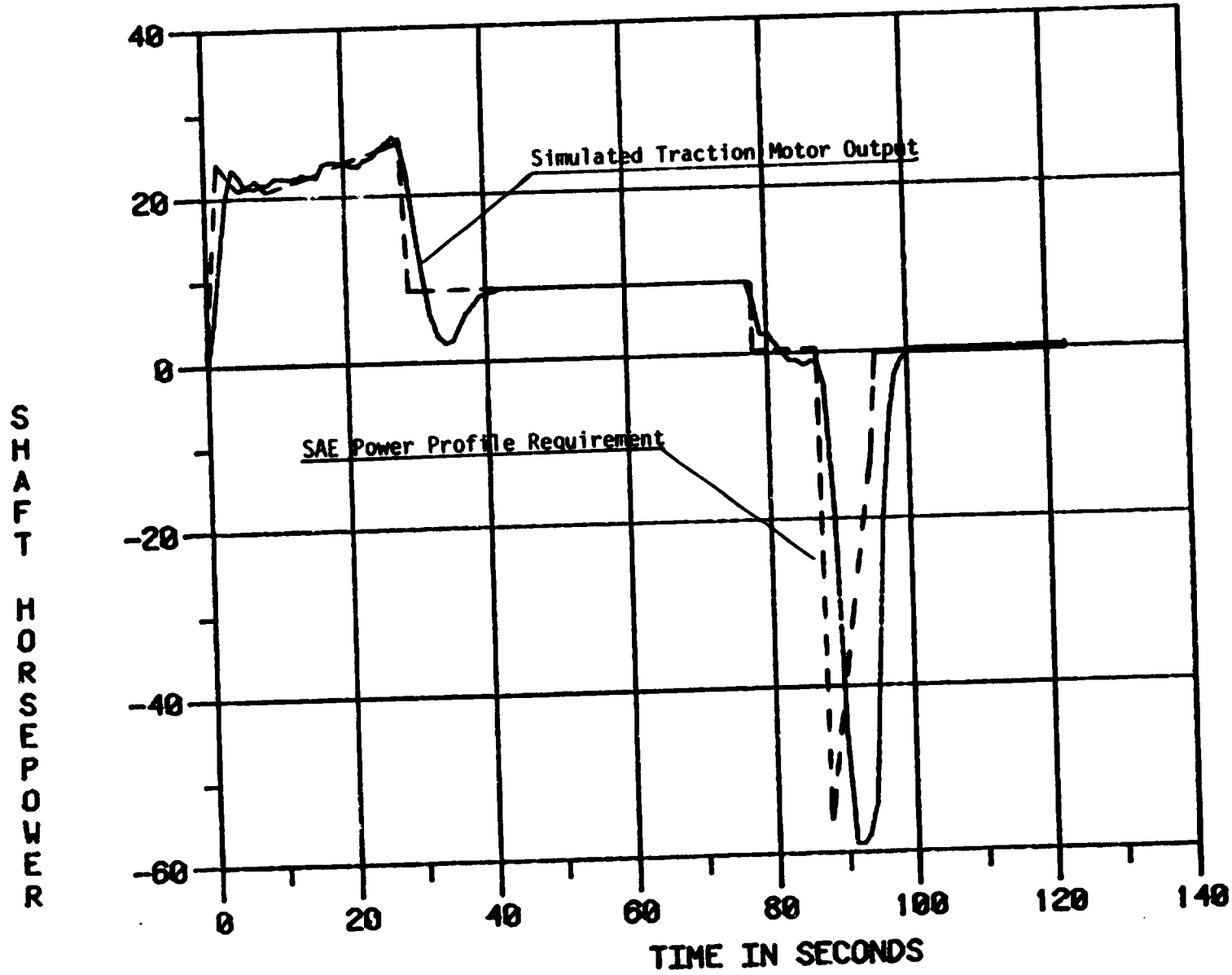

Figure 29. Traction Motor Shaft Output During SAE Profile

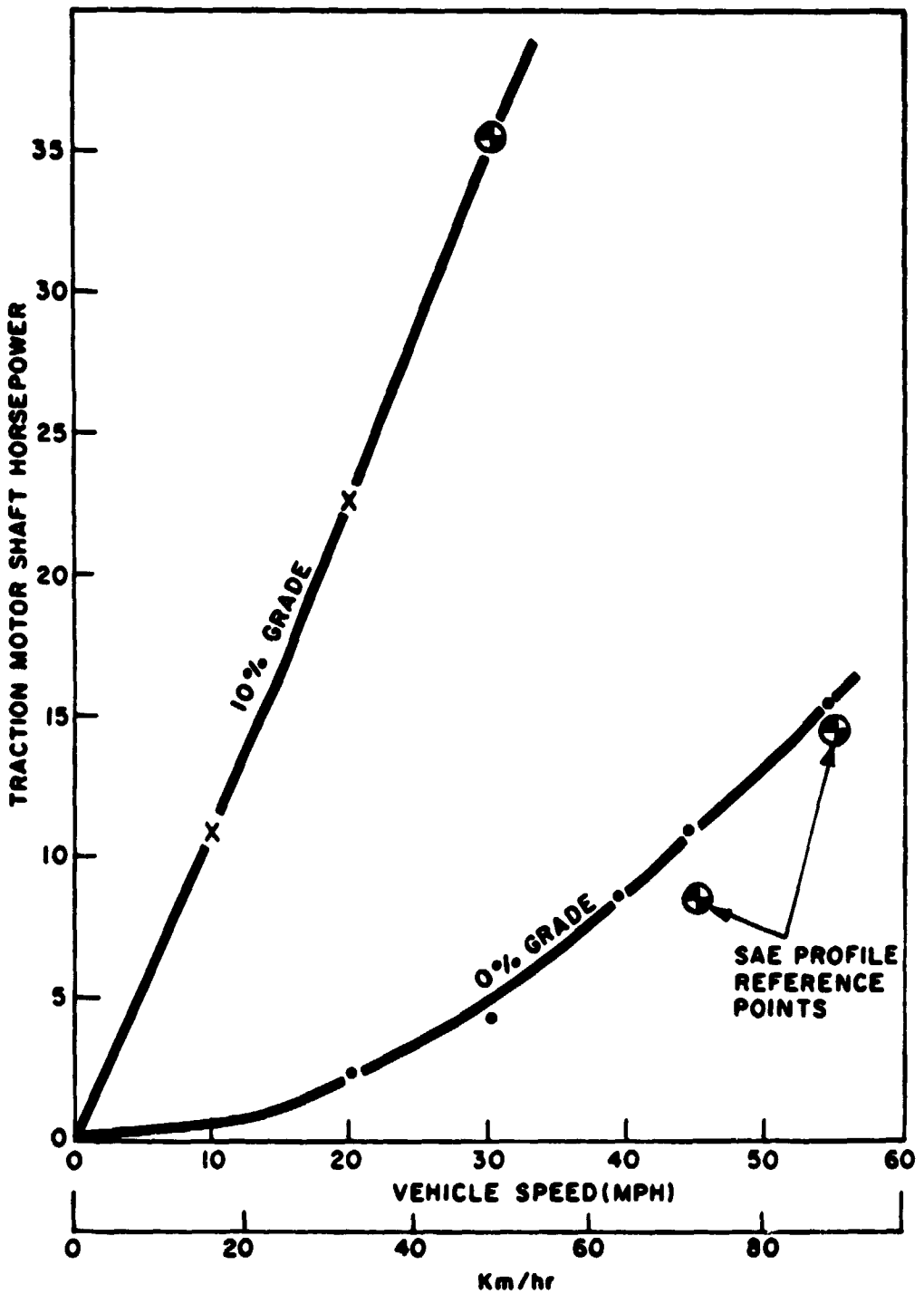

Figure 30. Traction Motor Horsepower Versus Vehicle Speed

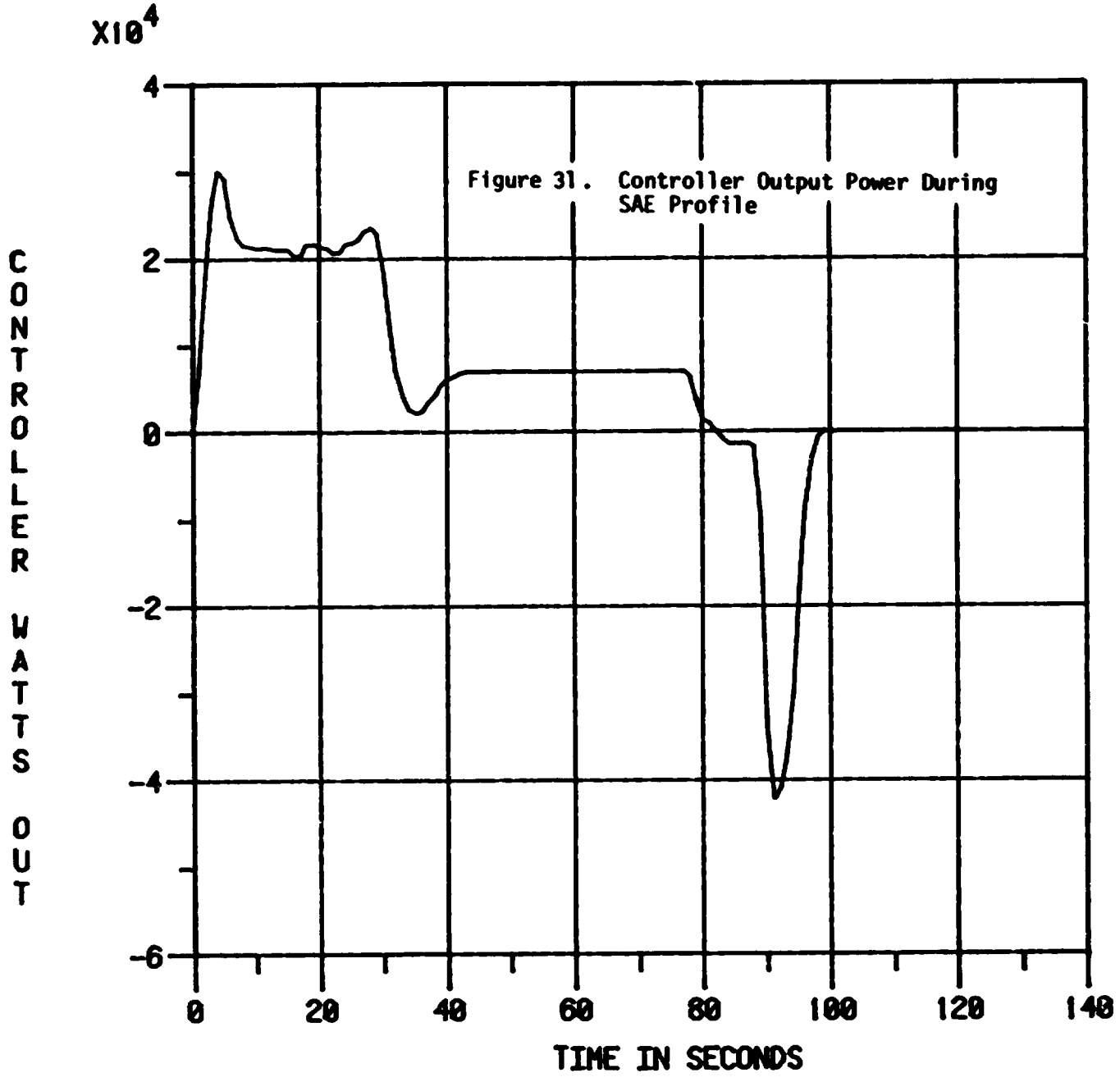

Figure 31. Controller Output Power During SAE Profile

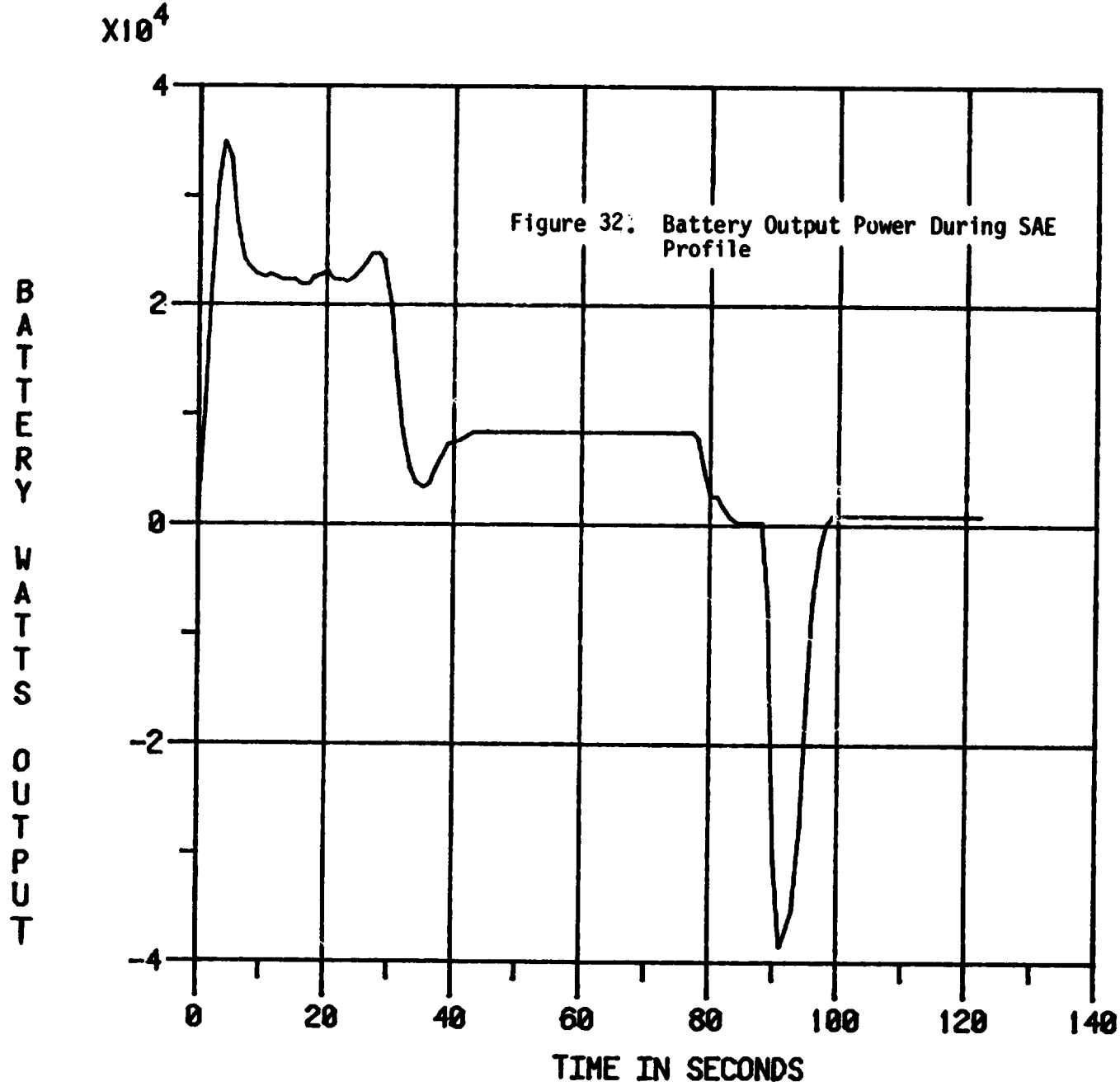

Figure 32. Battery Output Power During SAE Profile

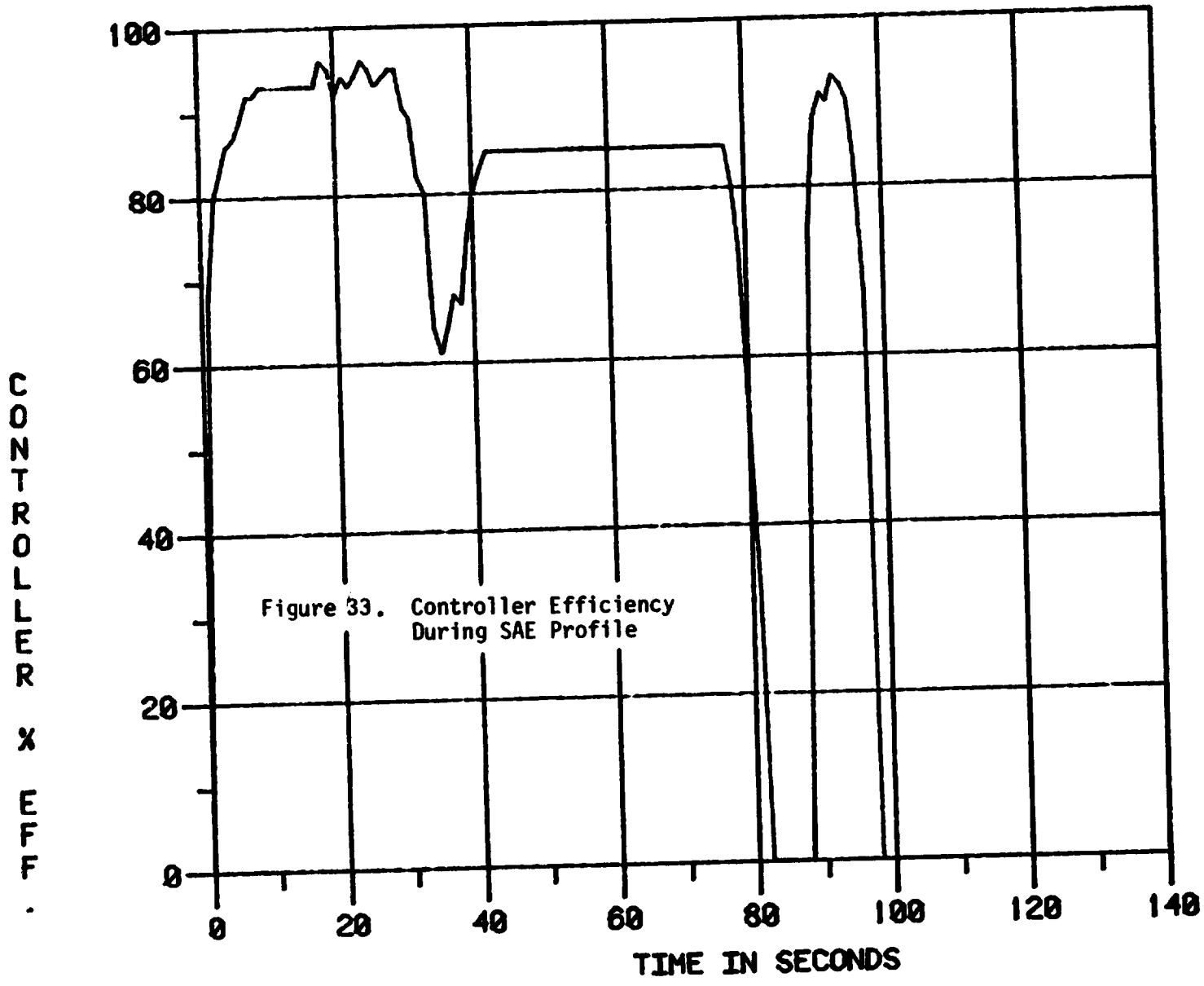

Figure 33. Controller Efficiency During SAE Profile

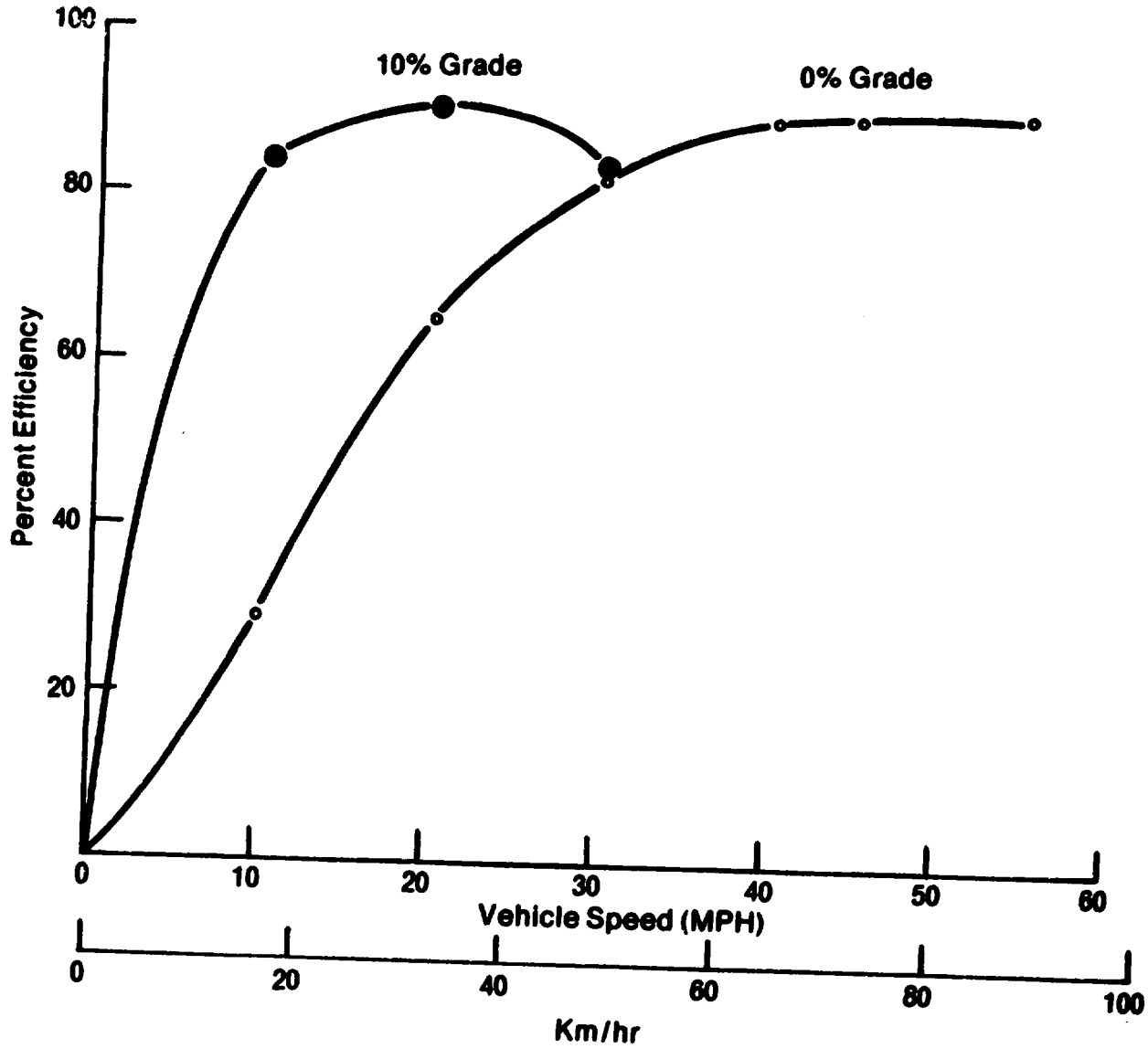

Figure 3.. Controller Efficiency Versus Vehicle Speed

ASSUMED 100,000 UNITS/YEAR

YEAR	1	2	3	4	5	6	7	8	9	10
PURCHASE PRICE	635	-	-	-	-	-	-	-	-	-
MAINTENANCE @ $16/HR	8	8	8	8	8	8	8	8	8	8
REPAIR @ $16/HR	-	-	-	-	-	-	36	-	-	-
SALVAGE VALUE	-	-	-	-	-	-	-	-	-	-318
ENERGY	10.17	10.17	10.17	10.17	10.17	10.17	10.17	10.17	10.17	10.17
WARRANTY	-	-	-	-	-	-	-	-	-	-
TOTALS	653.17	18.17	18.17	18.17	18.17	18.17	54.17	18.17	18.17	(-299.83)

	TOTAL LIFETIME COST	COST PER KILOMETER	COST PER MILE
100,000/YR	$534.70	$0.0033	$0.0052
10,000/YR	615.70	0.0038	0.0060

Figure 35. Summary of Life Cycle Costs

APPENDIX A

LIST OF SYMBOLS

PRECEDING PAGE BLANK NOT FILMED

SYMBOLS

A	armature amperes
A_f	field amperes
Amps	amperes
^oC	degrees centigrade
cm	centimeters
dc	direct current
DC	direct current
DOE	Department of Energy
E/M	electromagnetic
EMF	electromotive force
EV	electric vehicle
^oF	degrees fahrenheit
FRC	Franklin Research Center
ft	foot
GE	General Electric Company
hp	horsepower
hr	hour
I_b	battery current
I_d	drive motor armature current
I_f	field current
I_m	traction motor armature current
in	inches
J_D	drive motor inertia
J_L	reflected vehicle inertia

J_m	traction motor inertia
K_e	generated voltage constant
K_D	drag coefficient
K_f	friction and windage coefficient
K_t	torque constant
kg	kilogram
km	kilometer
kw	kilowatt
kwh	kilowatt hour
kw-sec	kilowatt second
lb	pound
MG	motor-generator
mi	mile
mph	miles per hour
NASA	National Aeronautics and Space Administration
Nm	newton meter
O.E.M.	original equipment manufacturer
P_o	power output
R&D	research and development
R_a	armature resistance
R_D	drive motor armature resistance
R_f	field resistance
R_g	generator armature resistance
R_m	traction motor armature resistance

rms	root mean square
rpm	revolutions per minute
S	Laplace transformer operator, d/dt
$S\theta_D$, $S\theta_m$	motor shaft speed
$S\theta_g$	generator shaft speed
SAE	Society of Automotive Engineers
sec	seconds
T_L	grade load torque
T_m	traction motor torque
v	volts
ϕ_D	drive motor field flux
ϕ_g	generator field flux
ϕ_m	traction motor field flux
Σ	summation

APPENDIX B

VALIDATION OF THE COMPUTER PROGRAM

Manual Calculations

Data recorded from the computer simulation of the Proof-of-Principle system during acceleration and deceleration are shown in Figure B1. Reference lines are provided for convenience in identifying the response with the discussion and in comparing the simulated results with the system test results in Figure B2.

Prior to Reference #201 and beginning at the top of Figure B1, the controller drive motor shaft velocity is 1000 rpm and the armature current 5.0 amperes, the level required to satisfy the friction and windage losses of the MG set.

The generator field is set to the value required to produce a terminal voltage of +12.0 volts, in these machines, 1.65 amperes. Since there is zero net voltage to the traction motor the motor velocity and the armature current are zero.

Under these conditions the power drawn from the battery will be the sum of the drive motor power, P_D the generator power P_g and the traction motor power P_m or

$$P_{in} = P_D + P_g + P_m$$

In this case

$$P_d = (I_D \times E_b) + (I_{fD} \times E_b)$$

$$P_d = (5.0 \times 12) + (1.65 \times 12) = 79.8 \text{ watts} \quad \text{(drive motor)}$$

$$P_g = (I_m \times E_g) + (I_{fg} \times E_b)$$

$$P_g = (0 \times 12) + (1.65 \times 12) = 19.8 \text{ watts} \quad \text{(generator)}$$

$$P_m = (I_m \times E_m) + (I_{fm} \times E_b)$$

$$P_m = (0 \times 0) + (1.65 \times 12) - 19.8 \text{ watts} \quad \text{(traction motor)}$$

and

$$P_{in} = 79.8 + 19.8 + 19.8 = 119.4 \text{ watts} \quad \text{(total)}$$

The computer simulation yields a value of approximately 115 watts.

At Reference #201 the generator field is suddenly reduced to zero. At zero the power required by the MG set drive motor should be no different because the loading is

$$P_D = P_{f+w} + P_g$$

or

$$P_D = P_{f+w} + I_m E_g$$

and in the previous case (maximum field)

$$P_D = P_{f+w} + (0 \times 12) = P_{f+w}$$

now

$$P_D = P_{f+w} + (I_m \times 0) = P_{f+w}$$

The computer simulation indicates a small change during the transition. This is due to the finite time it takes for the field to change from maximum to zero. During this transition the generator acts as a motor feeding back torque that increases the MG set shaft velocity and reduces the loss current to the drive motor from 5.0 to 2.2 amperes. When the field current has reached zero, there is no difference in drive motor power as predicted in the above analysis.

When the field excitation is zero, the generator terminal voltage will be due only to its IR armature drop. Since the <u>generated</u> voltage is zero, the terminal voltage is calculated from

$$E_g = E_b \left(\frac{R_g}{R_g + R_m} \right)$$

In the simulation an armature resistance of 0.165 ohms was used for all machines. Therefore at zero field the generator voltage should be half the battery voltage or 6.0 volts. However, taking into account the increase in generator speed during the transition (1000 to 1050 rpm), the generator terminal voltage can be

$$E_g = \frac{1050}{1000} \times 6.0 = 6.3 \text{ volts}$$

assuming an average of half the field current. The simulation indicates approximately 6.5 volts.

The traction motor peak current is due to the difference between battery and generator volts applied to its armature resistance or

$$I_m = \frac{E_b - E_g}{R_m} = \frac{12 - 6.5}{0.165} = 33 \text{ amperes}$$

The computer simulation indicates 32 amperes.

The peak battery power during this transition is

$$P_D = (2.2 \times 12) + (1.65 \times 12) = 46.2 \text{ watts}$$

$$P_g = (32 \times 6.5) + \left(\frac{1.65}{2} \times 12\right) = 217.9 \text{ watts}$$

$$P_m = \left[32(12 - 6.5)\right] + (1.65 \times 12) = 195.8 \text{ watts}$$

$$P_{in} = P_d + P_g + P_m = 459.9 \text{ watts}$$

The computer simulation shows approximately 470 watts at the peak.

Following the peak conditions after Reference #201, the traction motor reaches full speed in about 20 seconds with the inertia used in the simulation, 0.097 Nm sec^2 (0.86 lb in sec^2). At Reference #202, the generator field is zero and the traction motor is running at a constant no-load speed. Under these conditions the power drawn from the battery is distributed as follows:

$$P_d = (5.2 \times 12) + 19.8 = 82.2 \text{ watts}$$

$$P_g = (2^2 \times 0.165) + (0 \times 12) = 0.66 \text{ watts}$$

$$P_m = 2(12 - 0.33) + 19.8 = 43.14 \text{ watts}$$

$$P_{in} = P_d + P_g + P_m = 126 \text{ watts}$$

The simulation indicates about 135 watts.

The traction motor top speed (1000 rpm @ 12V) is limited by the IR drop in the generator armature or

$$S\theta_m = \left(E_b - I_m R_g\right) \frac{1000}{12}$$

$$S\theta_m = \left[12 - (2 \times 0.165)\right] \frac{1000}{12} = 978 \text{ rpm}$$

The simulation indicates about 975 rpm.

At Reference #203 the generator field is suddenly increased to its initial value and the generated voltage, added to the back emf of the running traction motor, causes the current in the armature circuit to reverse. Now the MG set drive motor must deliver the power developed by the generator. The drive motor shaft velocity decreases and the armature current increases. Using measured values of the peaks after Reference #203, the peak armature current is calculated

$$I_m = \frac{E_b - (E_m + E_g)}{R_m + R_g} + \frac{E_b - (E_m + E_g)}{R_d + R_m + R_g}$$

but

$$E_m = S\theta_m \left(\frac{12 \text{ volts}}{1000 \text{ rpm}}\right) = 975 \left(\frac{12}{1000}\right) = 11.7 \text{ volts}$$

then

$$I_m = \frac{12 - (11.7 + 5.5)}{0.33} + \frac{12 - (11.7 + 5.5)}{4.95}$$

$$I_m = -15.8 - 10.5 = -26.3 \text{ amperes}$$

The computer simulation shows a peak current of -26 amperes.

The power input during this transient is

$$P_d = (22 \times 12) + 19.8 = 283.8 \text{ watts}$$

$$P_g = (126 \times 5.5) + \frac{19.8}{2} = -133.1 \text{ watts}$$

$$P_m = (-26 \times 11.7) + 19.8 = -284.4 \text{ watts}$$

$$P_{in} = P_d + P_g + P_m = \quad = -134 \text{ watts}$$

The computer shows a peak of 135 watts being returned to the battery.

After 2 seconds the traction motor has slowed down to 680 rpm so the power distribution is:

$$P_D = (22.5 \times 12) + 19.8 = 289.8 \text{ watts}$$

$$P_g + (-14 \times 6.5) + 19.8 = -71.2 \text{ watts}$$

$$P_m = (-14 \times 8.16) + 19.8 = -94.4 \text{ watts}$$

$$P_{in} = P_D + P_g + P_m = 124.2 \text{ watts}$$

The computer simulation indicates 135 watts.

In conclusion, these manual calculations confirm that the computer program is accurately simulating the mathematical model of the Advanced DC Motor Controller with exceptional fidelity.

Graphical Comparison of Dynamic Test Results

The graphical test results from the Demonstration System in Figure B2 were compared with the results of the computer simulation in Figure B1. Superimposing the traces shows a remarkable similarity in transient responses. For example, we superimpose the two sets of traces in Figure B3. Some differences in peak and steady-state magnitudes are evident but the character of the response is the same. The differences are explained as follows.

Immediately after Reference #201, the peak armature current in the Demonstration System is considerably lower than in the simulated system. This is due to several factors as follows:

- The actual value of armature resistance at this current, taken from the nonlinear characteristic curve recorded earlier, is 0.185 ohms. A value of 0.165 ohms was used in the simulation.

- The actual value of the battery bus voltage is 11.5 volts as opposed to the 12 volts in the simulated system. Furthermore, the internal resistance of the battery is not inlcuded in the simulation.

- The field of the real generator has residual magnetism that accounts for another 0.5 volt reduction of voltage applied to the motor in the Demonstration System. This is not included in the simulation.

- Armature circuit inductances are not included in the simulation.

After the traction motor has reached a steady speed, that speed is 740 rpm in the Demonstration System and 1000 rpm in the simulation system. This difference is due to the following:

- The actual armature resistance is 0.48 ohms at a current of 4 amps. The linearized value used in the simulation was 0.165 ohms.

- The battery bus voltage is lower in the Demonstration System.

- The residual generator voltage is not simulated.

- There is higher level of friction at the lower speed due to the extremely nonlinear characteristics of the machines. A value of $K_f = 2.24 \times 10^{-4}$ Nm/rpm was used in the simulation.

At Reference #203 in Figures B1 and B2, the generator field is increased to decelerate the traction motor. The peak reverse current in the armature circuit is considerably lower in the Demonstration System than in the simulated system. In this case the armature current is very low so the armature resistances are high (0.5 ohms as measured in the initial bench tests).

The decay in traction motor speed of the Demonstration Systems appears different from the simulated systems' response. It is obviously the result of a non-linearity; specifically, the friction and windage characteristic. The largest component of friction in these small machines is the coulomb friction of the brushes riding on the commutator. It requires an armature current of 3 amperes to overcome this friction at starting and the total no-load running current at 740 rpm is only 4 amperes. This results in the sudden stop of the traction motor in the Demonstration System. Friction was treated in its viscous form (proportional to velocity) in the computer simulation.

In conclusion the validity of the computer simulation program has been firmly established in manual calculations and in a direct comparison with the results of tests on the Proof-of-Principle System. The computing accuracy is better than $\pm$ 5%. Differences are shown to be mainly a result of non-linearities which are not included in the simulation but are only predominant in small machines. For example, the brush friction in the Proof-of-Principle machines is 75% of the no-load losses while in a 20 hp machine, it is in the order of 40%. Therefore the computer simulation, with the proper parameter adjustments, is a reliable tool for predicting the performance of full-scale systems with good reliability.

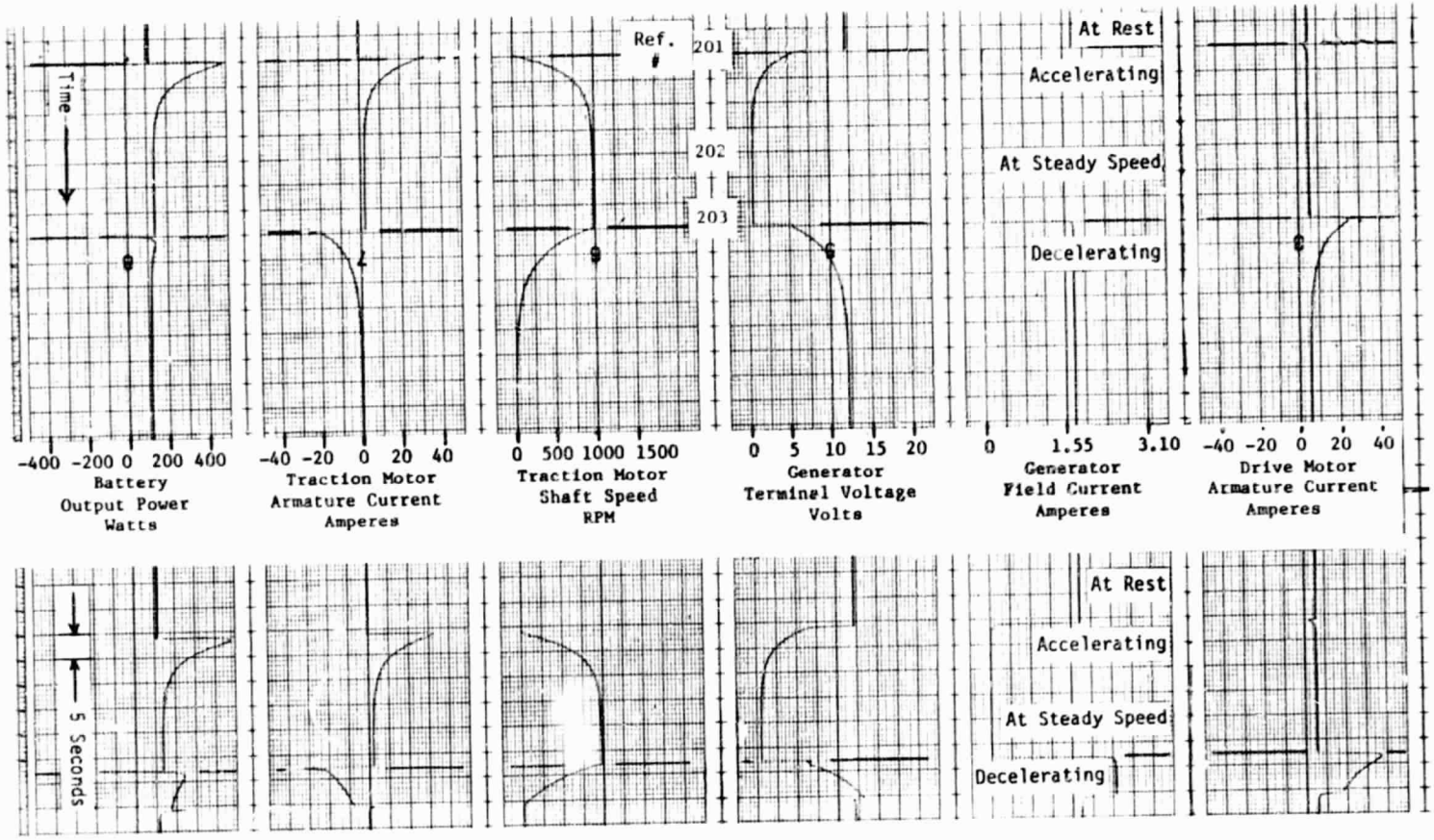

Figure B-1. Simulated Proof-of-Principle System -- Acceleration and Deceleration on Level Grade

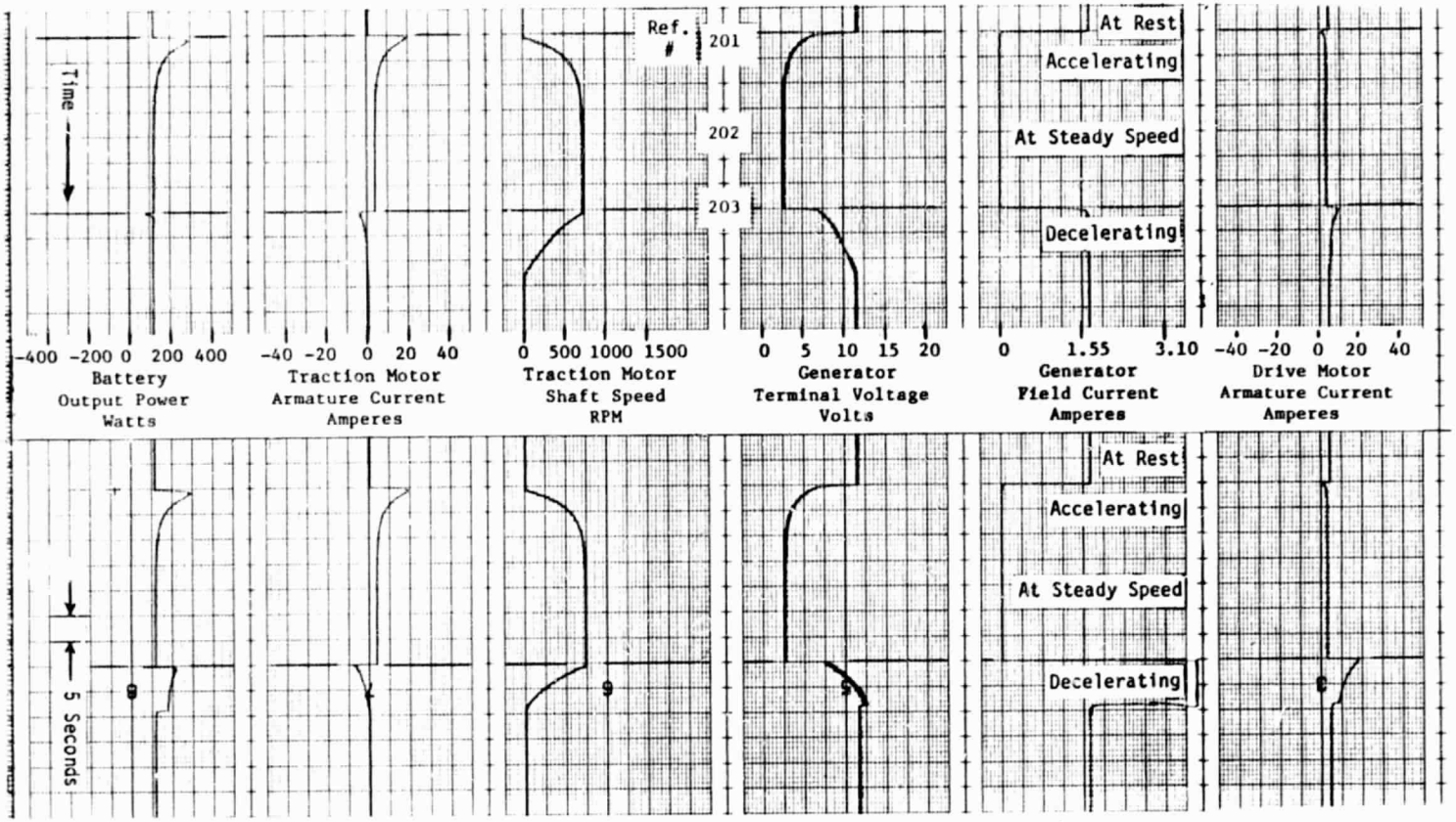

Figure B-2. Proof-of-Principle Demonstration System Test Results - Acceleration and Deceleration of a Vehicle on Level Grade

ORIGINAL PAGE IS OF POOR QUALITY

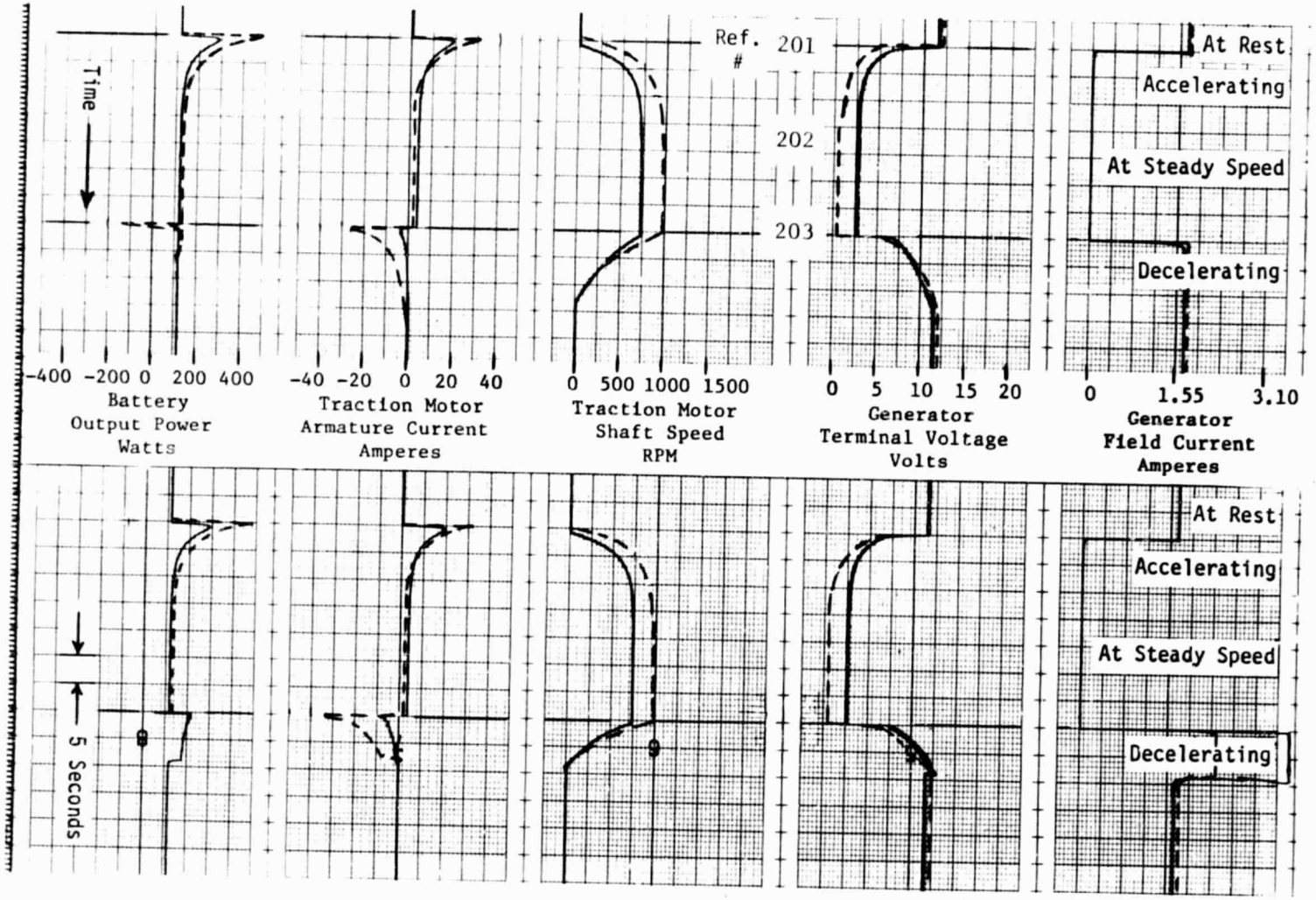

Figure B-3. Superposition of Figures B-1 and B-2 to Validate Computed Dynamic Performance

APPENDIX C

ADDITIONAL ENGINEERING MODEL CONTROLLER DRAWINGS

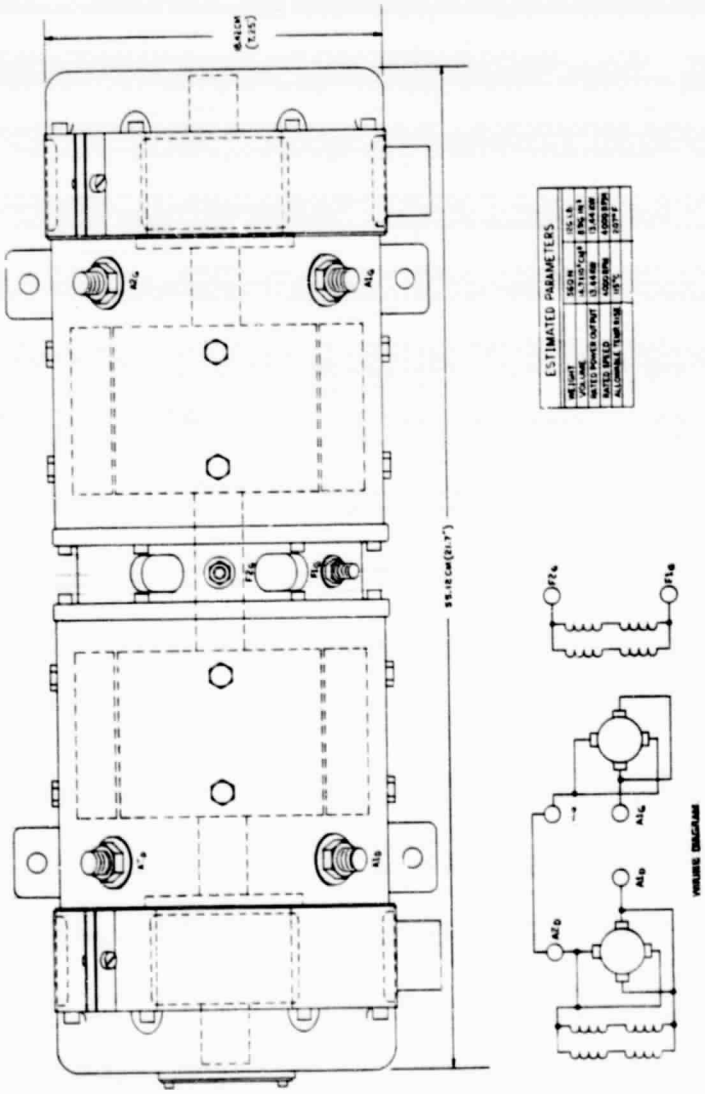
ESTIMATED PARAMETERS
WEIGHT
VOLUME
RATED POWER OUTPUT
RATED SPEED
ALLOWABLE TEMP RISE
WIRING DIAGRAM

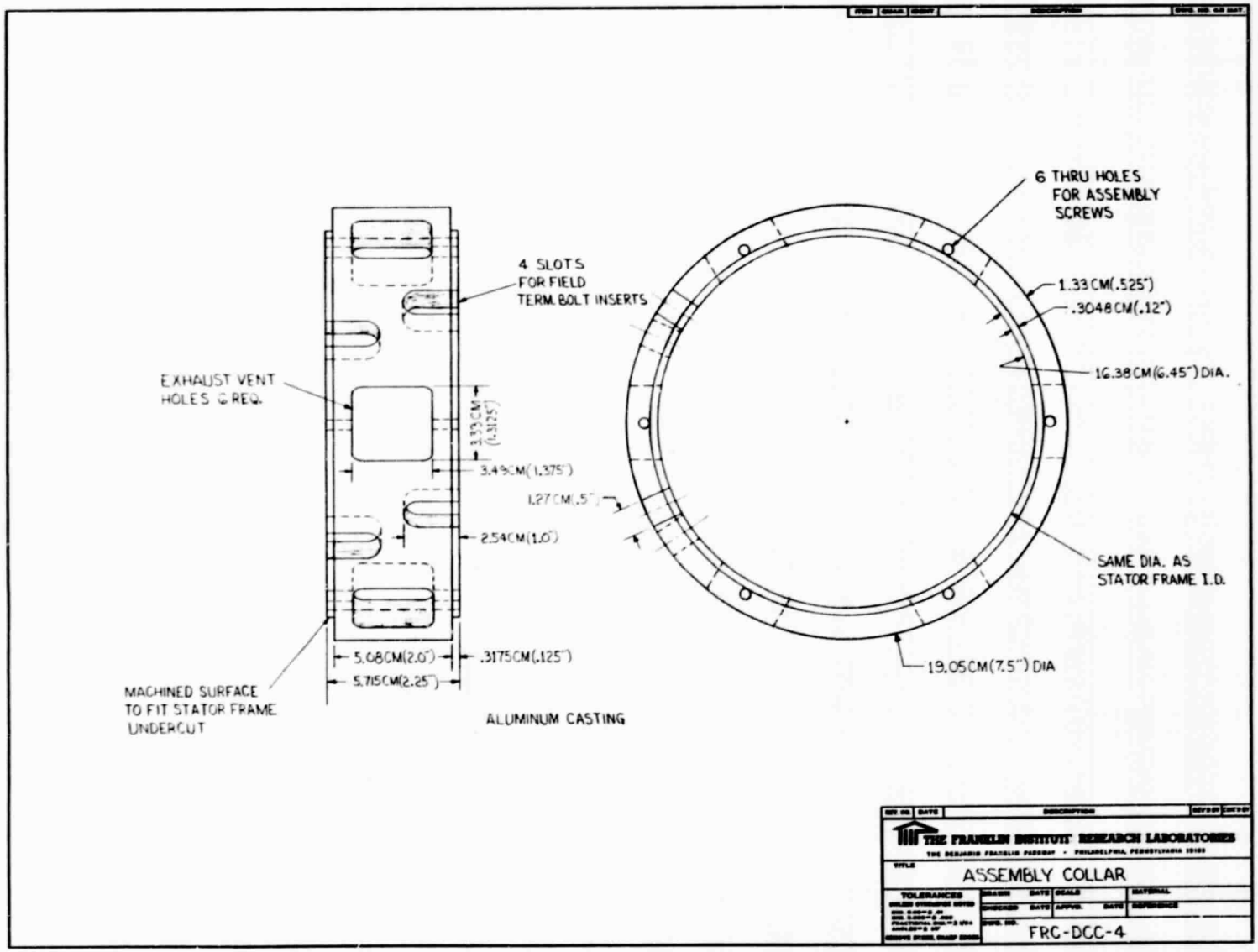
6 THRU HOLES
FOR ASSEMBLY
SCREWS
4 SLOTS
FOR FIELD
TERM. BOLT INSERTS
1.33 CM(.525")
.3048 CM(.12")
16.38 CM(6.45") DIA.
EXHAUST VENT
HOLES @ REQ.
3.33 CM
(1.3125")
3.49 CM(1.375")
1.27 CM(.5")
2.54 CM(1.0")
SAME DIA. AS
STATOR FRAME I.D.
5.08 CM(2.0")
.3175 CM(.125")
5.715 CM(2.25")
19.05 CM(7.5") DIA
MACHINED SURFACE
TO FIT STATOR FRAME
UNDERCUT
ALUMINUM CASTING
THE FRANKLIN INSTITUTE RESEARCH LABORATORIES
ASSEMBLY COLLAR
FRC-DCC-4

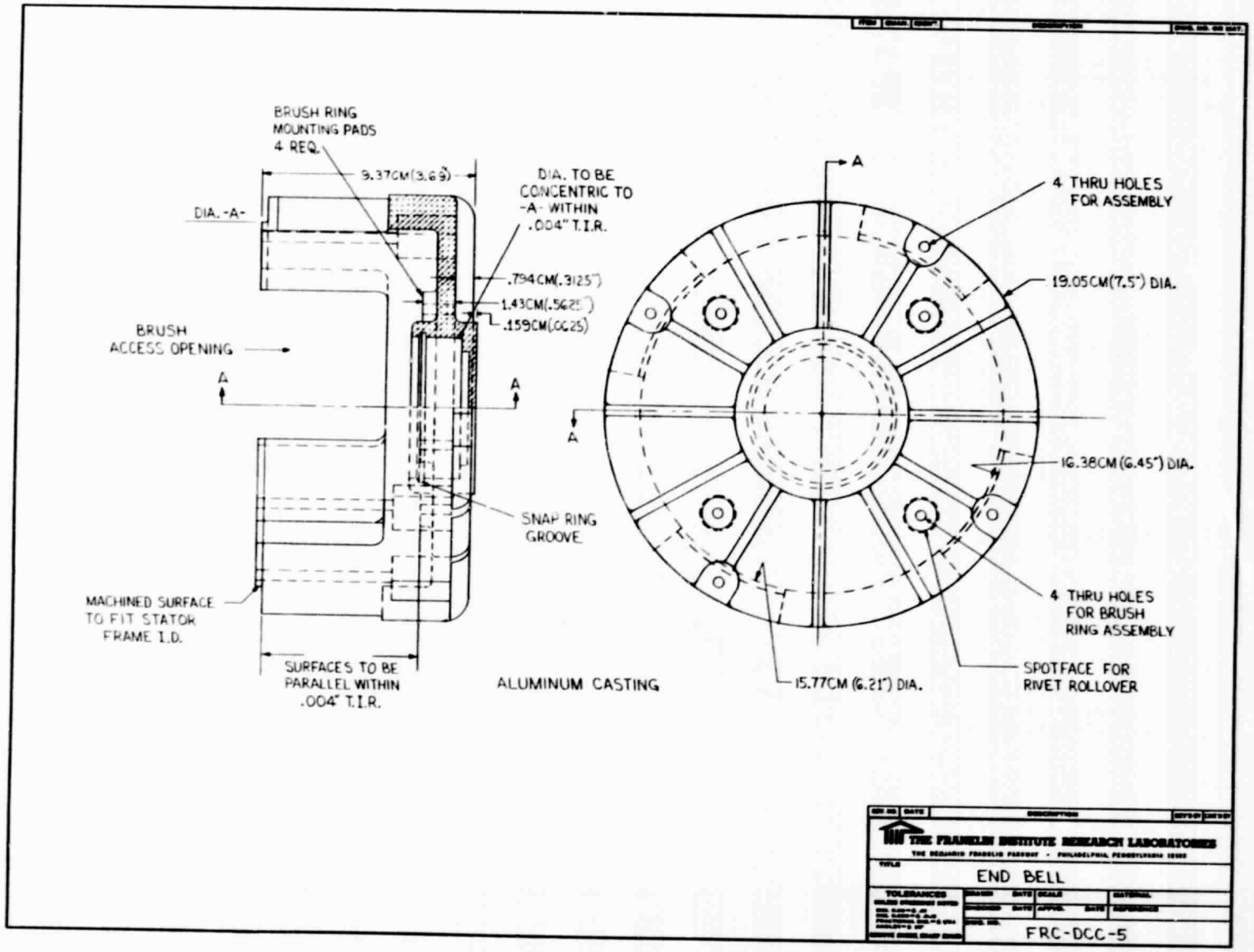
BRUSH RING
MOUNTING PADS
4 REQ.
9.37CM(3.69")
DIA. -A-
DIA. TO BE
CONCENTRIC TO
-A- WITHIN
.004" T.I.R.
.794CM(.3125")
1.43CM(.5625")
.159CM(.0625)
BRUSH
ACCESS OPENING
A
A
SNAP RING
GROOVE
MACHINED SURFACE
TO FIT STATOR
FRAME I.D.
SURFACES TO BE
PARALLEL WITHIN
.004" T.I.R.
ALUMINUM CASTING
A
A
4 THRU HOLES
FOR ASSEMBLY
19.05CM(7.5") DIA.
16.38CM(6.45") DIA.
4 THRU HOLES
FOR BRUSH
RING ASSEMBLY
SPOTFACE FOR
RIVET ROLLOVER
15.77CM (6.21") DIA.
THE FRANKLIN INSTITUTE RESEARCH LABORATORIES
END BELL
FRC-DCC-5

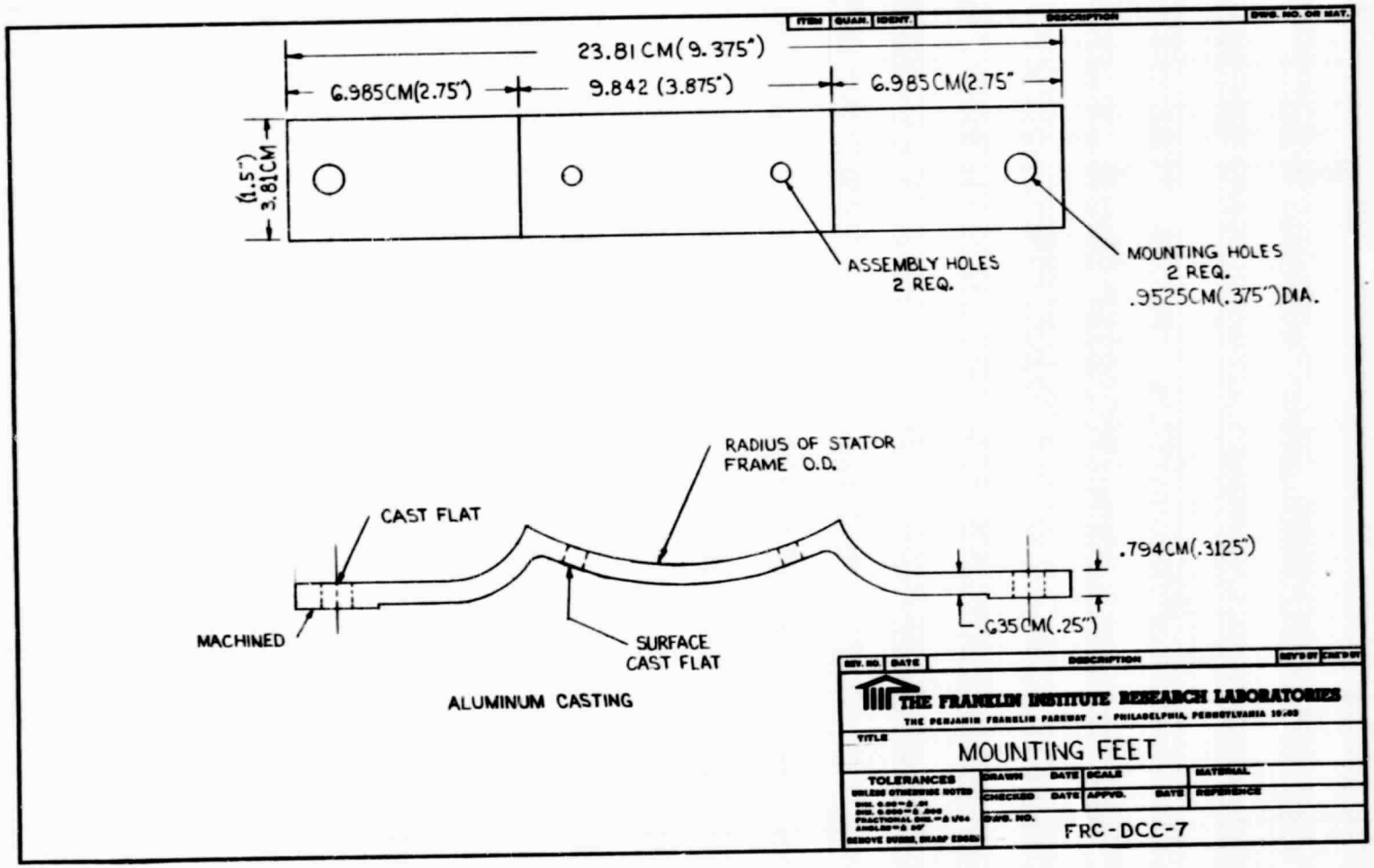
23.81 CM (9.375")
6.985CM(2.75")
9.842 (3.875")
6.985CM(2.75"
(1.5")
3.81CM
ASSEMBLY HOLES
2 REQ.
MOUNTING HOLES
2 REQ.
.9525CM(.375")DIA.
RADIUS OF STATOR
FRAME O.D.
CAST FLAT
.794CM(.3125")
MACHINED
SURFACE
CAST FLAT
.635CM(.25")
ALUMINUM CASTING
THE FRANKLIN INSTITUTE RESEARCH LABORATORIES
TITLE
MOUNTING FEET
TOLERANCES
DRAWN
DATE
SCALE
MATERIAL
CHECKED
APPVD.
REFERENCE
DWG. NO.
FRC-DCC-7

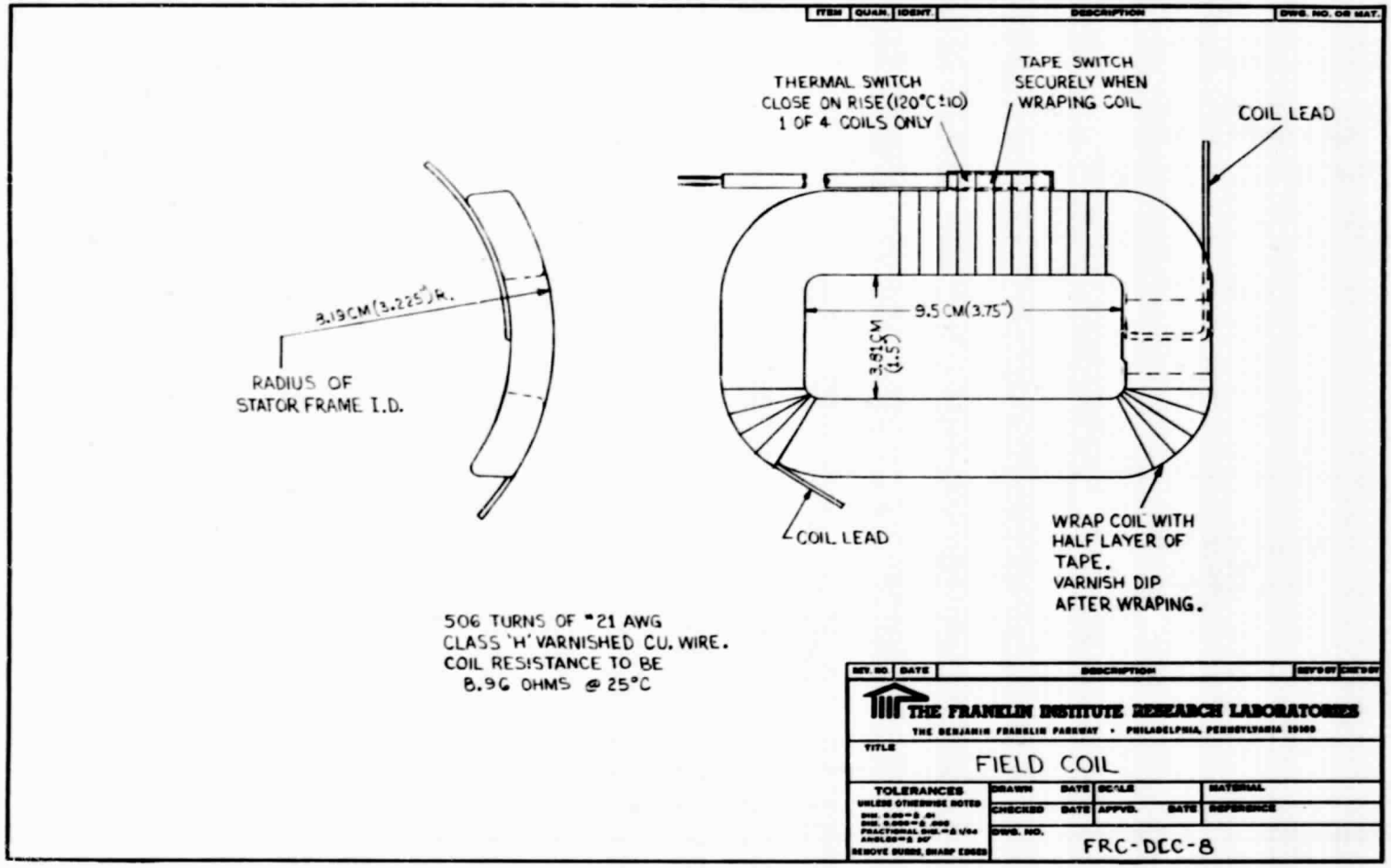
ITEM
QUAN.
IDENT.
DESCRIPTION
DWG. NO. OR MAT.
THERMAL SWITCH
CLOSE ON RISE (120°C ±10)
1 OF 4 COILS ONLY
TAPE SWITCH
SECURELY WHEN
WRAPING COIL
COIL LEAD
8.13CM (3.225") R.
RADIUS OF
STATOR FRAME I.D.
9.5 CM (3.75")
3.81CM
(1.5")
COIL LEAD
WRAP COIL WITH
HALF LAYER OF
TAPE.
VARNISH DIP
AFTER WRAPING.
506 TURNS OF #21 AWG
CLASS 'H' VARNISHED CU. WIRE.
COIL RESISTANCE TO BE
8.96 OHMS @ 25°C
REV. NO.
DATE
DESCRIPTION
REV'D BY
CHK'D BY
THE FRANKLIN INSTITUTE RESEARCH LABORATORIES
THE BENJAMIN FRANKLIN PARKWAY • PHILADELPHIA, PENNSYLVANIA 19103
TITLE
FIELD COIL
TOLERANCES
UNLESS OTHERWISE NOTED
REMOVE BURRS, SHARP EDGES
DRAWN
DATE
SCALE
MATERIAL
CHECKED
DATE
APPVD.
DATE
REFERENCE
DWG. NO.
FRC-DEC-8

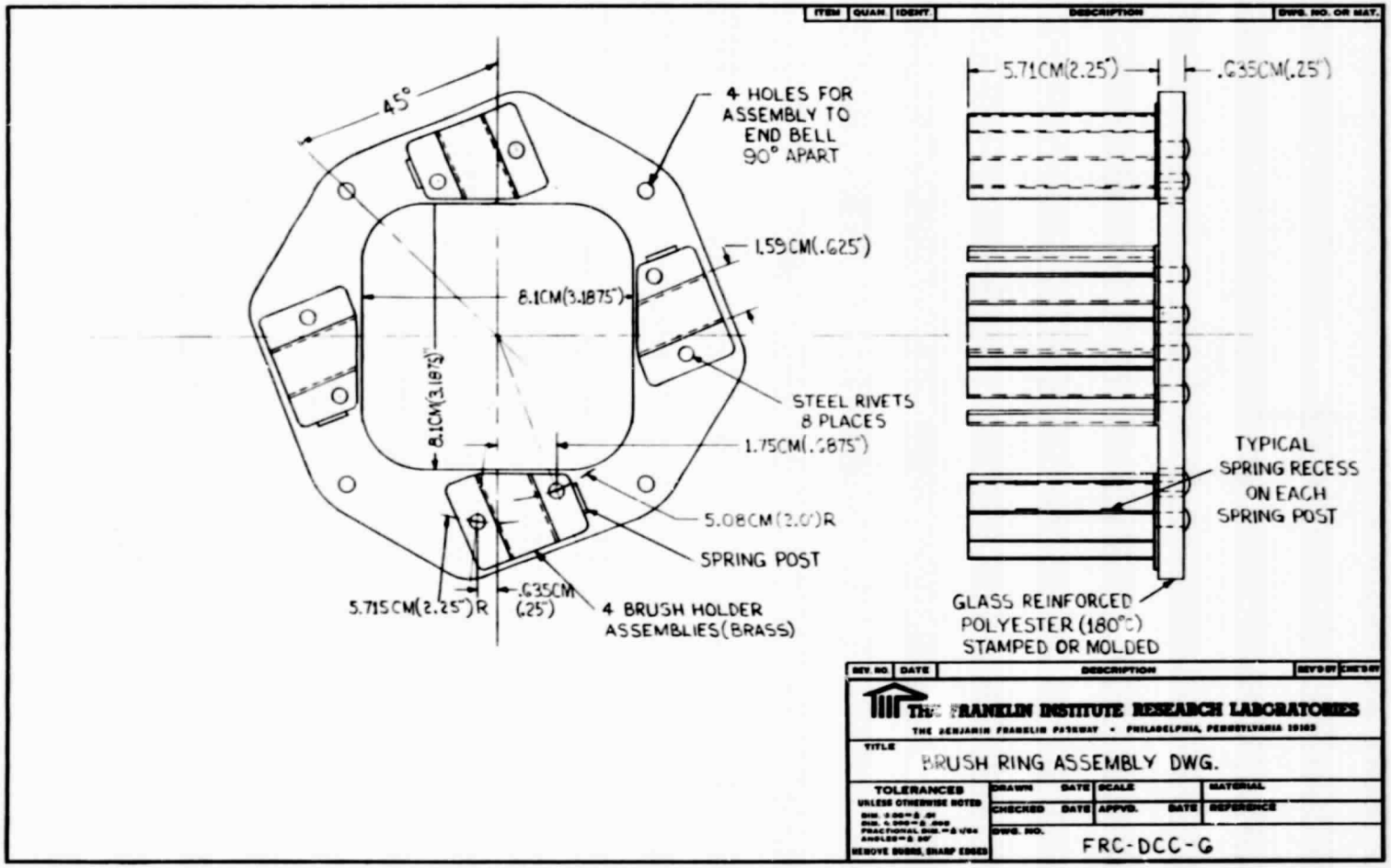
ITEM
QUAN
IDENT
DESCRIPTION
DWG. NO. OR MAT.
45°
4 HOLES FOR ASSEMBLY TO END BELL 90° APART
1.59CM(.625")
8.1CM(3.1875")
8.1CM(3.1875")
STEEL RIVETS 8 PLACES
1.75CM(.6875")
5.08CM(2.0")R
SPRING POST
5.715CM(2.25")R
.635CM (.25")
4 BRUSH HOLDER ASSEMBLIES(BRASS)
5.71CM(2.25")
.635CM(.25")
TYPICAL SPRING RECESS ON EACH SPRING POST
GLASS REINFORCED POLYESTER (180°C) STAMPED OR MOLDED
REV. NO
DATE
DESCRIPTION
REV'D BY
CHK'D BY
THE FRANKLIN INSTITUTE RESEARCH LABORATORIES
THE BENJAMIN FRANKLIN PARKWAY • PHILADELPHIA, PENNSYLVANIA 19103
TITLE
BRUSH RING ASSEMBLY DWG.
TOLERANCES
UNLESS OTHERWISE NOTED
REMOVE BURRS, SHARP EDGES
DRAWN
DATE
SCALE
MATERIAL
CHECKED
DATE
APPVD.
DATE
REFERENCE
DWG. NO.
FRC-DCC-G

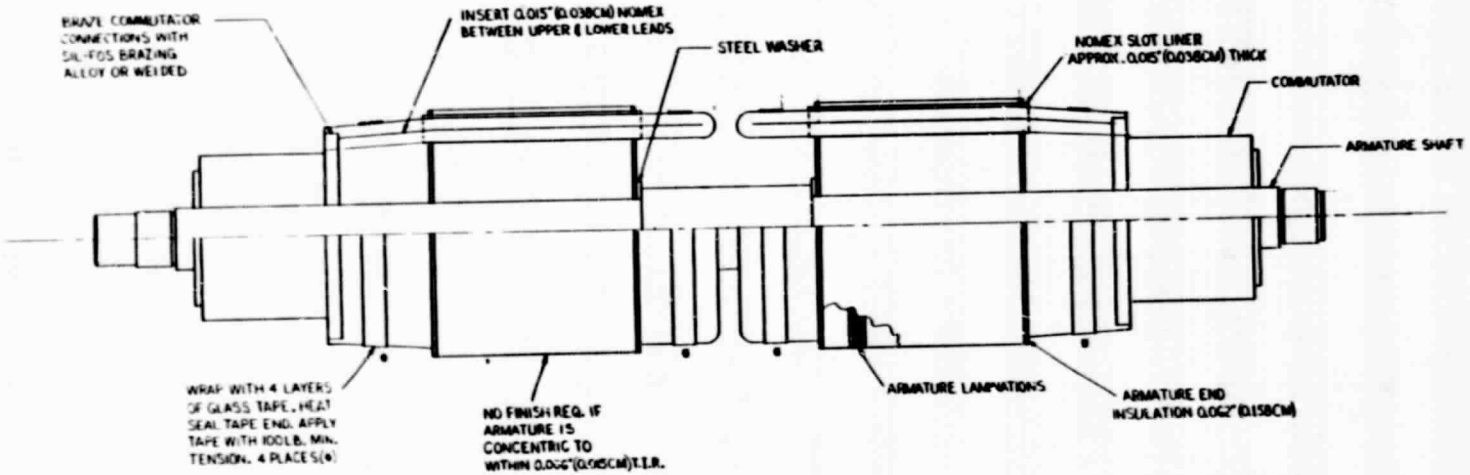

NOTE: ALL INSTRUCTIONS APPLY TO BOTH ARMATURE ASSEMBLIES

VARNISH COMPLETE ASSEMBLY WITH CLASS "H" INSULATION.
SPIN TEST AT 5000 RPM, 165°C
BALANCED WITHIN .3 OZ. IN.
RESISTANCE 0.005 OHMS @ 25°C

Armature Assembly

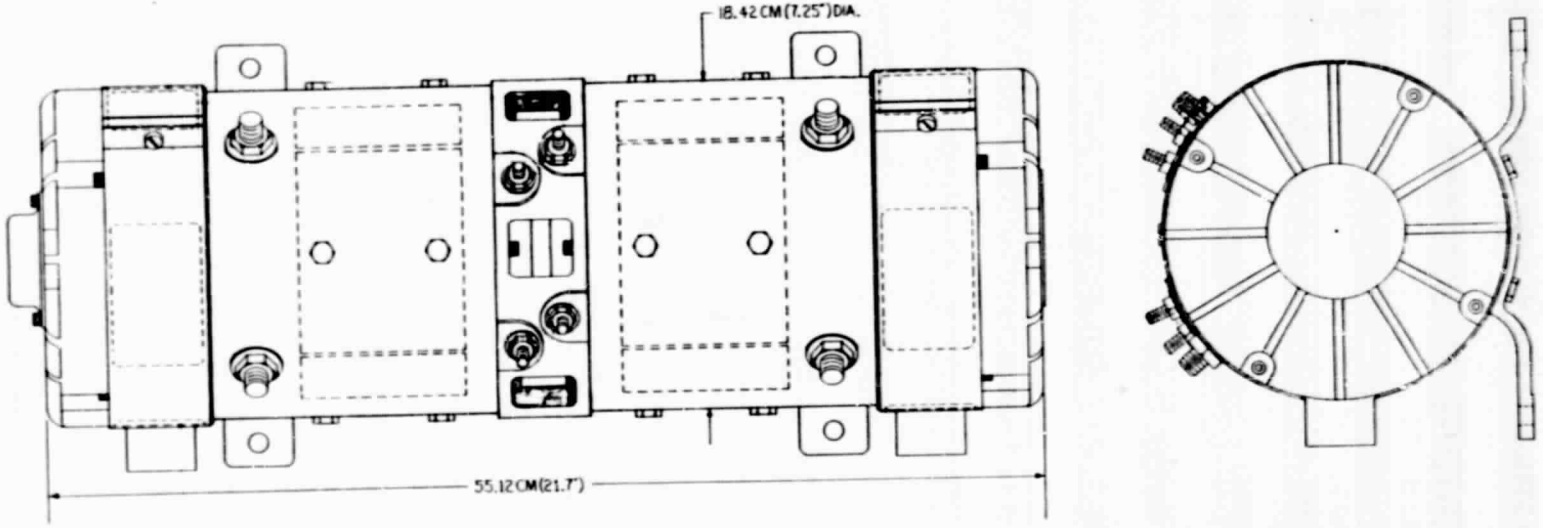

DC MG Set Outline Drawing